THE EFFECTS OF MESO-SCALE AND SMALL-SCALE INTERACTIONS ON GLOBAL CLIMATE

Systems, Science and Software

Prepared for:

Army Research Office (Durham)
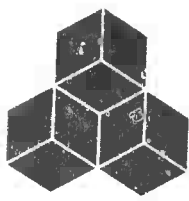Advanced Research Projects Agency

15 September 1972

QROD-9951.4-A

SYSTEMS, SCIENCE AND SOFTWARE

SSS-R-72-1255

THE EFFECTS OF MESO-SCALE AND SMALL-SCALE
INTERACTIONS ON GLOBAL CLIMATE

Quarterly Management/
Semiannual Technical Report

for Period

15 February 1972 through 14 August 1972

Sponsored by:

Advanced Research Projects Agency
ARPA Order No. 1752
Program Code No. G1101D

Contract No.: DAHC 04-71-0018
Effective Date of Contract: 15 February 1971
Contract Expiration Date: 14 August 1972
Amount of Contract: $298,559.00

D D C
OCT 27 1972
RECEIVED
B

15 September 1972

202

SYSTEMS, SCIENCE AND SOFTWARE

SSS-R-72-1255

THE EFFECTS OF MESO-SCALE AND SMALL-SCALE INTERACTIONS ON GLOBAL CLIMATE.

Quarterly Management/
Semiannual Technical Report,

15 Feb~~~~~~~~~~~~~-14 Aug~~~~ 1972,

Details of illustrations in
this document may be better   AROD – 9951.4-A
studied on microfiche.

Sponsored by:

Advanced Research Projects Agency
ARPA Order No. 1752
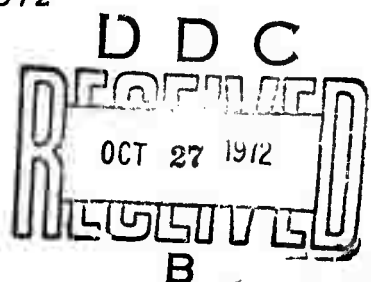Program Code No. G1101D

Contract No.:   DAHC 04-71-0018
Effective Date of Contract: 15 February 1971
Contract Expiration Date: 14 August 1972
Amount of Contract: $298,559.00

15 September 1972

388 507

TABLE OF CONTENTS

TABLE OF CONTENTS, contd.

TABLE OF CONTENTS, contd.

LIST OF ILLUSTRATIONS

LIST OF ILLUSTRATIONS, contd.

1. INTRODUCTION

The results reported herein are the continuation of numerical studies of meso-scale phenomena related to the effects of orography on momentum and energy transfer in the atmosphere and the interaction of solar radiation with the Earth's atmosphere. [1,2]

1.1   OROGRAPHIC EFFECTS ON GLOBAL CLIMATE

The scope of work during the past six months study has emphasized a continuing effort to develop and expand numerical codes which may be used to understand the physical processes which influence momentum transfer. Further developments on the HAIFA code were completed which enable us to calculate the time dependent effects of Coriolis forces and turbulence on two-dimensional flow over mountain ranges. In addition, a linear steady-state code based on an analysis by Bretherton[3] was completed and several problem sets investigating the effects of wind profile and atmospheric stabilities were completed. Where possible, the steady state results were compared with the time dependent results of HAIFA.

Some parameterization work was completed using the steady-state results for an exponential wind profile and a constant lapse rate in the atmosphere. Further work along this line is expected to be completed during the follow-on contract; in addition, we expect to develop three-dimensional

codes using the same assumptions present in our two-dimensional codes. This will allow us to calculate the effects of two-dimensional topography.

1.2 RADIATIVE TRANSFER

The atmospheric radiation code was completed during the past six months and calculational results were compared with the Mintz-Arakawa parameterization presently used in the UCLA global circulation model (GCM). These comparisons are reported in Sections 4 and 5. In addition, an updated description of the code (superceding our last report[2]) and a glossary of the input parameters required to operate it are included. Parameterization efforts using the existing code will be the main emphasis of the work and shall represent the bulk of the work during the next six months.

In addition, further modifications of the code are expected during the next six month period. In particular, we expect to study the effects of aerosols and the surface boundary conditions.

2. MODIFICATIONS TO THE HAIFA CODE

Two modifications were made to the basic HAIFA code during the past six months efforts. These were the inclusion of (1) the Coriolis forces and (2) an heuristic turbulence model in the basic code. These modifications are detailed in this section of the report.

2.1 CORIOLIS TERMS IN 2-D MESO-SCALE EQUATIONS

One of the major tasks undertaken in this contract period was the modification of the HAIFA code to enable one to study the effects of Coriolis forces on the flow over mountain ranges. An outline of the basic theory, previously presented, is repeated here for completeness.

In the 2-D calculations previously reported, lee waves were formed over the mountain in a time interval of about one hour, during which dynamic effects from the Coriolis force were small. (The geostrophic wind used for the unperturbed flow, of course, is strongly influenced by the Coriolis terms.) If the mountain range were more extensive or if the fate of the waves radiated by the mountain were followed to larger distances it is to be expected that larger effects from the Coriolis terms would be realized.

The characteristic distance scale for the Coriolis force is $L_f = u/f$, where u is a typical wind speed and f is the Coriolis parameter (if $u \sim 10$ m/s, we obtain $L_f \sim 100$ km).

When the mountain range is comparable to L_f, an appreciable modification of the gravity waves will result to form a complex system of gravity-inertia waves.

Since the Coriolis force induces a turning of the wind it is necessary to take into account several new factors in the calculations:

(1) the component of the wind parallel to the mountain;

(2) pressure gradients in directions parallel and perpendicular to the mountain must be included to establish geostrophic balance in the unperturbed flow; and

(3) the vertical atmosphere structure is slightly modified to account for the Coriolis contribution to the hydrostatic balance condition.

In the following formulation we attempt to parallel the numerical treatment of the HAIFA code as closely as feasible in order to be able to compare the effects of the Coriolis terms with those pertaining to a non-rotating Earth.

2.1.1 Formulation

The differential equations of the dry atmosphere are formulated in a system of reference fixed to a rotating Earth. As discussed by Thompson[4] we incorporate the centrifugal terms into the definition of the local gravity to obtain

$$\frac{d\vec{U}}{dt} + 2\vec{\Omega} \times \vec{U} = -\frac{1}{\rho} \nabla P - \hat{k}g \quad , \tag{2.1}$$

where $\vec{U}$ is the velocity relative to the Earth's surface, $\vec{\Omega}$ is the rotational velocity of the Earth, P is the pressure, ρ is the density of the atmosphere, g is the local acceleration of gravity which is assumed to act in the vertical direction $\hat{k}$. The time derivative is that evaluated following the fluid motion. The equations of mass and energy conservation are not affected by the Coriolis force.

Neglecting the curvature of the Earth's surface (and the resulting centrifugal terms associated with the relative velocity), Eq. (2.1) can be resolved into components. We choose a Cartesian coordinate system in which the x-axis lies in the surface and forms an angle ϕ with the eastward direction, the y-axis lies in the surface at the same angle ϕ with the northward direction, and the z-axis is perpendicular positive upward. We shall subsequently assume that the x-axis is perpendicular to the 2-D mountain range which is oriented at the angle ϕ with the northward direction (see figure below). Denoting x, y, and z components of the velocity by u, v, w, the component equations are:

5
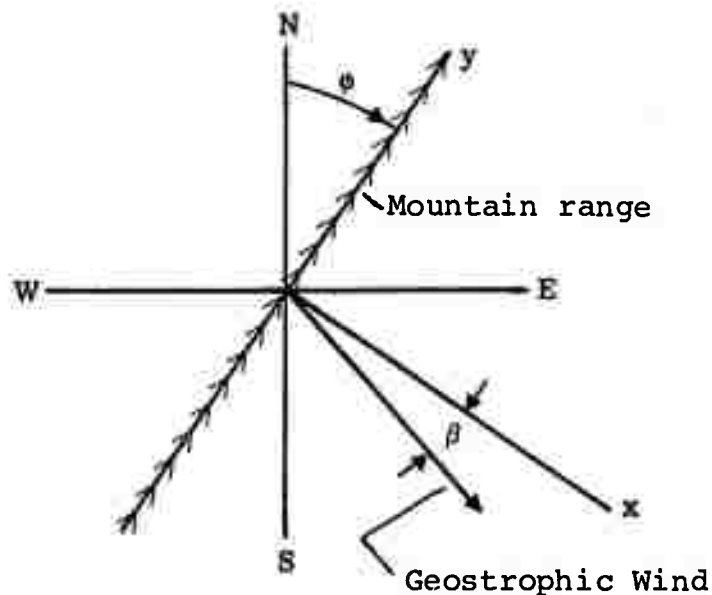
$$\frac{du}{dt} - 2\Omega \sin\theta \, v + 2\Omega \cos\theta \, \cos\phi \, w = - \frac{1}{\rho} \frac{\partial P}{\partial x} \ ,$$

$$\frac{dv}{dt} + 2\Omega \sin\theta \, u - 2\Omega \cos\theta \, \sin\phi \, w = \frac{1}{\rho} \frac{\partial P}{\partial y} \ ,$$

$$\frac{dw}{dt} - 2\Omega \cos\theta \, (u \cos\phi - v \sin\phi) = - \frac{1}{\rho} \frac{\partial P}{\partial z} - g \ , \qquad (2.2)$$

where Ω is the magnitude of the rotational velocity, θ is the latitude of the position, and the time derivatives are those formed following the fluid motion.

In the absence of the mountain varrier we consider the atmosphere to be in geostrophic balance; the motion is unaccelerated, the vertical velocity component w is zero, and the pressure gradients are just balanced by the Coriolis and gravity terms. Denoting the geostrophic state by subscripts g we obtain

$$-2\Omega \sin\theta \, v_g = - \frac{1}{\rho_g} \frac{\partial P_g}{\partial x} \ ,$$

$$2\Omega \sin\theta \, u_g = - \frac{1}{\rho_g} \frac{\partial P_g}{\partial y} \ ,$$

$$-2\Omega \cos\theta \, (u_g \cos\phi - V_g \sin\phi) + g = - \frac{1}{\rho_g} \frac{\partial P_g}{\partial z} \ . \qquad (2.3)$$

Since the velocity of the unperturbed state is taken to be independent of x and y , Eq. (2.3) shows that the pressure at most need depend linearly on x and y .

When the mountain is present the pressure, density and velocity are perturbed from their geostrophic values. It

will be convenient to introduce the deviation P' of the
pressure from the geostrophic value:

$$P' = P - P_g \; .$$ (2.4)

We also introduce the Boussinesq approximation, in which the
departure of density from the geostrophic value is taken into
account only in the gravity term of Eq. (2.3). In all other
terms, we use the geostrophic density:

$$\frac{du}{dt} - 2\Omega \sin\theta\,(v-v_g) + 2\Omega \cos\theta \cos\phi\, w = -\frac{1}{\rho_g}\frac{\partial P'}{\partial x} \; ,$$

$$\frac{dv}{dt} + 2\Omega \sin\theta\,(u-u_g) - 2\Omega \cos\theta \sin\phi\, w = -\frac{1}{\rho_g}\frac{\partial P'}{\partial y} \; ,$$

$$\frac{dw}{dt} - 2\Omega \cos\theta\,[(u-u_g)\cos\phi - (v-v_g)\sin\phi] = -\frac{1}{\rho_g}\frac{\partial P'}{\partial z} + \left(1 - \frac{\rho}{\rho_g}\right) g \; .$$ (2.5)

These equations constitute the Boussinesq approximation for
the equations of motion when the geostrophic flow, assumed
steady and independent of x and y, is perturbed. Clearly,
they are only approximately satisfied in a local region, since
u_g and v_g are not constant on the synoptic scale.

We now consider the special case in which the initial
and boundary equations are independent of the y-coordinate,
corresponding to a uniform but obliquely incident wind en-
countering a two-dimensional ridge, the topography of which
is independent of y. In this case, the initial and bound-
ary conditions and the equations depend only on the coordi-
nates x and z. The resulting 2-D equations derived from
Eq. (2.5) are:

$$\frac{\partial u}{\partial t} + u\frac{\partial u}{\partial x} + w\frac{\partial u}{\partial z} - 2\Omega \sin\theta (v-v_g) + 2\Omega \cos\theta \cos\phi \; w = -\frac{1}{\rho_g}\frac{\partial P'}{\partial x} \quad ,$$

$$\frac{\partial v}{\partial t} + u\frac{\partial v}{\partial x} + w\frac{\partial v}{\partial z} + 2\Omega \sin\theta (u-u_g) - 2\Omega \cos\theta \sin\phi \; w = 0 \quad ,$$

$$\frac{\partial w}{\partial t} + u\frac{\partial w}{\partial x} + w\frac{\partial w}{\partial z} + 2\Omega \cos\theta [(u-u_g)\cos\phi - (v-v_g)\sin\phi] =$$

$$-\frac{1}{\rho_g}\frac{\partial P'}{\partial z} + \left(1 - \frac{\rho}{\rho_g}\right)g \quad . \tag{2.6}$$

Equations (2.6) are to be supplemented with the equations of incompressibility and the temperature equation. The equations are unchanged from those in Ref. 2; they appear in that document as Eqs. (2.3) and (2.10).

There are two major modifications of the equations which have resulted from the treatment of the rotation of the Earth:

(1) The component of the wind parallel to the range influences both the x and z momentum equations through the Coriolis terms. The y momentum component equation is only weakly coupled to the others and may be solved in a similar way to the temperature equation.

(2) Additional terms from the Coriolis force enter the momentum equations giving rise to new terms in the vorticity equation.

2.1.2   Difference Equations

The difference equation formulation corresponding to Eq. (2.6) and supplementary equations can be chosen to parallel that of the HAIFA code. The equation for the y-component of

8

vorticity is obtained by cross-differentiation of the x and z components of the momentum, thereby eliminating the pressure from the equations entirely. The resulting equations are:

$$\frac{\partial \eta}{\partial t} + u\frac{\partial \eta}{\partial x} + w\frac{\partial \eta}{\partial z} - 2\Omega \sin\theta\left(\frac{\partial v}{\partial z} - \frac{\partial v_g}{\partial z}\right) - 2\Omega \cos\theta \sin\phi\frac{\partial v}{\partial x} = \frac{g}{\rho_g} \frac{\partial \rho}{\partial x} \quad ,$$

$$\frac{\partial v}{\partial t} + u\frac{\partial v}{\partial x} + w\frac{\partial v}{\partial z} + 2\Omega \sin\theta (u-u_g) - 2\Omega \cos\theta \sin\phi\, w = 0 \quad , \qquad (2.7$$

where the y-component of vorticity, η, is defined by

$$\eta = \frac{\partial u}{\partial z} - \frac{\partial w}{\partial x} \quad .$$

A quantity, v', is now introduced which is the difference between the y-component of wind velocity and the y-component of the geostrophic wind,

$$v' = v - v_g \quad .$$

The system of equations that HAIFA solves now becomes

$$\nabla^2 \psi = \eta \quad ; \qquad u = \frac{\partial \psi}{\partial z} \quad ; \qquad w = -\frac{\partial \psi}{\partial x} \quad ;$$

$$\frac{\partial T'}{\partial t} + \frac{\partial (uT')}{\partial x} + \frac{\partial (wT')}{\partial z} = -w\frac{\partial T_o}{\partial z} + \Gamma \quad ;$$

$$\frac{\partial \eta}{\partial t} + \frac{\partial (u\eta)}{\partial x} + \frac{\partial (w\eta)}{\partial z} - 2\Omega \sin\theta \frac{\partial v'}{\partial z}$$

$$- 2\Omega \cos\theta \sin\phi \frac{\partial v'}{\partial x} = \frac{g}{\rho_g} \frac{\partial \rho}{\partial x} \quad ;$$

9

$$\frac{\partial v'}{\partial t} + \frac{\partial (uv')}{\partial x} + \frac{\partial (wv')}{\partial z} = - w\frac{\partial v_g}{\partial z} \qquad (2.8)$$

$$- 2\Omega \sin\theta (u-u_g) + 2\Omega \cos\theta \sin\phi \, w = 0 \quad .$$

The difference approximations for the above equations follows that of the basic HAIFA formulation. The time-dependent equations are solved in an explicit two-level formulation. The advection terms are obtained by using a high order conservation scheme in which the two directions are integrated by the splitting technique. Additional terms are all centered in space from quantities available at the current time cycle. The additional equation for v' is similar to the temperature equation in structure. The vorticity equation is modified by gradients in the velocity perturbation. Changes in v' are due to both forcing terms which are the result of the Coriolis force actions on the u- and w-components of velocity and advection of the V_g-component of geostrophic velocity in the vertical direction. Depending on the geostrophic wind structure the advection term could dominate the change in the v' parameter.

2.1.3 Initial Conditions

The initial conditions for HAIFA modified to include Coriolis forces are the same as basic HAIFA except that the angle between the mountain range and the north-south direction and the angle between the geostrophic wind and the mountain range must be specified.

The figure in section 2.1.1 defines the parameters used to describe the orientation of the geostrophic wind and the mountain range. The angles, ϕ and β, are both specified in degrees; ϕ is the angle that the mountain range makes with the

north-south coordinate, and β is the angle the geostrophic wind makes with respect to the direction normal to the mountain range. The x- and y-axis in the code corresponds to the direction along the mountain range and normal to the mountain range, respectively.

The other parameter required in the Coriolis terms is the latitude, θ, which is specified in the usual manner, in degrees from the equator.

The initial geostrophic wind, u_g, is simply the wind which would be present without the mountain. This wind is assumed not to vary in direction to the vertical. Thus, it is similar to the initial u velocity in basic HAIFA except that the wind is not necessarily normal to the mountain. Noting that

$$\vec{u}_g(z) = u(z)\hat{x} + v(z)\hat{y} \qquad (2.9)$$

and referring to the figure above we can calculate the initial u- and v-velocities by

$$u(z) = \cos\beta \ \vec{u}_g(z)$$

$$v(z) = \sin\beta \ \vec{u}_g(z)$$

The gradient of the u_g-velocity in the vertical is simply

$$\frac{\partial u_g}{\partial z} = \sin\beta \ \frac{\partial \vec{u}_g(z)}{\partial z} \qquad (2.10)$$

2.1.4   Test Problem

Several preliminary runs were made using HAIFA with Coriolis forces. The first runs were made with the angular

velocity, Ω, set to zero and with the initial wind perpendicular to the mountains in an attempt to duplicate the double wave problem run with the basic HAIFA code.

After verifying that HAIFA with Coriolis forces duplicates the standard double wave problem, additional runs were made with the angular velocity, Ω, set to its nominal value, and with the wind perpendicular to the mountain range (i.e., $\beta = 0$). The results of this run showed virtually no effects of the Coriolis terms incorporated in HAIFA. This result is not unexpected when we recall that the mountain range in the double wave problem is only 625 meters high and 4500 meters long.

However, problems simulating much larger mountains, for example, the Andes or the Sierras, should be significantly affected by the Coriolis forces, and the resulting lee waves produced would be a system of both inertia and gravity waves. These complex wave systems could appreciably change the drag from what one would expect considering only gravity waves.

The test problems were not continued pending completion of a linear steady state code described in Section 3 of this report. The primary reason for this was the desirability of determining the relationship between steady state and transient results of the vertical flux of horizontal momentum. In particular, the cyclic behavior of the Reynolds stress as a function of time previously reported must be related to the steady state value and further test calculations were delayed in order to attempt to determine this relationship.

2.2   HEURISTIC NUMERICAL MODEL OF TURBULENCE

In incompressible flow, whether laminar or turbulent, the equations of momentum and continuity, along with the boundary and initial conditions, suffice to establish completely the exact fluid motion. If the flow happens to be turbulent, however, the motion involves such small and rapid changes that, although it is in principle determinate, its actual calculation would impose an overwhelming computational burden and, in addition, the detailed initial conditions are not known.

The usual way around this difficulty is to average the equations of momentum and continuity to obtain mean flow quantities which are smooth. This results, of course, in an enormous simplification. Unfortunately, it also involves a significant and irretrievable loss of essential information. Consequently, owing to the presence of the unknown Reynolds stresses which are created by this averaging process, the averaged equations of momentum and continuity do not in themselves comprise a determinate set. Additional relations are required to fix the unknown Reynolds stresses. Equations can also be derived for the fluctuations and for averages of products of them. However, these equations form a coupled system involving ever higher order variances. No first-principles method for terminating this system of equations is known.

A plausible heuristic approach has been developed by Gawain and Pritchett.[5] Since the necessary supplementary relations cannot be established from the original equations by an analytic procedure, Gawain and Pritchett closed the system with the addition of empirical hypotheses. Their philosophy and rationale is quoted below:

"From another viewpoint, it may be stated that the averaged equations of motion show the effect of the Reynolds

stresses upon the mean flow. However, the reciprocal effect of the mean flow upon the Reynolds stresses is lost in the averaging process. Hence some adequate hypothesis must be found for representing this relation, at least approximately."

"For this purpose, a heuristic approach which seems plausible is to postulate a relation between the Reynolds stresses and the mean flow which is analogous to the relation that is known to govern the viscous stresses. The analogue of the ordinary molecular kinematic viscosity is the so-called eddy kinematic viscosity. The problem becomes, therefore, to determine empirically the general law which governs this mean effective eddy viscosity at every space/time point in the flow field."

"The eddy viscosity presumably depends on a number of variables, one of the most important of which is the local kinetic energy of turbulence. Therefore, it becomes necessary to find the space/time distribution of the turbulent energy. Fortunately, the governing energy equation can be deduced rigorously from the original equations of motion. However, the energy equation itself introduces two additional unknowns which can only be approximated in the same heuristic and empirical fashion as the eddy viscosity itself. The additional unknowns are the rate of dissipation of turbulent energy into heat, and the rate of turbulent diffusion of energy."

"Theory and experiment both show that the eddy viscosity, and the dissipation and diffusion functions as well, depend not only on the turbulent energy itself, but also on a local length scale parameter which can be associated with each space/time point in the flow field. Von Karman was perhaps the first to point out how a physically meaningful characteristic length can be defined in terms of local space derivatives of the mean velocity at any point in the flow.

In the present paper, the original approach of von Karman is further developed and refined. It now takes into account not only the velocity derivatives at the designated point itself, but also the values in the general vicinity of the point."

"By employing dimensional analysis, and by applying the available experimental data, we finally obtain three empirical expressions which determine to a reasonable approximation the eddy viscosity, the heat dissipation and the turbulent diffusion, respectively. These expressions also involve the turbulent energy, the local length parameter, and the distance to the nearest fixed wall (if any). Of course, these empirical expressions are amenable to further investigation and development."

"In this way a single consistent and determinate set of equations is established which applies in principle to any incompressible turbulent flow field. Only the boundary conditions differ for each specific application."

2.2.1 Formulation

The formulation of equations as developed by Gawain and Pritchett must be modified for flow of an incompressible fluid to flow of a fluid characterized by the Boussinesq approximation. Starting with the momentum and continuity equations shown below, the derivation of equations follows.

$$\frac{\partial u}{\partial x} + \frac{\partial w}{\partial z} = 0 \qquad \text{(continuity)} \tag{2.11}$$

$$\frac{\partial u}{\partial t} + u\frac{\partial u}{\partial x} + w\frac{\partial u}{\partial z} = \frac{1}{\rho_o}\frac{\partial p}{\partial x} + \nabla \cdot (K_\nu \, \nabla u) \tag{2.12}$$

$$\frac{\partial w}{\partial t} + u\frac{\partial w}{\partial x} + w\frac{\partial w}{\partial z} = -\frac{1}{\rho_o}\frac{\partial p}{\partial z} + \nabla\cdot(K_\nu \, \nabla w) - \frac{\rho}{\rho_o}\,g \tag{2.13}$$

(momentum)

15

Here K_ν is the molecular viscosity. The velocity components, the pressure, and density can be separated into mean and fluctuating parts,

$$u = \overline{u} + u'$$

$$w = \overline{w} + w'$$

$$p = \overline{p} + p'$$

$$\rho = \overline{\rho} + \rho'$$

These are to be inserted into the equations of motion and ensemble averaged. Eqs. (2.) and (2.) give the mean momentum equations.

$$\frac{\partial \overline{u}}{\partial t} + \overline{u}\frac{\partial \overline{u}}{\partial x} + \frac{\partial}{\partial x}(\overline{u'^2}) + \overline{w}\frac{\partial \overline{u}}{\partial z} + \frac{\partial}{\partial z}(\overline{u'w'})$$

$$= -\frac{1}{\rho_0}\frac{\partial \overline{p}}{\partial x} + \nabla \cdot K_\nu \, \nabla \overline{u} \qquad (2.14)$$

and

$$\frac{\partial \overline{w}}{\partial t} + \overline{u}\frac{\partial \overline{w}}{\partial x} + \frac{\partial}{\partial x}(\overline{u'w'}) + \overline{w}\frac{\partial \overline{w}}{\partial z} + \frac{\partial}{\partial z}(\overline{w'^2})$$

$$= -\frac{1}{\rho_0}\frac{\partial \overline{p}}{\partial z} + \nabla \cdot K_\nu \, \nabla \overline{u} + \frac{\rho}{\rho_0} g \qquad (2.15)$$

Following Gawain and Pritchett, the Reynolds stresses are postulated to be related to the strain rates of mean flow through

16

$$-\overline{u_i' u_j'} = -\frac{1}{3}\overline{u_k' u_k'}\delta_{ij} + \varepsilon\left(\frac{\partial \overline{u}_j}{\partial x_i} + \frac{\partial \overline{u}_i}{\partial x_j}\right) \tag{2.16}$$

where $\delta_{ij} = 0$ for $i \neq j$, and $=1$ otherwise; ε is called the eddy kinematic viscosity.

The postulate of Eq. (2.16) provides four necessary relationships,

$$-\overline{u'^2} = -\frac{1}{3}\left(\overline{u'^2} + \overline{v'^2} + \overline{w'^2}\right) + 2\varepsilon\frac{\partial \overline{u}}{\partial x}$$

$$-\overline{u'w'} = \varepsilon\left(\frac{\partial \overline{w}}{\partial x} + \frac{\partial \overline{u}}{\partial z}\right)$$

$$-\overline{w'^2} = -\frac{1}{3}\left(\overline{u'^2} + \overline{v'^2} + \overline{w'^2}\right) + 2\varepsilon\frac{\partial \overline{w}}{\partial z}$$

$$-\overline{w'u'} = -\overline{u'w'} \; . \tag{2.17}$$

Applying the postulate of Eq. (2.16) to Eq. (2.14) and substituting the kinematic pressure

$$\Phi = \overline{p} - \frac{1}{3}\left(\overline{u'^2} + \overline{v'^2} + \overline{w'^2}\right)$$

one has

$$\frac{\partial \overline{u}}{\partial t} + \overline{u}\frac{\partial \overline{u}}{\partial x} + \overline{w}\frac{\partial \overline{u}}{\partial z} = -\frac{1}{\rho_o}\frac{\partial \Phi}{\partial x} + (\varepsilon + K_\nu)\nabla^2\overline{u}$$

$$+ 2\frac{\partial \varepsilon}{\partial x}\frac{\partial \overline{u}}{\partial x} + \frac{\partial \varepsilon}{\partial z}\left(\frac{\partial \overline{w}}{\partial z} + \frac{\partial \overline{u}}{\partial z}\right) \; , \tag{2.18}$$

and for Eq. (2.15) one obtains

17

$$\frac{\partial \overline{w}}{\partial t} + \overline{u}\frac{\partial \overline{w}}{\partial x} + \overline{w}\frac{\partial \overline{w}}{\partial z} = -\frac{1}{\rho_O}\frac{\partial \Phi}{\partial z} + (\varepsilon + K_v)\nabla^2 \overline{w} + \frac{\rho}{\rho_O}g$$

$$+ \frac{\partial \varepsilon}{\partial x}\left(\frac{\partial \overline{w}}{\partial x} + \frac{\partial \overline{u}}{\partial z}\right) + 2\frac{\partial \varepsilon}{\partial z}\frac{\partial \overline{w}}{\partial z} \quad . \tag{2.19}$$

Equations (2.18) and (2.19) are reformulated in terms of the vorticity η and the stream function ψ, which satisfy the relations $\eta = \frac{\partial u}{\partial z} - \frac{\partial w}{\partial x}$ and $\nabla^2 \psi = \eta$. The vorticity equation then has the form

$$\frac{D\eta}{Dt} = (\varepsilon + K_v)\nabla^2 \eta - \frac{g}{\rho_O}\frac{\partial \rho}{\partial x} + \left(\frac{\partial^2 \varepsilon}{\partial z^2} - \frac{\partial^2 \varepsilon}{\partial x^2}\right)\left(\frac{\partial^2 \psi}{\partial z^2} - \frac{\partial^2 \psi}{\partial x^2}\right)$$

$$+ 4\frac{\partial^2 \varepsilon}{\partial x \partial z}\frac{\partial^2 \psi}{\partial x \partial z} + \frac{\partial \varepsilon}{\partial z}\frac{\partial \eta}{\partial z} + \frac{\partial \varepsilon}{\partial x}\frac{\partial \eta}{\partial x} + \frac{\partial \varepsilon}{\partial x}\left[\nabla^2 \frac{\partial \psi}{\partial z}\right]$$

$$+ \frac{\partial \varepsilon}{\partial z}\left[\nabla^2 \frac{\partial \psi}{\partial x}\right] \quad . \tag{2.20}$$

The energy equation is formed by multiplying the momentum equation by velocity. As before, the resultant equation is rewritten with mean and fluctuating terms, and the averaged energy equation is subtracted to yield the turbulent energy equation. It is convenient to express the result in Cartesian tensor notation,

$$\frac{\partial}{\partial t}\left(\frac{\overline{u_j' u_j'}}{2}\right) + \frac{\partial}{\partial x_k}\left(\overline{u}_k \frac{\overline{u_j' u_j'}}{2}\right) = - \frac{\overline{u_j' u_k'}}{2}\left(\frac{\partial \overline{u}_j}{\partial x_k} + \frac{\partial \overline{u}_k}{\partial x_j}\right)$$

$$- \frac{K_\nu}{2}\overline{\left(\frac{\partial u_j'}{\partial x_k} + \frac{\partial u_k'}{\partial x_j}\right)^2}$$

$$- \frac{\partial}{\partial x_k}\left[\overline{u_k'\left(\frac{u_j' u_j'}{2} + \phi'\right)}\right]$$

$$+ K_\nu \frac{\partial}{\partial x_k}\left[\frac{\partial}{\partial x_k}\left(\frac{\overline{u_j' u_j'}}{2}\right) + \frac{\partial}{\partial x_j}\overline{(u_j' u_k')}\right] \quad (2.21)$$

ϕ' is the perturbation of kinematic pressure, pressure/density. The terms on the right-hand side of the energy equation represent, respectively, turbulent energy production corresponding to the work done by the mean flow against the Reynolds stresses, dissipation of turbulent energy to heat, turbulent diffusion of energy, and molecular diffusion. For problems at high Reynolds number the last term is vanishingly small; it will be ignored hereafter.

Denoting by E the turbulent kinetic energy,

$$E = \frac{\overline{u_j' u_j'}}{2} = \frac{1}{2}\left(\overline{u'^2} + \overline{v'^2} + \overline{w'^2}\right) \quad (2.22)$$

and applying the postulate of Eq. (2.16) to Eq. (2.21), the turbulent energy equation becomes

$$\frac{\partial E}{\partial t} + \frac{\partial}{\partial x_k}(\overline{u}_k E) = \frac{\varepsilon}{2}\left(\frac{\partial \overline{u}_j}{\partial x_k} + \frac{\partial \overline{u}_k}{\partial z_j}\right)^2 - \frac{K_\nu}{2}\overline{\left(\frac{\partial u_j'}{\partial x_k} + \frac{\partial u_k'}{\partial x_j}\right)^2}$$

$$- \frac{\partial}{\partial x_k}\left[\overline{u_k'\left(\frac{u_j' u_j'}{2} + \phi'\right)}\right] \quad . \quad (2.23)$$

19

At this point, neither the vorticity equation nor the turbulent energy equation are closed. It should also be noted here that the development of the turbulent energy equation (2.23) as described by Gawain and Pritchett neglects the temperature stratification term $- \overline{\rho' u_i'} \frac{g}{\rho_o}$ on the right-hand side of the

equation, which for our applications can be a significant effect. For the initial development of the turbulent scheme, however, this term was also ignored as it requires that the fluctuating density component be described in some heuristic and empirical fashion, i.e., that $\overline{\rho' u_i'} \equiv \varepsilon' \frac{\partial \rho}{\partial z}$. The value of ε' remains to

be determined from experimental data in much the same manner as the kinematic eddy viscosity ε itself needs to be determined. As work on the turbulence scheme itself progresses, investigations of this term will be made through literature searches in order to incorporate its effect in mountain wave problems.

To enable the kinematic eddy viscosity ε to be determined, Gawain and Pritchett postulated the formulation

$$\varepsilon = \alpha \lambda \sqrt{2E} \ . \tag{2.24}$$

where α is a dimensionless, slowly varying universal function not predictable from theory, but estimable from experimental data and λ is a length scale of turbulence in the vicinity of a point. Thus, there is a λ associated with every point of the flow field. It was hypothesized that the definition of λ in the vicinity of an arbitrary point should depend only on the mean flow conditions in a finite region surrounding that point. By use of a weighting function which falls off rapidly with increasing separation, dependence on all points in the flow field can be avoided.

The weighting function chosen was

$$
\hat{w}(\vec{x}) = \frac{\exp\left(-\frac{\vec{\Delta x} \cdot \vec{\Delta x}}{\lambda^2(\vec{x})}\right)}{\displaystyle\int_{\substack{\text{all} \\ \text{space}}} \exp\left(-\frac{\vec{\Delta x} \cdot \vec{\Delta x}}{\lambda^2(\vec{x})}\right)} \quad .
\tag{2.25}
$$

A strain rate tensor was defined,

$$
\Gamma_{ij} = \frac{\partial \bar{u}}{\partial z} + \frac{\partial \bar{w}}{\partial x} \quad .
\tag{2.26}
$$

Note that $\Gamma_{ii} = 0$ for the incompressible case from continuity. Next a generalized strain rate, Ω^2, an a generalized strain rate gradient, Ω'^2, were defined as follows:

$$
\Omega^2 = \frac{1}{2} \Gamma_{ij}\Gamma_{ij}
\tag{2.27}
$$

$$
\Omega'^2 = \left(\frac{\partial \Omega}{\partial x_i}\right) \left(\frac{\partial \Omega}{\partial x_i}\right)
\tag{2.28}
$$

It was also found useful to define

$$
(\Omega\Omega')^2 = \frac{1}{4} \left(\frac{\partial \Omega^2}{\partial x_i}\right) \left(\frac{\partial \Omega^2}{\partial x_i}\right)
\tag{2.29}
$$

λ^2 can be defined in terms of Ω^2 and $(\Omega\Omega')^2$:

$$
\lambda^2(\vec{x}) = I^2(\vec{x})/J^2(\vec{x})
\tag{2.30}
$$

where

21

$$I^2(\vec{x}) = \int_{\substack{\text{all} \\ \text{space}}} \hat{w}(\vec{x},\vec{x}')\,\Omega^4(\vec{x})\,dv' \qquad (2.31)$$

$$J^2(\vec{x}) = \int_{\substack{\text{all} \\ \text{space}}} \hat{w}(\vec{x},\vec{x}')\,(\Omega\Omega'(\vec{x}))^2\,dv' \qquad (2.32)$$

and

$$\hat{w}(\vec{x},\vec{x}') = \frac{\exp\left(-\dfrac{(\vec{x}-\vec{x}')\cdot(\vec{x}-\vec{x}')}{\lambda^2(\vec{x})}\right)}{\displaystyle\int_{\substack{\text{all} \\ \text{space}}} \exp\left(-\dfrac{(\vec{x}-\vec{x}')\cdot(\vec{x}-\vec{x}')}{\lambda^2(\vec{x})}\right)} \qquad (2.33)$$

The last term in the turbulent energy equation (Eq. 2.23) is not in a form amenable to calculation. It was postulated to be expressible in the form

$$\overline{u_k'\left(\frac{u_j'u_j'}{2} + \phi\right)} = -\gamma\varepsilon\left(\frac{\partial E}{\partial x_k}\right) \qquad (2.34)$$

Dimensional considerations suggested to Gawain and Pritchett that the dissipation of turbulent energy into heat could be expressed in the form

$$\dot{E}_H = \frac{K_\nu}{2}\overline{\left(\frac{\partial u_j}{\partial x_i} + \frac{\partial u_i}{\partial x_j}\right)^2} = \frac{K_\nu(2E)}{\lambda_D^2} \qquad (2.35)$$

which amounts to a definition of a dissipation length λ_D. To define λ_D, Gawain and Pritchett turned to the results of experimental studies at high Reynolds number, where heat dissipation effect tended to become independent of Reynolds number. Two lengths L_1 and L_2 were defined,

$$L_1^2 = \frac{K_\nu}{2E} \tag{2.36}$$

$$L_2^2 = \frac{2E}{J} \tag{2.37}$$

and the relation

$$\frac{L_1 L_2}{\lambda_D^2} = \beta \tag{2.38}$$

was postulated. The energy dissipation term becomes

$$\dot{E}_H = \beta (2E)^{7/6} J^{1/3} . \tag{2.39}$$

The complete turbulent energy equation, including heuristic substitutes, is then written as follows:

$$\frac{\partial E}{\partial t} + \frac{\partial}{\partial x} (\bar{u}E) + \frac{\partial}{\partial z} (\bar{w}E) = \alpha\lambda \sqrt{2E} \, \Omega^2 - \beta (2E)^{7/6} J^{1/3}$$

$$+ \frac{\partial}{\partial x} \left(\alpha\gamma\lambda \sqrt{2E} \frac{\partial E}{\partial x} \right) + \frac{\partial}{\partial z} \left(\alpha\gamma\lambda \sqrt{2E} \frac{\partial E}{\partial z} \right) \tag{2.40}$$

To complete the formulation, it is necessary to specify the computation of the three dimensionless coefficients, α, β, and γ. Gawain and Pritchett used the following expressions, based on experimental data:

$$\alpha = 0.065 \{1 + \exp[-(y/\lambda-1)^2]\}$$

$$1/\beta = 3.7 \{1 + \exp[-(y/\lambda-1)^2]\} \tag{2.41}$$

$$\gamma = 1.4 - 0.4 \exp[-(y/\lambda-1)^2]$$

where y is the distance to the nearest fixed boundary.

Thus, the modifications to the usual incompressible formulation required to incorporate the heuristic turbulence scheme of Gawain and Pritchett are

(1) the revised vorticity equation [Eq. (2.20)], and

(2) the inclusion of an heuristic equation for turbulent energy (Eq. 2.21).

These modifications have been carried out, and the results are detailed in the following sections.

2.2.2 Numerics

The modifications to the vorticity equation were coded and incorporated using typical finite difference formulations, and treating the sum $(K_\nu + \varepsilon)$ as a total diffusion term.

The solution of the turbulent energy equation was carried out in a new code subpackage, subroutine TURB. The flow logic of this subroutine is displayed in Figure 2.1.

The turbulent energy code was debugged exercised on some test problems. It became apparent that a major calculational burden was imposed by the development of the I^2 and J^2 terms, and the associated weighting terms required for each grid point. This is despite the fact that the potentially expensive "exponential" evaluations can be reduced to a one pass computation, with tabular evaluation thereafter each cycle. The cost in computer time to simply form all the I^2 and J^2 terms, when only the nearest 36 cells are used in the weights, is about 12 seconds. The cost of a complete calculational cycle for the turbulent formulation approached 7 seconds in this case, nearly 10 times the cost of the standard HAIFA solution. In one test, the problem characteristics were such that the weights did not fall off sufficiently rapidly, and it was required to include

24
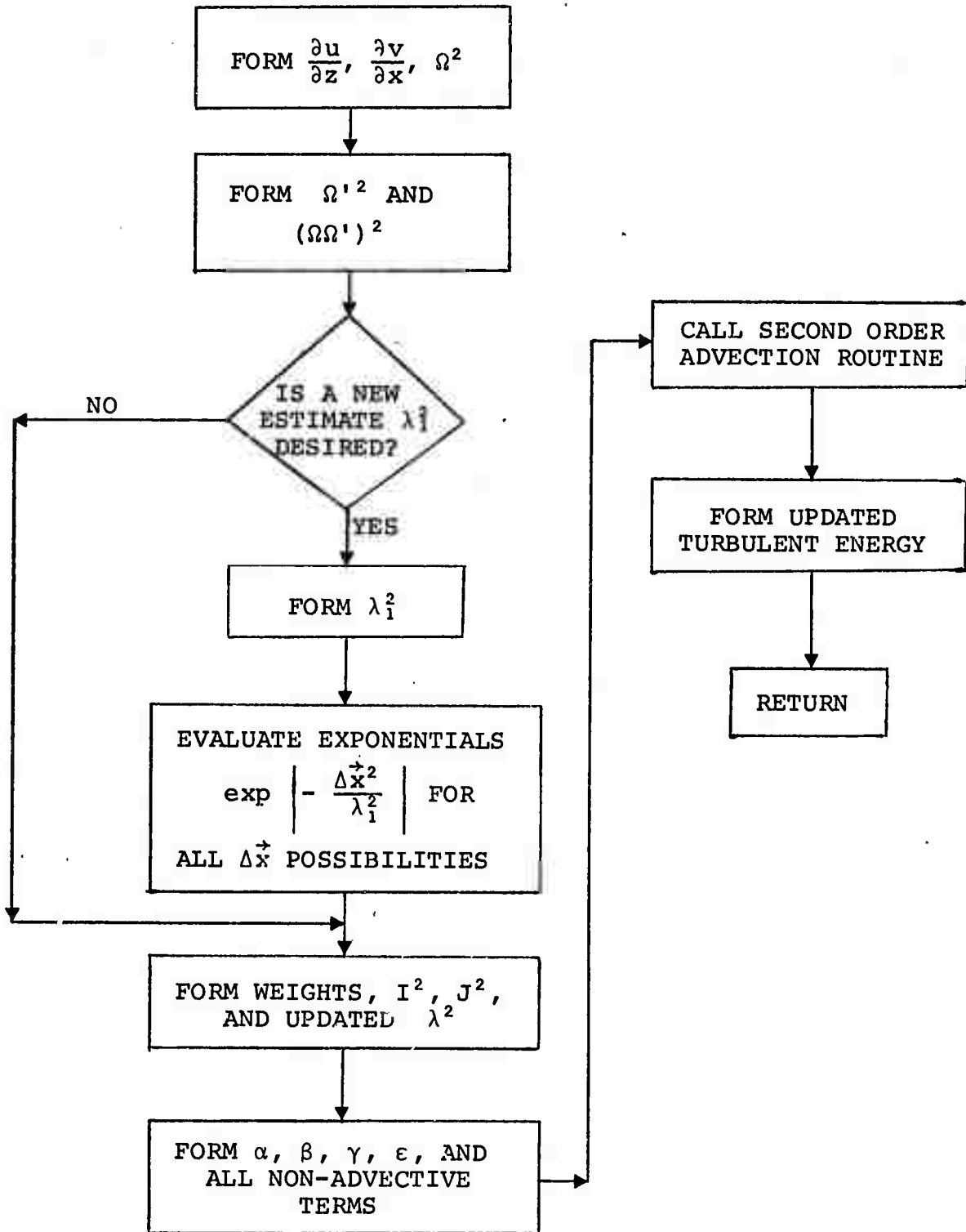
SUBROUTINE TURB

Figure 2.1 — Flow Logic for Subroutine TURB

the entire grid in the calculation of the weights. The computer required 55 seconds each cycle to form I^2 and J^2 in this case.

Because of the great expense involved in carrying out the numerical solution of the turbulence equations, the approach was not pursued beyond this point. It is expected, however, that some effort will be committed during the next year, to the modification of the present turbulence scheme to speed up the computational time over that obtained in our first efforts. Only then, will it be practical to attempt calculation of the mountain wave problem with turbulence.

3. LINEAR STEADY STATE CODE DEVELOPMENT

The calculation of the vertical flux of horizontal momentum (wave drag) using the HAIFA codes as described previously[1,2] has led to results which are cyclic with time. These results, because of their behavior, are not well understood and thus have not been parameterized. In order to more fully understand the transient results and to aid in developing an initial parameterization for use in the RAND global circulation model (GCM), a linear steady state numerical model of gravity waves was developed. It is important to note that both the motion of the flow field and the obstacle placed in the stream must be small for the linear code to be valid. Some of the problems calculated previously using the HAIFA code do fall in this category and it was felt that detailed comparisons could be made with reported results to aid in the accomplishment of the above goals.

The code description, some results of the code and a parameterization of some of the linear steady state results are described in this chapter. Comparisons between the transient results of HAIFA and the steady state results are also made and discussed although further work in this is required before the transient results are understood well enough to parameterize for use in the GCM.

3.1   LINEAR STEADY STATE ANALYSIS

Bretherton[3] and Danielsen and Bleck,[6] among others, have published linear steady state analyses on the calculation of momentum transport by gravity waves. After an examination of both procedures, the analysis of Bretherton was chosen as the basis of the numerical model to be developed at Systems, Science and Software. The primary reason for the selection was Bretherton had extended his analysis to three dimensions and arbitrary topography while the Danielsen and Bleck model was more limited in scope. The analysis is briefly outlined below. The reader is referred to the referenced papers for a more complete discussion of the model.

Small perturbations to a stratified shear flow may be analyzed in terms of a single Fourier component of vertical velocity

$$w(x,z) = R \; \hat{w}(k,z)e^{ikx} \quad ,$$

where k is the wave number and R indicates the real part of the complex vertical velocity $w(x,z)$. Assuming the motion to be steady, invisid and adiabatic, making the Boussinesq approximation and neglecting the Earth's rotation, $\hat{w}$ satisfies an equation

$$\frac{d^2\hat{w}}{dz^2} + \left\{ l^2(z) - k^2 \right\}\hat{w} = 0 \tag{3.1}$$

which is known as Scorer's equation.[7] The parameter l, sometimes referred to as Scorers parameter or number, is

28

$$1^2 = \frac{N^2(z)}{u^2(z)} - \frac{1}{u(z)} \frac{d^2 u(z)}{dz^2} \tag{3.2}$$

where N is the Brunt-Vaisala frequency. Eliassen and Palm[8] showed that the Reynolds stress or wave drag associated with this component satisfies the equation

$$\frac{d}{dz}(\rho \overline{uw}) = \frac{d}{dz}\left\{\frac{\rho}{zik}\left(\frac{d\hat{w}^*}{dz}\hat{w} - \frac{d\hat{w}}{dz}\hat{w}^*\right)\right\} = 0 \quad, \tag{3.3}$$

where ρ is the mean air density, and $\hat{w}^*$ denotes the complex conjugate of $\hat{w}$.

The equations above are solved subject to boundary conditions at the lower surface and at the top of the atmosphere. The lower boundary condition is based upon a Fourier transformation of the actual topography of the region under study. For the upper boundary condition, Bretherton divides the problem into two separate parts and treats each part separately. The drag associated with waves which are assumed to be propagating upwards in the atosphere above the arbitrary height of the numerical grid (H) are calculated separately from those associated with waves which are trapped with the computational atmospheric grid.

The first boundary condition

$$\frac{d\hat{w}}{dz} = + i\sqrt{1^2 - k^2} \, \hat{w} \, [\text{sgn. } U] \qquad \text{at} \quad z = H \tag{3.4}$$

where U is the horizontal free stream velocity, is applied when $k^2 < 1^2(H)$ and implies only upward propagating waves above $Z=H$. The second boundary condition,

29

$$\frac{d\hat{w}}{dz} = - \sqrt{k^2 - l^2} \; \hat{w} \qquad \text{at} \quad Z = H \qquad (3.5)$$

is applied if $k^2 \geq l^2(H)$ and implies that, should the basic state of the atmosphere be imagined to continue upwards to infinity with $l^2 = l^2(H)$, the total perturbation energy in this wave number would be finite. The solution to this second mode (trapped waves) will be discussed in more detail after presenting the more general case for the continuous drag calculation.

The solution of Eq. (3.3) for the Reynolds stress is accomplished in the following manner:

(1) The actual surface topography is Fourier analyzed to obtain the wave number dependence of the lower boundary condition.

The complex Fourier transform is defined by

$$\hat{h}(k) = \frac{1}{2\pi} \int_0^X h(x) \; e^{-ikx} \; dx \qquad (3.6)$$

where $h(x)$ is the ground level height of the position x. A spectrum function is defined as

$$A(k) = \frac{2\pi}{X} \hat{h}^*\hat{h} \qquad (3.7)$$

where X is the maximum grid length and $\hat{h}^*$ is the complex conjugate of $\hat{h}$.

(2) The equation for the complex velocity w, Eq. (3.1), is solved subject to the upper boundary condition, Eq. (3.4). The value of H at which this boundary condition is applied is somewhat arbitrary and its effect is investigated in test problems, the results of which are presented later in this section.

From the results of the integration, a parameter $F(k)$, independent of surface topography, may be computed as

$$F(k) = \frac{\frac{1}{2i}\left\{\frac{d\hat{w}}{dz}\hat{w}^*(z) - \frac{d\hat{w}^*}{dz}\hat{w}(z)\right\}}{\hat{w}^*(0)\,\hat{w}(0)} \; . \tag{3.8}$$

$F(k)$, which is independent of height, has the property that it vanishes if $1^2(H) < k^2$. To obtain the entire Reynolds stress, we add the effects all possible wave numbers, with excitation amplitudes determined from

$$\hat{w}(o) = ik\, U\hat{h} \; . \tag{3.9}$$

The total Reynolds stress from Eq. (3.3) is then

$$\rho\overline{uw} = 2\rho(0)\, U^2(0) \int_{o}^{\ell(H)} k\, A(k)\, F(k)\, dk \tag{3.10}$$

where $\rho\overline{uw}$ = Reynolds stress, $U(0)$ is the free stream horizontal velocity at the surface (lower) boundary, and $\rho(0)$ is the fluid density at the lower boundary. It may happen for a range of values $k_c < k \le 1(H)$, that $F(k)$ is extremely close to zero except for very narrow wave number intervals within which $F(k)$ becomes large. These correspond to

31

trapped modes with a very slight upwards energy leak. Although in principle $F(k)$ is still a continuous function of k, in practice it would be very inefficient to compute it numerically from Eq. (3.10); the narrow bands where $F(k)$ differs appreciably from zero are more efficiently treated analytically. Consequently, the upper limit of the integral in Eq. (3.10) is reduced to k_c (defined arbitrarily as the point where $F(k)$ approaches zero) and the trapped wave contributions are added analytically.

The trapped wave analysis outlined in Bretherton gives for the Reynolds stress

$$\rho\overline{uw} = 2\rho(0) \ U^2(0) \sum_i \frac{\pi}{2} \frac{\left|\frac{d\hat{w}_i}{dz}(0)\right|^2}{\int_0^H \left|\hat{w}_i(z)\right|^2 dz} A(k_i) \qquad (3.11)$$

where the subscript i is the _ith_ wave number greater than k_c but less than $\ell(H)$ for which $w(0) = 0$. The w_i is the solution of Eq. (3.1) with the boundary condition specified by Eq. (3.4).

As noted, for $k > \ell(H)$, $F(k)$ is zero. However, eigensolutions satisfying Eq. (3.5) with $\hat{w} = 0$ at the ground may exist; in this case the lower boundary condition, Eq. (3.9), cannot be satisfied. In this case, $F(k)$ is indeterminate. The solutions of Eq. (3.1) subject to the upper boundary condition specified in Eq. (3.5) are found and the drag is calculated using Eq. (3.11) for each wave number for which $\hat{w}(0) = 0$.

3.1.1 Method of Numerical Solution

The basic scheme used in the solution for the Reynolds stresses associated with linear steady state gravity waves is shown in Figure 3.1.1. The integrals for the Reynolds stresses are calculated using the Gaussian quadrature method while the solution for the complex velocity at a given k value is found using a Glauz-Adams integration routine, a modification of the Adams-Moulton predictor-corrector method. [9]

3.1.2 Test Problems

The linear steady state code is general enough to accept any temperature stratification and horizontal velocity profile as input. However, in order to compare with previous work, the problems described herein have constant atmospheric lapse rates and exponential velocity profiles described by $U_o e^{UEXP*Z}$ where U_o and UEXP are constants for each problem. In this way, transient results of problems previously calculated using HAIFA would be compared with the steady state results. In particular, the two wave and single wave calculations used as test problems[1,2] which were checked using the analysis of Palm and Foldvik,[10] could be compared with the results of this new code.

A matrix of problems was run varying the atmospheric stability and the exponential velocity coefficient, using a rectangular mountain 625 meters high and 4.5 km long. H was arbitrarily selected as 12.0 km, roughly corresponding to the grid height used in the HAIFA calculations. The effect of this height on the results is discussed later in this section. The results arising from each calculation are (1) the continuous drag, (2) the drag associated with each trapped wave, (3) the trapped wave numbers (wave length), and

33

INPUT DATA

CALCULATE SCORER PARAMETER

SOLVE FOR COMPLEX VELOCITY
AT INITIAL K VALUE
LESS THAN $\ell(H)$.
SOLVE FOR A(k), F(k).

$F(k) < 10^{-3}$ — YES / NO

$K < \ell(H)$ — YES

UPDATE K

1) INTEGRATE FOR REYNOLDS
STRESS-CONTINUOUS
2) DEFINE $K_C < \ell(H)$

BEGIN SEARCH FOR
TRAPPED WAVES
$K_C < K < \ell(H)$

UPDATE K

$K < \ell(H)$ — NO / YES

1) SOLVE FOR $\hat{w}(0)$
FROM EQS. (3.1)
AND (3.4)
2) SIGN $\hat{w}(0)$
CHANGE — NO / YES

SEARCH BETWEEN LAST TWO
K VALUES FOR
$|\hat{w}(0)| < 10^{-4}$
FROM EQ. (3.1) SUBJECT
TO B.C. in EQ. (3.4)

SOLVE FOR A(k), F(k)

INTEGRATE REYNOLDS STRESS
FOR TRAPPED WAVE

$K_C < K < \ell(H)$ — YES / NO

SOLVE FOR w(0)
FROM EQ. (3.1)
SUBJECT TO B.C.
IN EQ. (3.5)

UPDATE K

SIGN w(0) CHANGE
FOR LAST TWO
VALUES OF K

SEARCH BETWEEN LAST
TWO K VALUES FOR
$|\hat{w}(0)| < 10^{-4}$ FROM
EQS. (3.1) AND (3.5)

UPDATE K

$K > KMAX$ — NO / YES

SOLVE FOR
w(0) WITH
EQS. (3.1)
AND (3.5)

PRINT, EXIT

Figure 3.1.1 — Flow chart for linear steady state code

34

(4) the complex velocity perturbations as a function of height in the atmosphere. While it is possible to compare the wave lengths from these calculations with those of Palm and Foldvik, no direct comparison is available of the drag values. The trapped wavenumbers are tabulated in Table 3.1, as a function of the exponential velocity coefficient UEXP and T', the atmospheric lapse rate divided by Γ, the adiabatic lapse of the atmosphere (0.01 °C/m).

In Figures 3.1.2 and 3.1.3, the real part of the velocity perturbation as a function of altitude is shown for two problems. The first is the two-wave problem resulting from T'/Γ = 0.5 and UEXP = 0.795 10^{-4}. The second is a problem having three waves defined by the velocity profile U = U_oEXP (1×10^{-4}*Z) and an atmospheric lapse rate of 0.002 °C/meter.

The drag associated with each wave number denoted in Table 3.1 multiplied by the wavenumber is presented in Table 3.2 as a function of UEXP and T'. The general trend of the results indicates larger drag values as (1) the lapse rate decreases compared to the adiabatic lapse rate and (2) the velocity profile approaches a uniform value (UEXP = 0). The stronger effect appears to be associated with the lapse rate. Continuous drag values occur only at low values of the velocity exponential coefficient.

The two wave problem, described previously, was computed with a grid height (H) of both 12 km and 15 km. The drag associated with the longer wave length (K = 0.1475) decreased from 2.91 dynes/cm² to 2.62 dynes/cm². The wave number itself also changed by approximately 2.5 percent while the shorter wave and its associated drag were identical in both cases.

TABLE 3.1

WAVENUMBERS (K) OF TRAPPED WAVES
AS A FUNCTION OF
LAPSE RATE AND WIND PROFILE

UEXP*10^4* (1/m)	T'/Γ**	K_1 (1/km)	K_2 (1/km)	K_3 (1/km)
0.5	0.1	1.421	1.2037	.1.0289
1.5	0.1	1.0895	0.6331	0.2673
2.5	0.1	0.8146	0.0748	
3.0	0.1	0.6787		
3.5	0.1	0.5354		
1.5	0.2	1.0074	0.5624	
1.795	0.2	0.9246	0.4142	
1.0	0.25	1.1140	0.7842	0.5442
2.0	0.25	0.8261	0.2661	
3.0	0.25	0.5522		
4.0	0.25	0.2265		
0.5	0.40	1.1450	0.9581	
1.0	0.40	0.9725	0.6610	
1.795	0.40	0.7447	0.250	
3.5	0.40	0.2392		
1.0	0.50	0.8679	0.5701	
1.795	0.50	0.6431	0.1475	
2.0	0.50	0.5875		
3.0	0.50	0.3688		
1.0	0.75	0.5475		
2.0	0.75	0.2638		
0.5	0.90	0.4138		
1.5	0.90	0.1072		

Mountain height = 625 meters   Mountain length = 4.5 km

*$U = U_o \exp[UEXP*Z]$ **$\Gamma = 0.01$ °C/m
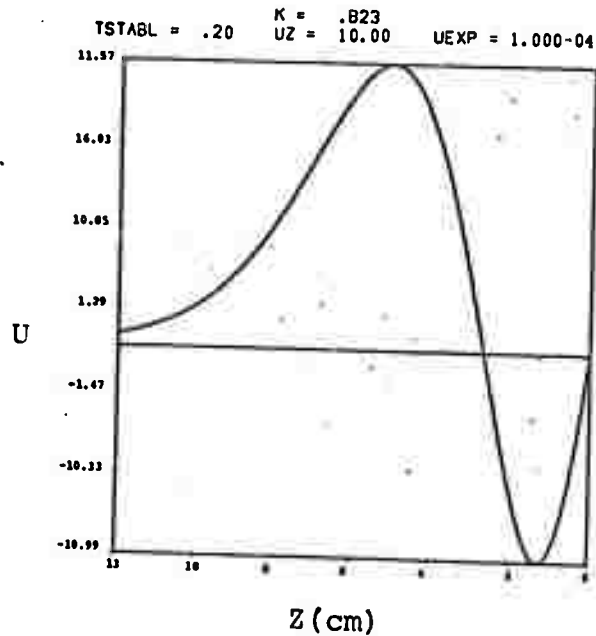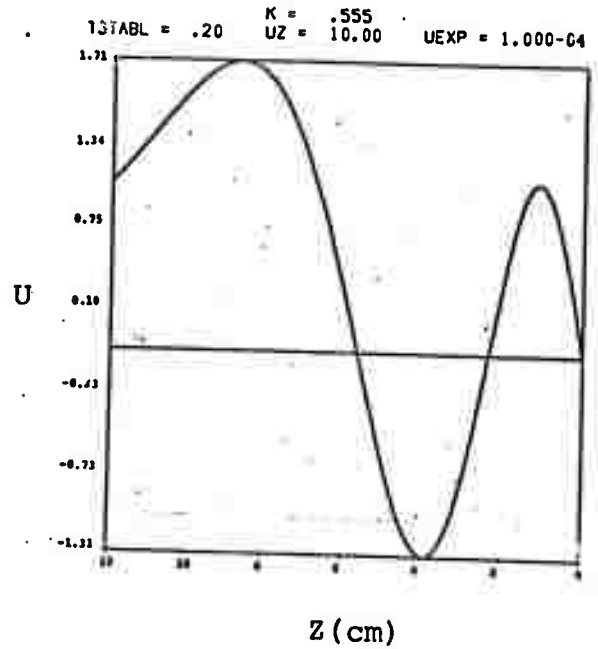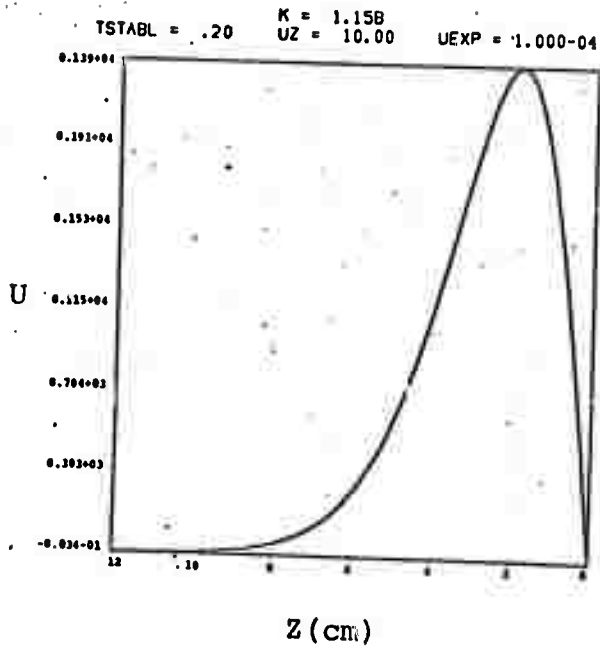
Figure 3.1.2 — Horizontal Velocity Perturbation as a
Function of Wind Profile and Lapse Rate

37
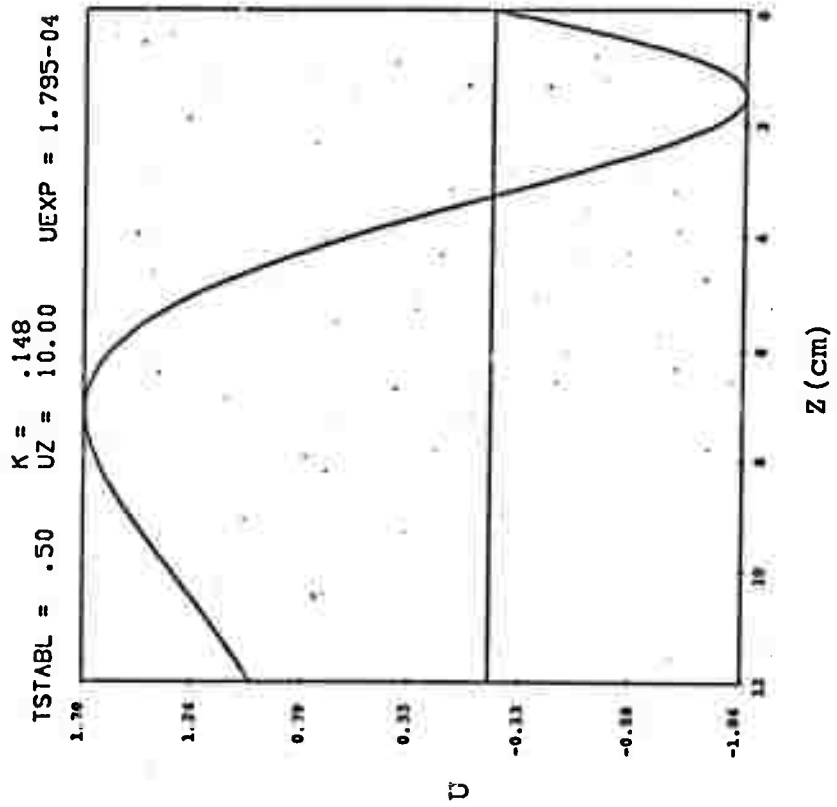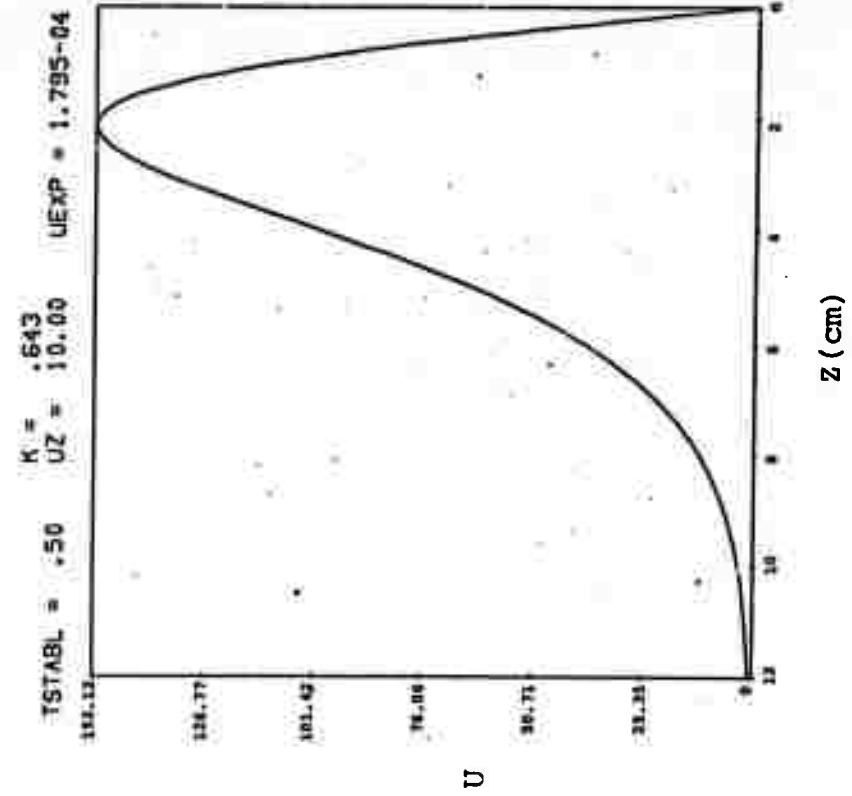
Figure 3.1.3 — Horizontal Velocity Perturbation as a Function of Wind Profile and Lapse Rate

TABLE 3.2

DRAG (K) AS A FUNCTION OF LAPSE RATE, WIND PROFILE, AND WAVE NUMBER

UEXP	T'/Γ	K$_1$*DRAG(K$_1$)	K$_2$*DRAG(K$_2$) (dynes/cm² × km)	K$_3$*DRAG(K$_3$)
0.5	0.1	0.0047	0.20	0.601
1.5	0.1	1.407	3.132	1.097
2.5	0.1	5.354	0.312	
3.0	0.1	7.0		
3.5	0.1	7.505		
1.5	0.2	1.91	2.709	
1.795	0.2	2.941	2.34	
1.0	0.25	0.736	1.879	1.60
2.0	0.25	3.806	1.373	
3.0	0.25	5.826		
4.0	0.25	2.558		
0.5	0.40	0.249	0.578	
1.0	0.40	1.213	1.673	
1.795	0.40	3.241	0.982	
3.5	0.40	2.13		
1.0	0.50	1.425	1.399	
1.795	0.50	2.963	0.430	
2.0	0.50	3.17		
3.0	0.50	2.91		
1.0	0.75	0.957		
2.0	0.75	0.791		
0.5	0.90	0.249	0.166	
1.5	0.90	0.0	0.0875	

3.1.2.1 <u>Scaling of the Results</u> — The drag values calculated from the linear steady state mathematical model may be separated into a continuous value and a value associated with each trapped wave (or angle wave number k). Since the topography spectrum enters as a multiplicative factor in the drag calculation, the drag values in the tables may be applied to any topography by multiplying them by the ratio of the A(k) for the new topography data to A(k) from the existing runs. For rectangular obstacles the scaling may be found as follows:

$$A(k) = \frac{2\pi}{X} \, \hat{h} * \hat{h} \tag{3.12}$$

where

$$h = \frac{1}{2\pi} \int_{0}^{X} h(x) \, e^{-ikx} \, dx \tag{3.13}$$

h(x) corresponds to a rectangular mountain for which the height, h, is assumed constant over a given region x_1 to x_2 and zero elsewhere in the grid.

X is the grid length

$$h = \frac{h}{2\pi} \int_{x_1}^{x_2} [\cos kx - i \sin kx] dx$$

$$= \frac{h}{2\pi k} [\sin kx_2 - \sin kx_1 + i(\cos kx_2 - \cos kx_1)] \tag{3.14}$$

$$\hat{h} * = \frac{h}{2\pi k} [\sin kx_2 - \sin kx_1 - i(\cos kx_2 - \cos kx_1)] \tag{3.15}$$

$$A(k) = \frac{h^2}{X2\pi k^2} [(\sin kx_2 - \sin kx_1)^2 + (\cos kx_2 - \cos kx_1)^2] \tag{3.16}$$

40

Thus, we note that for rectangular mountain, the drag for
any single wave number is proportional to the height squared
and to the mountain length in a more complicated function of
the square of the sum of sines and cosines. The formula can
be further simplified by noting that $x_2 - x_1 = L$ where L
is the mountain length. Making this substitution, $A(k) =
(h^2/X\pi k^2)(1-coskL)$.

The results of the calculations have been parameterized
so that (1) the primary and secondary wave numbers may be
found as a function of UEXP and T'/Γ and (2) the drag associ-
ated with each wave may be calculated from the same two param-
eters. Figures 3.1.4 and 3.1.5 present the wave number cal-
culations and contours selected to represent the results. The
equation for k_1 (the primary wave number) was found to be

$$k_1 = -0.328[(UEXP \times 10^4) + 4(T'/\Gamma)] + 1.78 \qquad (1/km) \qquad (3.17)$$

and k_2 (the secondary wave number) as

$$k_2 = -0.431[(UEXP \times 10^4) + 2(T'/\Gamma)] + 1.48 \qquad (1/km) \ . \qquad (3.18)$$

While some of the cases calculated showed the presence of a
third wave, an insufficient number of points were available
to parameterize the results. It is important to point out
that the above equations may be improved upon as more data
from the calculations become available. Also, it was deter-
mined that in general a negative value of k_1 or k_2 indicates
no wave is present in that region.

The $k_1(Drag(k_1)/A(k_1))$ and $k_2(Drag(k_2)/A(k_2))$ are
shown in Figures 3.1.6 and 3.1.7. These values were also
parameterized as functions of UEXP and T'/Γ and can be repre-
sented by the equations:

41
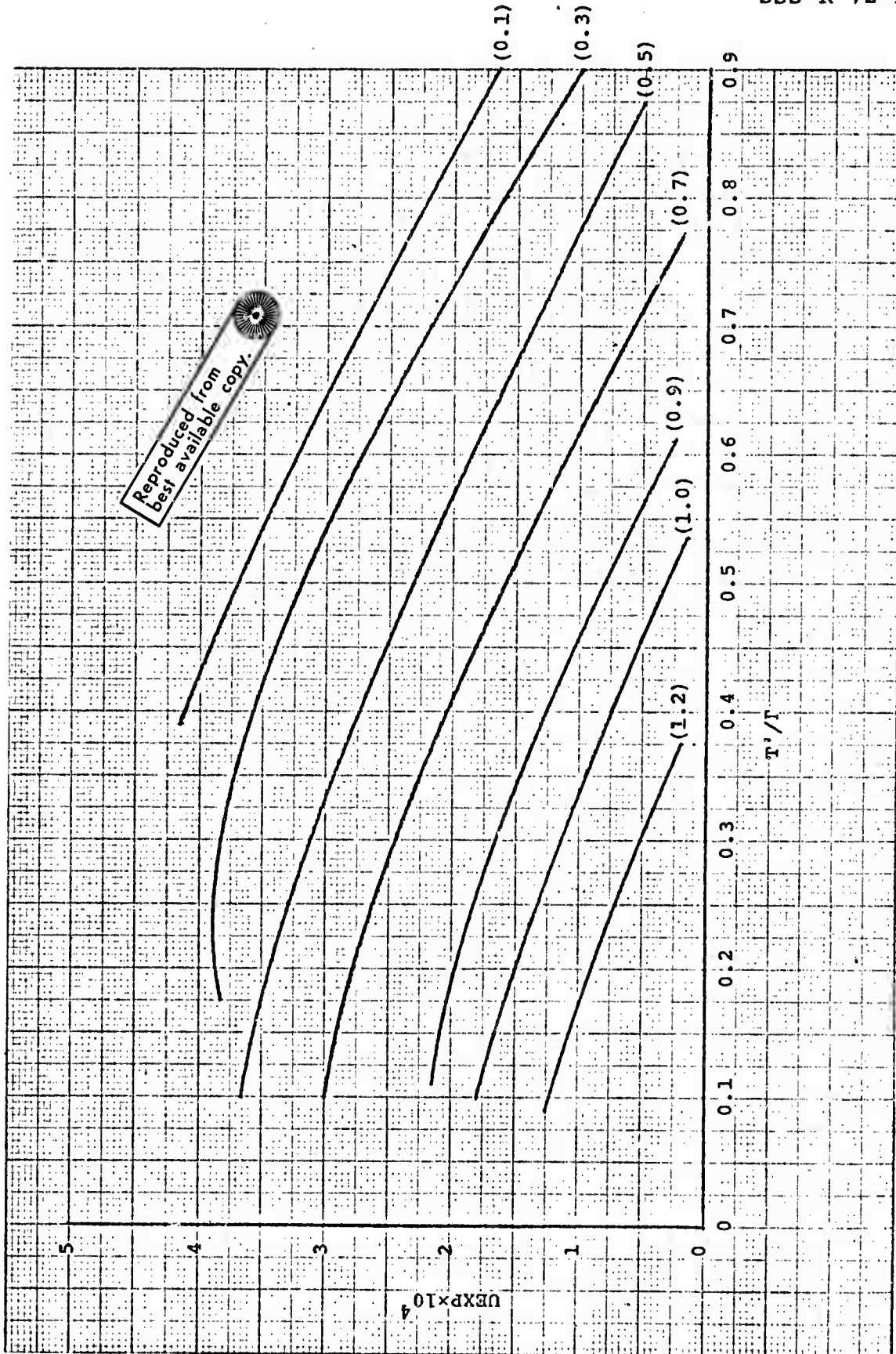
Figure 3.1.4 – Primary Wave Number as a Function of Velocity Profile and Lapse Rate

42
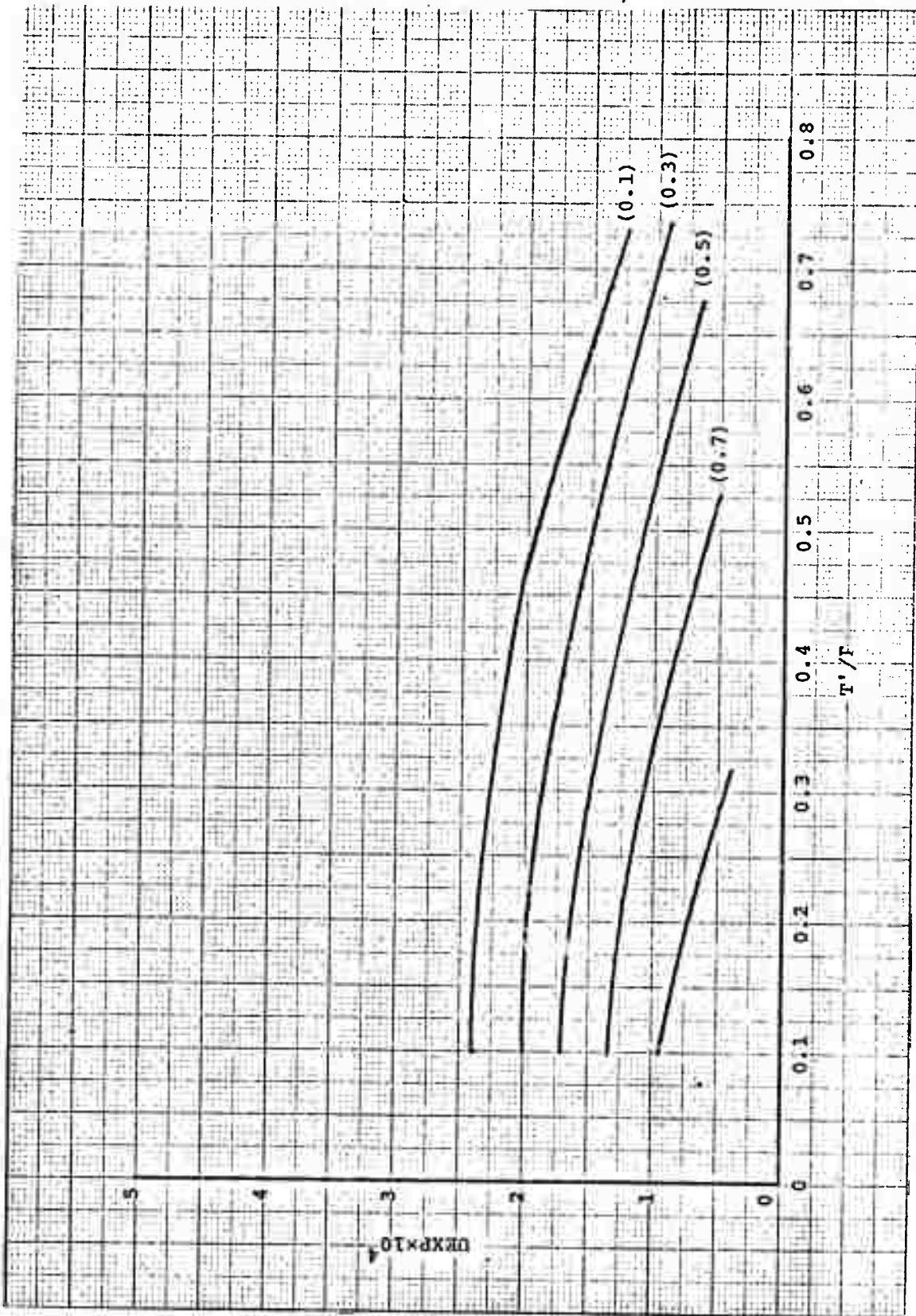
Figure 3.1.5 — Secondary Wave Number as a Function of Velocity
Profile and Lapse Rate
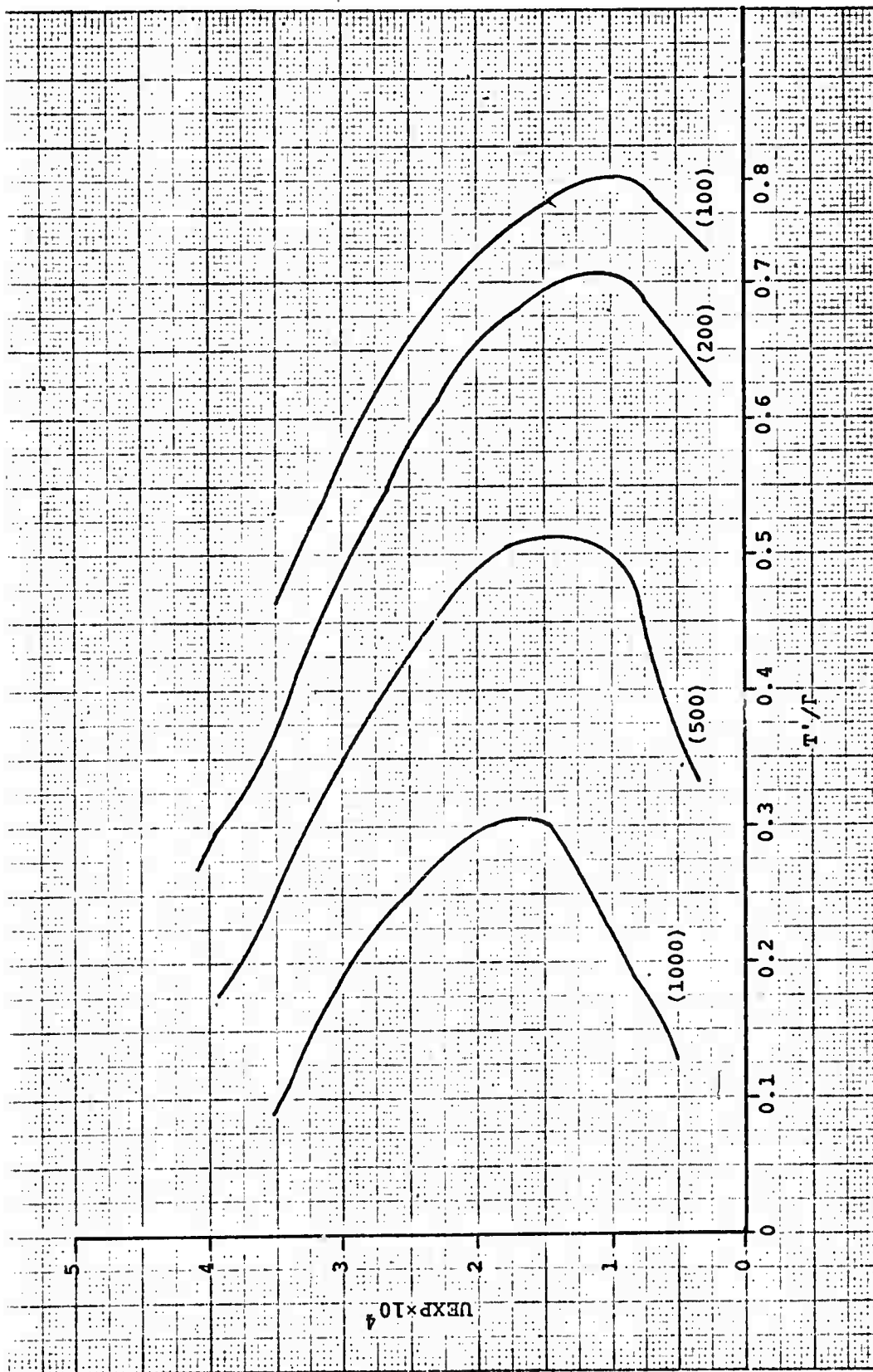
Figure 3.1.6 — Primary Trapped Wave Drag as a Function of
Lapse Rate and Velocity Profile

44
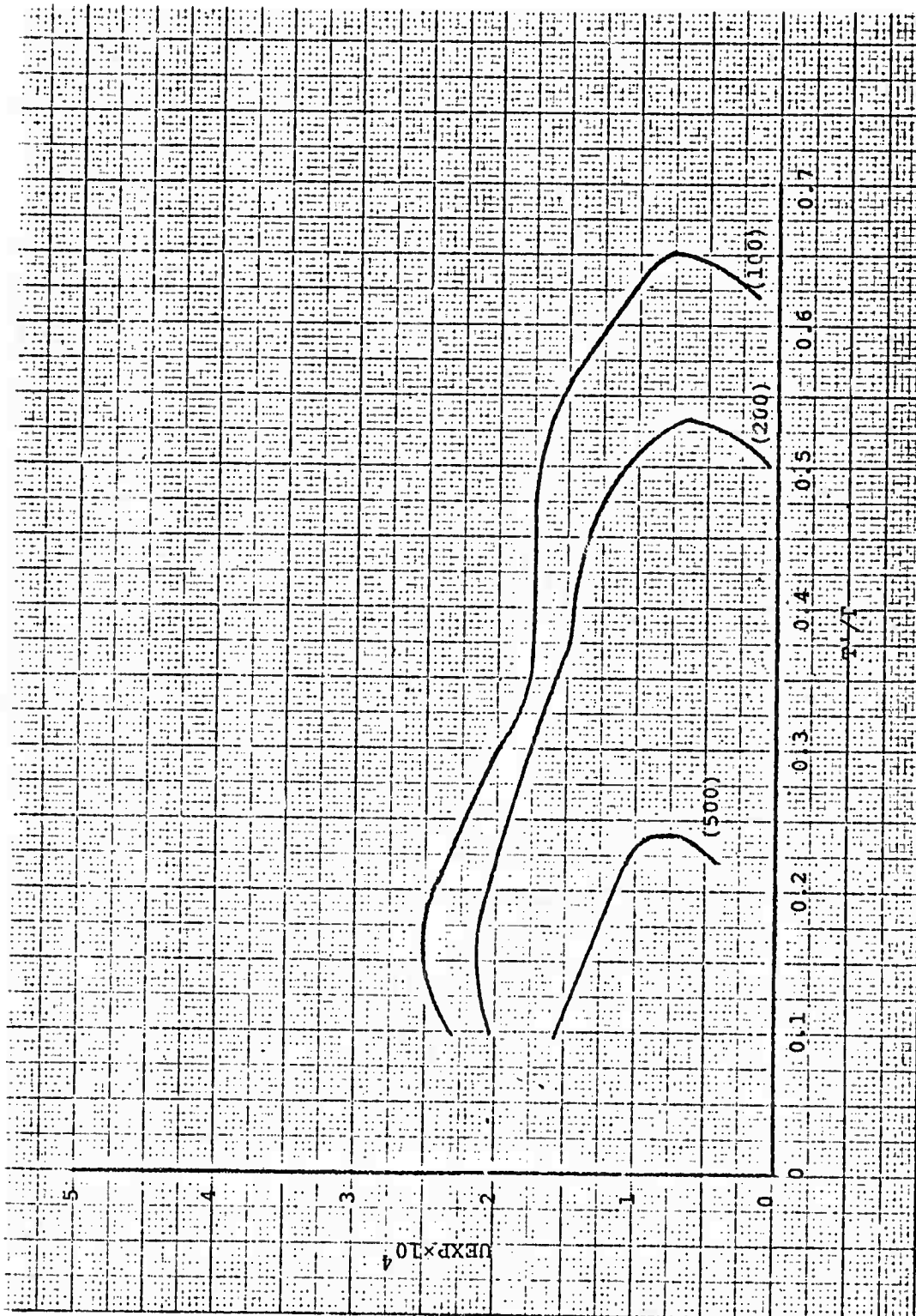
Figure 3.1.7 – Secondary Trapped Wave Drag as a Function of
Lapse Rate and Velocity Profile

$$k_1\left(\text{Drag}(k_1)/A(k_1)\right) = \frac{10^4}{7.5}\left\{- 6.45 + (\text{UEXP}\times10^4)\right.$$

$$\left.\pm\left[-11\times\text{UEXP}\times10^4 - 16.8\times\frac{T'}{\Gamma} + 54.2\right]^{1/2}\right\} \quad (3.19)$$

and

$$k_2\left(\text{Drag}(k_2)/A(k_2)\right) = - 9.44\times10^2\ \frac{T'}{\Gamma} + 7.26\times10^2$$

$$- 2.36\times10^2\left\{\text{UEXP}\times10^4 - 0.85\right\}^2 . \quad (3.20)$$

The actual values of $k(\text{Drag}(k)/A(k))$ used for the parameterization are included in Table 3.3 As previously noted, the drag can be scaled for any topography for which $A(k)$ can be calculated. Further efforts will be made to present the results in the manner most useful for incorporation into the GCM. In addition, the effects of using wind profiles other than exponential in shape and the effects of non-constant atmospheric lapse rate will be investigated.

3.2 COMPARISON OF NON-LINEAR TIME DEPENDENT AND LINEAR STEADY STATE SOLUTIONS

For two problems, a comparison between the linear steady state code and the time dependent HAIFA code can be made. These were the single wave and two wave problems reported in Reference 1 and which also have been compared with the results of Palm and Foldvik's analysis. The problem input is characterized in the following table.

Figure 3.2.1 presents the results of the drag as calculated using the two codes. It is seen that the HAIFA results would have to be compared to much later time in order to determine or justify an extrapolation of the results to the

TABLE 3.3

CALCULATED VALUES OF k (Drag(k)/$A(k)$)
USED IN THE PARAMETERIZATION

UEXP	T'/	k_2 (Drag/$A(k_2)$)	k_1 (Drag/$A(k_1)$)
1.5	0.2	378.35	1335.7
0.5	0.25	475.9	707.96
1.5	0.35	212.3	885.5
1.0	0.4	295.6	697.1
2.0	0.6		267.9
2.0	0.7		124.6
1.0	0.65	84.76	250.6
3.5	0.5		41.21
3.0	0.6		58.2
3.0	0.1		1299.0
2.5	0.3		848.4
2.5	0.45		457.4
1.795	0.2	249.7	1336.8
1.795	0.4	86.1	731.6
1.795	0.6	1.7	296.3
1.795	0.8		46.2
1.0	0.25	206.0	483.0
2.0	0.25	122.6	1139.0
3.0	0.25		796.0
4.0	0.25		220.5
1.0	0.75		129.5
2.0	0.75		70.6
3.5	0.1		990.1
2.5	0.1	25.0	1534.0
1.5	0.1	98.0	515.0
0.5	0.1	477.0	678.0
3.5	0.4		185.0
0.5	0.4	309.0	465.0
0.5	0.7		131.0
2.5	0.6		176.0
1.5	0.9		7.0
0.5	0.9		17.7
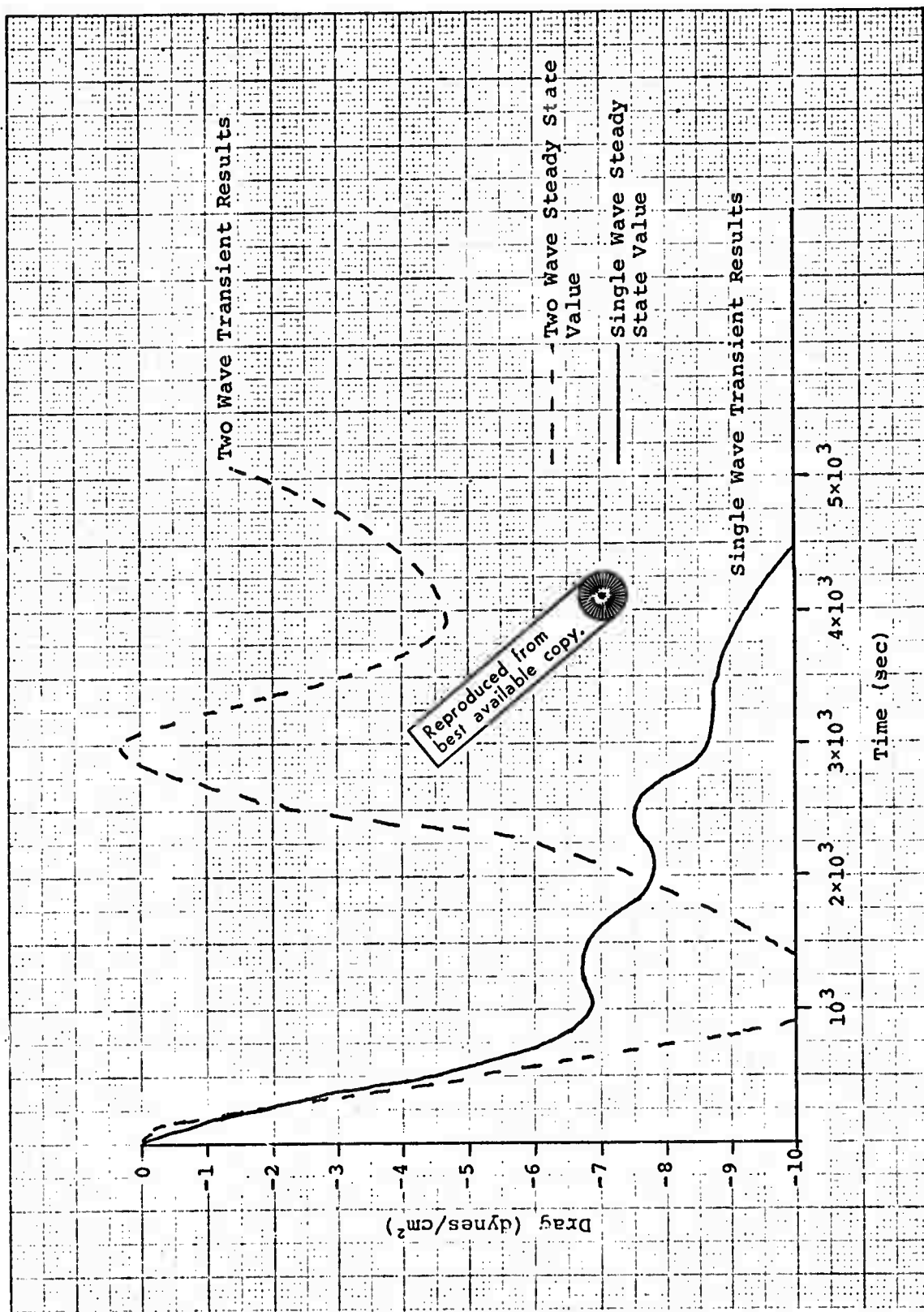
Figure 3.2.1 - Comparison of Steady State and Transient Drag Computations

48

PROBLEM	ATMOSPHERIC LAPSE RATE	OBSTACLE SIZE	HORIZONTAL VELOCITY PROFILE
Single Wave	$1/2 \Gamma$ [1]	635 meters high by 4.5 km long	$U = 9.43 \exp (3 \times 10^{-4} z)$ [2] $U = 10.0 \exp (3 \times 10^{-4} z)$ [3]
Two Wave	$1/2 \Gamma$	625 meters high by 4.5 km long	$U = 9.94 \exp (1.795 \times 10^{-4} z)$ [2] $U = 10.0 \exp (1.795 \times 10^{-4} z)$ [3]

[1] Γ = adiabatic lapse rate in the atmosphere

[2] HAIFA code

[3] Linear steady state code

steady state value. This agrees with the previous interpretation of the transient results in that the Reynolds stress was far from achieving a constant value as a function of height, a requirement for the steady state case.

3.3 COMPARISON OF RESULTS OF THE LINEAR STEADY STATE ANALYSIS AND A GCM PARAMETERIZATION

The parameterization of the drag currently used in the Rand Climate Dynamics version of the UCLA Global Circulation Model[ ] relates the surface stress (τ_s) to the total surface velocity, U_s, and a drag coefficient, C_D, by the relation

$$\tau_s = -\rho \; C_D \; |U_s + G| \; U_s \qquad (3.21)$$

where ρ is the air density, U_s is estimated by a linear extrapolation of U from the two known levels with respect to the vertical pressure coordinate and G is a gustiness factor taken to be 2.0 m/sec. The drag coefficient over land is taken to be

49

$$C_D = 0.002 + 0.006 \ Z_s/5000 \qquad (3.22)$$

where Z_s, the average altitude of the surface, is in meters.

The mountain range used in the linear steady state calculations was 625 meters high. The drag coefficient, C_D, in these circumstances (Eq. (3.)) is 0.00275 producing a constant drag of 3.30 dynes/cm^2 for a surface wind velocity of 10.0 meters/sec.

The results calculated from the linear steady state model indicate differences that should be included in the parameterization in at least two different areas. First, the results indicate a dependence of the drag on the horizontal velocity profile. Secondly, the variation of the mountain width and the atmospheric lapse rate calculated produced a variation in drag values which ranged from zero to values greater than 10.0 dynes/cm^2.

One concludes from the very limited studies completed that an average drag based on the surface roughness alone is not adequate to account for orographic effects of the vertical flux of horizontal momentum. The effects of lapse rate mountain widths, and horizontal velocity profiles should also be addressed. Further calculations in both two and three dimensions will be carried out in order to determine in a more definitive manner how the wave drag is affected by these variables.

4. RADIATION IN THE EARTH'S ATMOSPHERE: ATRAD THEORY ·

Since the previous semiannual report on this contract,[2] the atmospheric radiation code, called ATRAD, has become operational. It has been compared against several known radiative transfer solutions and the agreement has been excellent. Two comparison calculations have been made between ATRAD and the radiation subroutine of the Mintz-Arakawa code. The results of these comparisons and a description of ATRAD were presented at the American Meteorological Society's Conference on Atmospheric Radiation at Fort Collins, Colorado, August 7-9, 1972.[12] (This paper is included as Appendix C.)

Since the code ATRAD has reached operational status and fewer changes will be made in the future, it is useful now to summarize its theoretical basis. This is done in the present chapter, where elements from both of the prior semi-annuals[1,2] and code improvements which have not previously been reported are brought together. Chapter 5 contains a description of the Mintz-Arakawa radiation subroutine and of the method of obtaining data from it to form appropriate input data for ATRAD. The two comparisons between ATRAD and Mintz-Arakawa are also presented and discussed in Chapter 5. Finally, future plans for code development and code applications are presented in Chapter 6.

4.1   ASSUMPTIONS

The fundamental assumptions involved in the formulation of the ATRAD equations are:

(1)   plane-parallel atmosphere (rather than spherical) and horizontal surface,

(2)   horizontal homogeneity,

(3)   local thermodynamic equilibrium, so that true emission is described by the Planck function,

(4)   unpolarized radiation field ,

(5)   non-refractive air (rays are not curved),

(6)   spherical aerosol scatterers of uniform composition,

(7)   point source sun (no angular width), and

(8)   multiplying together the transmissions of individual molecular constituents yields the total transmission.

Assumptions (1) and (5) are only violated for large-zenith-angle rays, and such rays make only a very small contribution to vertical fluxes.

Assumption (2) probably represents the most serious approximation in the code, one whose impact has been largely ignored in the literature. The effect of the most important form of horizontal inhomogeneity, partial cloudiness, is customarily accounted for by taking a weighted sum of clear-air and totally-cloudy fluxes,

$$F = \alpha F_{cloud} + (1-\alpha) F_{clear}$$

where α is the fractional cloudiness. The only virtue of this scheme is that it reduces properly in the limits $\alpha = 0$ and $\alpha = 1$ and, therefore, cannot err too greatly for $0 < \alpha < 1$. A more reasonable scheme, in the context of ATRAD's numerical algorithm,[2] would be to take the weighted sum of the reflection and transmission matrices of a partially cloudy zone. This difficulty could be resolved with a three-dimensional Monte Carlo code such as that of Cox and McKee,* which should help to ascertain the relative importance of horizontal inhomogeneity and whether it is really significant for weather and climate radiation subroutines.

Assumption (3), which requires sufficiently high pressures that collisions maintain thermodynamic equilibrium in excited states, is valid below about 70 km.

Assumption (4) has been examined by several investigators, for example Howell and Jacobowitz,[13] who find that, especially in the presence of aerosols, the flux errors resulting from a polarization-independent treatment are generally less than one percent in the <u>visible</u> spectrum. Averaged over the whole spectrum, these errors are considerably smaller.

A standard Mie theory treatment[14] of aerosol scattering is made possible by assumption (6). Uniform composition is not essential, since layered spherical particles can be handled with some increase in computational complexity (see Kerker[15]). However, there is practically no experimental data on layered (water-sheathed, etc.) aerosol particles. Neither is sphericity essential since Mie theory has been extended to ellipsoids and circular cylinders. However, solid aerosol particles (with the exception of cirrus ice needles) are no more accurately representable as ellipsoids or

---

* S. Cox, Colorado State University, Fort Collins, Colorado, private communication.

cylinders than as spheres. And liquid aerosol particles are very nearly spherical, although the larger ones will tend to be slightly flattened by the air flow around them. Furthermore, as Hodkinson[16] argues, randomly oriented irregular particles produce the same forward diffraction, the same scattering due to external reflection, and the same scattering due to the first refraction as equivalent spheres (spheres having the same distribution of projected area). For moderately absorbing irregular particles, this would lead to a complete equivalence of scattering patterns. Measurements of Hodkinson,[16] Ellison,[17] and Holland and Gagne[18] tend to confirm the usefulness of Mie theory (with equivalent spheres) for predicting the scattering from irregular particles into the forward hemisphere, which contains almost all the scattered photons.

The one aerosol which, by virtue of its importance to the global radiative energy budget,[19,20] should probably not be approximated as spherical is cirrus cloud. Jacobowitz[21] has computed the phase function of randomly oriented hexagonal ice cylinders, typical of cirrus, and has found that as much energy is scattered into the halo, around 22°, as into the main diffraction peak. This effect is entirely missed by an equivalent sphere model. In the future, we intend to include cirrus in ATRAD more completely.

The error incurred by assumption (7), ignoring the angular width of the sun, has been estimated and found to be negligible as far as vertical fluxes are concerned.

Assumption (8), that individual transmissions are multiplicative, is firmly grounded in experiment,[23] and has virtually no detectable experimental error associated with it.

4.2 BASIC RADIATIVE TRANSFER EQUATIONS

The radiative transfer problem in the Earth's atmosphere reduces to the solution of the seemingly simple equation[24]

$$\frac{dI_\nu}{ds} = J_\nu - \kappa_\nu I_\nu \qquad (4.1)$$

which states that the monochromatic (frequency ν) radiant intensity I_ν, in traversing the element of length ds , will be augmented by sources in the amount J_ν ds and diminished by extinction in the amount $\kappa_\nu I_\nu$ ds . In general, the radiant intensity and J_ν , the source function, depend on both a spatial coordinate $\vec{r}$ and an angular coordinate (direction) $\vec{\Omega}$ at the point $\vec{r}$, as well as upon the frequency ν . The time dependence of these quantities is ignored because the radiative state of the atmosphere is established, for all practical purposes, instantaneously. κ_ν is the extinction coefficient, which describes the relative depletion in the intensity of the beam, dI_ν/I_ν , upon traversing the element of distance ds . κ_ν is in general the sum of an absorption part and a scattering part. J_ν describes the additions made to the beam intensity along ds by thermal (Planckian) emission and by scattering.

In ATRAD's plane-parallel geometry, which is illustrated in Figure 4.1, $\vec{r}$ is replaced by z, which is measured from the top of the atmosphere, and $\vec{\Omega}$ is represented as usual by the spherical coordinates $\mu = \cos\theta$ and ϕ . Using Kirchhoff's Law to obtain the source function J_ν , the radiative transfer equation (4.1) becomes in this geometry[25]
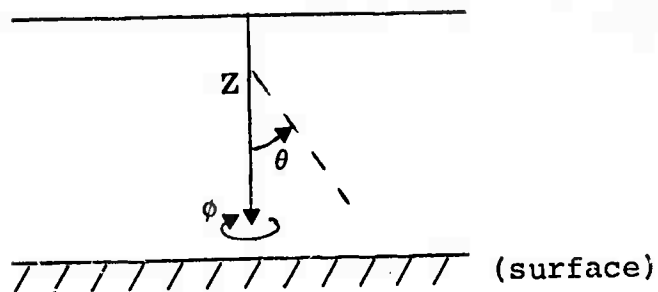
Figure 4.1 — ATRAD coordinate system

$$\mu \frac{\partial I_\nu}{\partial z} = \alpha_\nu'(z) B_\nu(T) + \frac{\beta_\nu(z)}{4\pi} \int_{4\pi} P_\nu(z,\vec{\Omega},\vec{\Omega}') \; I_\nu(z,\vec{\Omega}') \, d\Omega'$$

$$- \kappa_\nu(z) \; I_\nu \qquad (4.2)$$

where

$\kappa_\nu = \alpha_\nu' + \beta_\nu$ = volume extinction coefficient,

α_ν' = volume absorption coefficient, α_ν , corrected for stimulated emission (a correction usually ignored in the atmospheric radiation literautre),

$$= \alpha_\nu \left(1 - e^{-h\nu/kT}\right) \quad ,$$

T = temperature,

β_ν = volume scattering coefficient,

B_ν = Planck function

$$= \frac{2h\nu^3/c^2}{e^{h\nu/kT} - 1}$$

56

and P_ν is the phase function, defined so that

$$P_\nu(z,\vec{\Omega},\vec{\Omega}') \frac{d\Omega}{4\pi}$$

is the probability that a photon entering a volume element around z from direction $\vec{\Omega}'$ will be scattered into the cone $d\Omega$ of directions around $\vec{\Omega}$. Since absorption is explicitly represented in Eq. (4.2), the above probabilities must sum to one

$$\int_{4\pi} P_\nu(z,\vec{\Omega},\vec{\Omega}')\frac{d\Omega}{4\pi} = 1 \qquad (4.3)$$

In what follows, it is convenient to break the absorption coefficient into a "line" part and a "continuum" part,

$$\alpha_\nu' = \alpha_\nu^{line} + \alpha_\nu^{cont} \qquad (4.4)$$

α_ν^{cont} varies "slowly" with frequency and includes, for example, the water vapor 8-12μ continuum and the aerosol absorption; α_ν^{line} is the rapidly-varying part, due to absorption lines of atmospheric constituents. Since a continuum is often due to the wings of distant lines, the separation is to a certain extent arbitrary. Therefore, we shall adopt the convention that, with the exception of aerosol absorption, continua exist only in the gaps between absorption bands.

Because a volume element in the atmosphere exhibits the same scattering pattern no matter what the direction of incidence

$\vec{\Omega}'$, the phase function depends only on the scattering angle θ_s <u>between</u> $\vec{\Omega}$ and $\vec{\Omega}'$,

$$P_\nu = P_\nu(z, \mu_s)$$

where

$$\mu_s \equiv \cos\theta_s = \mu\mu' + \sqrt{1-\mu^2}\ \sqrt{1-\mu'^2}\ \cos(\phi-\phi')$$

In order to azimuthally-average the radiation transport equation (see below), it is necessary to azimuthally-average P_ν:

$$\overline{P}_\nu(z, \mu, \mu') \equiv \frac{1}{2\pi}\ \int_0^{2\pi} P_\nu(z, \mu_s)\, d\phi$$

$$= \frac{1}{2\pi}\ \int_0^{2\pi} P_\nu(z, \mu\mu' + \sqrt{1-\mu^2}\ \sqrt{1-\mu'^2}\ \cos\phi)\, d\phi \quad . \qquad (4.5)$$

The second step follows from the periodicity of the cosine. As a result, $\overline{P}_\nu$ does not depend on ϕ' .

For the computation of vertical fluxes and radiative heating rates, the retention of the ϕ-dependence of I_ν is unnecessary. It can be eliminated by ϕ-averaging Eq. (4.2) (operating on both sides with $\frac{1}{2\pi}\ \int_0^{2\pi} d\phi$) to obtain

$$\mu \frac{\partial \overline{I}_\nu}{\partial z} = \alpha'_\nu B_\nu + \frac{\beta_\nu}{2} \int_{-1}^{1} \overline{P}_\nu(z,\mu,\mu') \, \overline{I}_\nu(z,\mu') \, d\mu' - \kappa_\nu \overline{I}_\nu \qquad (4.6)$$

where

$$\overline{I}_\nu(z,\mu) = \frac{1}{2\pi} \int_{0}^{2\pi} I_\nu(z,\mu,\phi) \, d\phi \quad .$$

Knowing $\overline{I}_\nu$, the vertical flux F_ν is obtained from

$$F_\nu(z) \equiv \int_{4\pi} \mu \, I_\nu(z,\vec{\Omega}) \, d\Omega = 2\pi \int_{-1}^{1} \mu \, \overline{I}_\nu(z,\mu) \, d\mu \quad . \qquad (4.7)$$

From F_ν the total (spectrally-integrated) flux F can be computed:

$$F(z) = \int_{\nu_{min}}^{\nu_{max}} F_\nu(z) \, d\nu$$

where $[\nu_{min}, \nu_{max}]$ includes all spectral intervals in which F_ν is non-negligible. From F, the radiative heating rate at level z can be calculated from

$$\frac{\partial T}{\partial t} = - \frac{1}{\rho C_p} \frac{dF}{dz} \qquad (4.8)$$

where

$$\rho = \rho(z) = \text{air density}$$

$$C_p = \text{specific heat of air at constant pressure} \quad .$$

Using the hydrostatic approximation, this becomes

$$\frac{\partial T}{\partial t} = - \frac{g}{C_p} \frac{dF}{dp} \quad .$$

Rather than compute point-values of heating, ATRAD computes the average heating of a zone (z_i, z_{i+1}) in terms of the boundary fluxes:

$$\left\langle \frac{\partial T}{\partial t} \right\rangle \equiv \frac{1}{p_{i+1} - p_i} \int_{p_i}^{p_{i+1}} \frac{\partial T}{\partial t} \, dp$$

$$= - \frac{g}{C_p} \frac{F(z_{i+1}) - F(z_i)}{p_{i+1} - p_i} \tag{4.9}$$

(the slight vertical variation of g has been ignored).

The radiative transfer equation, Eq. (4.6), is a phenomenological equation requiring input data of three different types:

(a) atmospheric structure data

(b) boundary condition data

(c) absorption data for relevant atmospheric constituents.

The next three sections describe ATRAD's needs in each of these areas.

4.3 SPECIFICATIONS OF ATMOSPHERIC STRUCTURE

The atmospheric structure data needed to solve Eq. (4.6), with the use of Mie scattering theory for aerosols, consists of the pressure p, the temperature T, the water vapor density ρ_{H_2O}, the ozone density ρ_{O3}, and the aerosol (including cloud) number density, size distribution, and composition. These must all be given as a function of height. The atmospheric absorbers other than water vapor and ozone are assumed to be uniformly mixed.

The details as to how the structure data are supplied to ATRAD are given in Appendix A. A variety of analytic aerosol size distributions are available as options, or the user may supply his own size distributions in card form. Similarly, a variety of aerosol refractive indices are available as options, e.g. water, ice, sea-salt, dust, etc.

4.4 BOUNDARY CONDITIONS

The boundary condition at the top of the atmosphere is

$$I_\nu(0,\mu,\phi) = S_\nu \, \delta(\vec{\Omega} - \vec{\Omega}_o) \qquad \text{for} \qquad \begin{array}{c} 0 < \mu \leq 1 \\[4pt] 0 \leq \phi < 2\pi \end{array}$$

where S_ν is the solar flux at frequency ν at the position of the Earth and $\vec{\Omega}_o$ is the direction of the solar beam in ATRAD's coordinate system (Figure 4.1). Taking the ϕ-average,

$$\overline{I}_\nu(0,\mu) = \frac{S_\nu}{2\pi} \, \delta(\mu - \mu_o) \qquad 0 < \mu \leq 1 \qquad (4.10)$$

μ_O, the cosine of the solar zenith angle, is calculated following the prescription of Woolf[26] from user-supplied values of latitude, longitude, day of the year, and Greenwich time. The best measurements of S_ν are those of Thekaekara, et.al.,[27] which have been included in the code. (Actually, the values of

$$\int_o^\lambda S_\lambda \, d\lambda = \int_\nu^\infty S_\nu \, d\nu$$

are given by Thekaekara, and the code obtains from these the values

$$S_{\Delta\nu} = \frac{1}{\Delta\nu} \int_{\Delta\nu} S_\nu d\nu$$

for use in each frequency group $\Delta\nu$.) $S_{\Delta\nu}$ is adjusted according to the earth-sun distance, which is calculated from the day of the year.

The boundary condition at the surface requires, for its complete specification, the ground temperature T_g and the bidirectional reflectivity ρ_ν''. If a beam of intensity $I_{\nu,inc}$ is incident on a surface from direction $\vec{\Omega}_i$ and the resultant reflected intensity at angle $\vec{\Omega}_r$ is $I_{\nu,ref}(\vec{\Omega}_r;\vec{\Omega}_i)$, then ρ_ν'' is defined such that[28] (see Figure 4.2)

$$\pi I_{\nu,ref}(\vec{\Omega}_r;\vec{\Omega}_i) = \rho_\nu''(\vec{\Omega}_i,\vec{\Omega}_r) I_{\nu,inc} \cos\theta_i d\Omega_i \qquad (4.11)$$

By this definition, ρ_ν'' is of finite order, barring specular reflection, for $I_{\nu,ref}$ is of differential order with respect to $I_{\nu,inc}$. In case there is a specular component of reflection, we separate ρ_ν'' into a diffuse part $\rho_{\nu,d}''$ and a

62

specular part $\rho''_{\nu,s}$,

$$\rho''_\nu = \rho''_{\nu,d} + \rho''_{\nu,s}$$

where

$$\rho''_{\nu,s}(\vec{\Omega}_i,\vec{\Omega}_r) = \frac{\pi}{\cos\theta_i} \rho'_{\nu,s}(\vec{\Omega}_i)\delta(\mu_i-\mu_r)\delta(\phi_i+\pi-\phi_r) \quad . \qquad (4.12)$$

Some authors, for example Siegel and Howell[28], do not include the factor of π in Eq. (4.11). We find it convenient because when the reflection is diffuse, ρ''_ν reduces to an albedo (flux ratio), the customary measure of surface reflectivity.
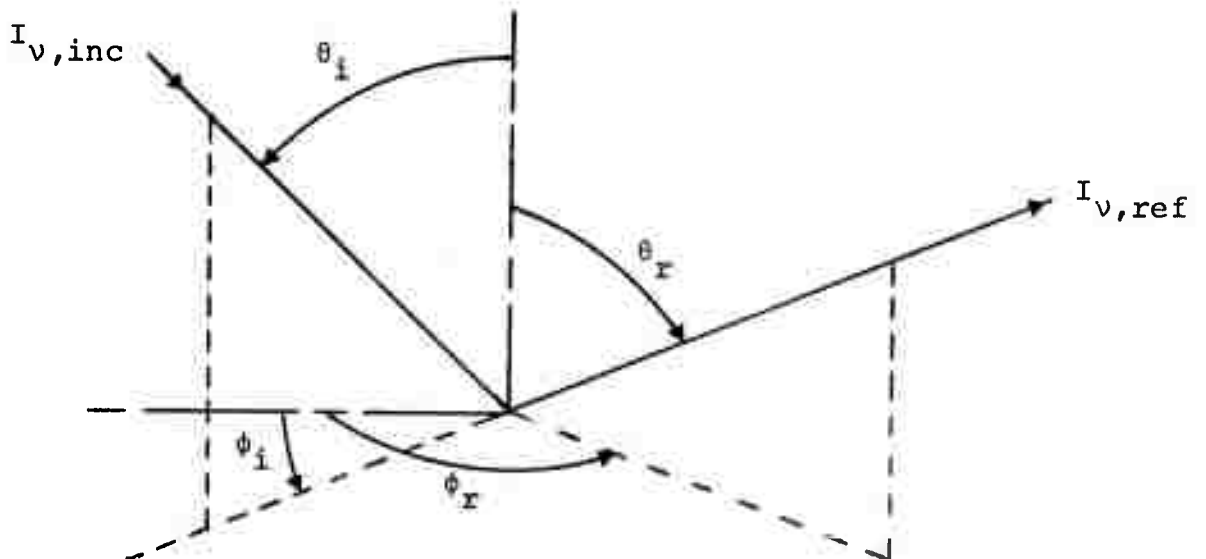
Figure 4.2. Geometry of reflection.

When radiation is incident from all $\vec{\Omega}_i$, the reflected intensity along $\vec{\Omega}_r$ is, by Eq. (4.11),

$$I_{\nu,ref}(\vec{\Omega}_r) = \frac{1}{\pi} \int_0^{2\pi} d\phi_i \int_0^1 d\mu_i \, \rho_\nu''(\vec{\Omega}_i,\vec{\Omega}_r) I_{\nu,inc}(\vec{\Omega}_i)\mu_i \quad .$$

Adding on the thermal emission from the ground and phrasing the whole result in terms of the ATRAD coordinate system (Figure 4.1), the surface boundary condition becomes

$$I_\nu(z_0,\mu,\phi) = \varepsilon_\nu'(|\mu|)B_\nu(T_g) + \rho_{\nu,s}'(|\mu|)I_\nu(z_0,|\mu|,\phi-\pi)$$

$$+ \frac{1}{\pi}\int_0^{2\pi} d\phi' \int_0^1 d\mu' \rho_{\nu,d}''(|\mu|,\mu',\phi-\phi')I_\nu(z_0,\mu',\phi')\mu' \tag{4.13}$$

for

$$-1 \leq \mu < 0$$
$$0 \leq \phi < 2\pi$$

where z_0 is the surface level, and ε_ν', the directional emissivity, has been written as a function of angle of emission.[28] The absolute value signs on μ in ε_ν', $\rho_{\nu,s}'$, and $\rho_{\nu,d}''$ are merely because these surface properties are customarily measured or calculated with the convention $0 \leq \theta_i$, $\theta_r \leq 90^\circ$, whereas ATRAD's coordinate system takes $0 \leq \theta_i < 90^\circ$ and $90^\circ < \theta_r \leq 180^\circ$.

It should be noted that, in Eq. (4.13), ϕ is entirely missing from the argument list of $\rho_{\nu,s}'$ and occurs in the combination $\phi-\phi'$ in the argument list of $\rho_{\nu,d}''$. In both cases, this is justified because the surface is isotropic, that is,

64

its reflecting properties do not change as we rotate the co-ordinate system in Figure 4.2 about the vertical axis.

Taking the ϕ-average of Eq. (4.13) leads to the final form of the surface boundary condition:

$$\bar{I}_\nu(z_0,\mu) = \epsilon_\nu'(|\mu|)B_\nu(T_g) + \rho_{\nu,s}'(|\mu|)\bar{I}_\nu(z_0,|\mu|)$$

$$+ 2\int_0^1 d\mu' \; \bar{\rho}_{\nu,d}''(|\mu|,\mu')\bar{I}_\nu(z_0,\mu')\mu' \tag{4.14}$$

for $-1 \leq \mu < 0$, where

$$\bar{\rho}_{\nu,d}''(\mu,\mu') \equiv \frac{1}{2\pi}\int_0^{2\pi} \rho_{\nu,d}''(\mu,\mu',\phi-\phi')d\phi$$

$$= \frac{1}{2\pi}\int_0^{2\pi} \rho_{\nu,d}''(\mu,\mu',\phi)d\phi$$

(the second step follows from the 2π-periodicity of $\rho_{\nu,d}''$ in its third argument).

There are three simplifications of the surface boundary condition (4.14) which are used in almost all of the other extant atmospheric radiation codes:

(a) $\epsilon_\nu' = 1$, $\rho_{\nu,s}' = \rho_{\nu,d}'' = 0$. This is used practically without exception by codes dealing with the infrared (IR) spectrum, ignoring the very real frequency-and angle-variations of ϵ_ν for natural surfaces. Furthermore, except for water, snow, and ice, the average IR emissivity

65

of natural surfaces is known to deviate considerably from unity.[22] Nevertheless, the mathematical consequences of using a non-unit emissivity (implying $\rho''_{\nu,d} \neq 0$) are disastrous for codes using a simple quadrature of the integral transport equation, for then they can no longer frequency-average the boundary term.

(b) $\rho''_{\nu,d} = 0$, $\rho'_{\nu,s}$ given by Fresnel formulae for reflection at a plane interface, ν so large that $B_\nu(T_g)$ is negligible. This is used primarily by codes dealing with single frequencies in the solar spectrum with water as the underlying surface.

(c) $\rho'_{\nu,s} = 0$, $\rho''_{\nu,d} =$ constant (independent of angle of incidence and angle of reflection), ν so large that $B_\nu(T_g)$ is negligible. This is used primarily by codes dealing with single frequencies in the solar spectrum with a solid underlying surface. $\rho''_{\nu,d}$ is the albedo, and the reflection is assumed diffuse.

We believe that it is important to include a fully general boundary condition, Eq. (4.14), as ATRAD does. Research to date suggests that such factors as the angular--and frequency--dependence of ε'_ν or $\rho''_{\nu,d}$ cannot be ignored.[28,30,31,32,33] While data with respect to these dependences are limited, they exist in sufficient quantities to warrant comparisons with calculations using frequency and/or angular averages. Such studies will be performed with ATRAD, and should indicate what level of detail is necessary in the boundary condition.

Two theoretical models of rough-surface reflectivity seem sufficiently realistic to warrant inclusion in ATRAD. The first is that for a rough water surface, in which it is assumed that the surface consists of planar elements each of which is a specular reflector. The slope distribution of the planar elements as a function of average surface wind speed can be taken from the experimental work of Cox and Munk.[29] Even with this model, the inclusion of shadowing and multiple reflections among planar elements is difficult. Therefore these effects can probably only be included approximately. Experimental measurements of sea surface bidirectional reflectivities[30] should prove useful in guiding the approximations.

The second theoretical model of rough-surface reflectivity is for land areas, and assumes that the surface consists of planar elements each of which is a diffuse reflector (of given albedo). This model is due to McStravick.[31] The slope distribution of the planar elements is presumed Gaussian. As with the first model, shadowing and multiple reflection can probably be included only approximately.

In practice, the full bidirectional reflectivity of the earth's surface is not available experimentally, nor is it likely to be available in the near future, as a function of latitude and longitude. Therefore the two theoretical models described above, particularly the water-surface model applying to so much of the earth's surface, assume special importance in filling this void. However, ATRAD also makes provision to use certain degraded forms of the bidirectional reflectivity and directional emissivity which are more readily available from experiment. These are (refer to Figure 4.2 for notation):

(a) the directional-hemispherical reflectivity,

$$\rho'_\nu(\vec{\Omega}_i) = \frac{\text{reflected flux}}{\text{incident flux from } \vec{\Omega}_i}$$

$$= \frac{\int_D I_{\nu,\text{ref}}(\vec{\Omega}_r;\vec{\Omega}_i)\cos\theta_r \, d\Omega_r}{I_{\nu,\text{inc}}(\vec{\Omega}_i)\cos\theta_i \, d\Omega_i}$$

$$= \frac{1}{\pi} \int_D \rho''_\nu(\vec{\Omega}_i,\vec{\Omega}_r) \cos\theta_r \, d\Omega_r$$

$$= 2\int_0^1 \overline{\rho}''_\nu(\mu_r,\mu_i)\mu_r \, d\mu_r \qquad (4.15)$$

(b)   the hemispherical reflectivity (albedo),

$$\rho_\nu = \frac{\text{reflected flux}}{\text{incident flux}}$$

$$= \frac{\int_D \rho'_\nu(\vec{\Omega}_i) I_{\nu,\text{inc}}(\vec{\Omega}_i)\cos\theta_i \, d\Omega_i}{\int_D I_{\nu,\text{inc}}(\vec{\Omega}_i)\cos\theta_i \, d\Omega_i} \qquad (4.16)$$

(c)   the hemispherical emissivity,

$$\varepsilon_\nu = \frac{\text{emitted flux}}{\text{black body flux at } T_g}$$

$$= \frac{\int_D I_{\nu,\text{em}}(\vec{\Omega})\cos\theta \, d\Omega}{\pi B_\nu(T_g)}$$

$$= \frac{1}{\pi} \int_D \varepsilon'_\nu(\mu)\mu \, d\Omega$$

$$= 2\int_0^1 \varepsilon'_\nu(\mu)\mu \, d\mu \qquad (4.17)$$

The solid-angle integrals in (a)-(c) are over the upward hemisphere. Note that, by the isotropy of the surface, ρ_ν' really only depends on μ_i. Also, the above quantities are not all independent. By Kirchhoff's Law for surfaces[28],

$$\epsilon_\nu'(\mu) + \rho_\nu'(\mu) = 1 \tag{4.18}$$

so that, if either ϵ_ν' or ρ_ν' is known, the other is determined.

If only the directional-hemispherical reflectivity ρ_ν' is given, nothing can be said about the angular dependence of the reflected radiation. Therefore ATRAD assumes diffuse reflection, which means $\overline{\rho}_\nu''$ in Eq. (4.15) is independent of μ_r and is equal to ρ_ν',

$$\overline{\rho}_\nu''(\mu_r, \mu_i) = \rho_\nu'(\mu_i)$$

If ϵ_ν' rather than ρ_ν' is known, Eq. (4.18) is used to obtain ρ_ν', and therefore $\overline{\rho}_\nu''$.

Note that the albedo ρ_ν, Eq. (4.16), is not an intrinsic surface property but depends on the incident radiation field $I_{\nu,inc}$, a fact familiar to experimenters.[32] Only when ρ_ν' is independent of angle does the albedo become independent of intensity, in which case Eq. (4.16) reduces to

$$\rho_\nu = \rho_\nu' \quad .$$

When only an albedo is available, ATRAD uses the approximation that $\overline{\rho}_\nu''$ is independent of both μ_r and μ_i, leading to

$$\overline{\rho}_\nu'' = \rho_\nu \quad .$$

To obtain the emissivity, observe that if the emission is isotropic or if ρ_ν' is independent of angle, then

$$\rho_\nu + \epsilon_\nu = 1$$

from Eq. (4.18). Since the second assumption holds, ϵ_ν can be obtained from ρ_ν. ATRAD then invokes the assumption of isotropic emission to obtain

$$\epsilon_\nu' = \epsilon_\nu$$

from Eq. (4.17).

A large amount of albedo data is available,[33] particularly as it relates to remote sensing from aircraft and satellites. Much more such data remains classified. However, as yet no comprehensive tabulation of albedos, bidirectional reflectivities, etc., has been incorporated into ATRAD; data for individual problems will be obtained as needed.

4.5 TRANSMISSION FUNCTIONS

Line-by-line absorption coefficients have been calculated and measured during the last two decades for all of the important atmospheric absorbers. However, it is computationally infeasible to use frequency groups small enough to resolve individual lines in ATRAD. Therefore, frequency-averaged absorption coefficient data in the form of transmission functions $T_{\Delta\nu}$ are employed. In terms of the optical depth for line absorption

$$\tau_{\nu,ab}(z_1, z_2) \equiv \int_{z_1}^{z_2} \alpha_\nu^{(line)}(z)\,dz, \qquad (4.19)$$

the transmission function is

70

$$T_{\Delta\nu}(z_1, z_2, \mu) \equiv \frac{1}{\Delta\nu} \int_{\Delta\nu} e^{-\tau_{\nu,ab}(z_1, z_2)/\mu} \, d\nu \quad . \qquad (4.20)$$

The frequency interval $\Delta\nu$ in general includes many lines.

The computation of transmission functions has a long history. The earliest attempts were based on band models, in which simple analytical representations of line strengths, positions, and shapes were assumed. As accurate line-by-line absorption data has become available, both from theory and experiment, transmission function computations have incorporated it. However, such detailed line-by-line transmission function computations are very expensive in terms of computer time. Considering that integration steps as small as 0.001 cm^{-1} may be required, and that the region of significant absorption extends from 10,000 cm^{-1} (1μ) to 250 cm^{-1} (40μ), with only a few gaps, the magnitude of the problem is apparent. As an example, Kyle[34] used 15 minutes of CDC 6600 time to compute transmission functions between a single pair of atmospheric levels z_1 and z_2, for a single value of μ, for the wavelength interval 1.7μ - 20μ with $\Delta\nu = 1$ cm^{-1}. Multiply this by the number of angles N_μ and by the number of pairs of levels $\frac{1}{2}N_z(N_z-1)$, and the computing time to obtain a complete set of transmission functions becomes truly formidable (for 4 angles and 20 levels Kyle would require 190 hours). While it is foreseeable that, with ingenuity, such computing times could be reduced substantially, it is apparent that for the present ATRAD cannot afford to calculate transmission functions line-by-line for each new problem. Therefore, a less exact method was sought.

A rather thorough literature survey revealed numerous less exact methods for computing transmission functions. These ranged from simple parameterized band models such as Elsasser's and Goody's,[35] through more sophisticated band models such as Wyatt's,[36] to approaches such as those of Smith[37] or

71

McClatchey[38] involving an empirically determined _function_ as
well as empirically determined parameters. The errors in the
methods of Smith or McClatchey are almost within the uncer-
tainties in the line-by-line calculations themselves, and in-
volve orders of magnitude less calculation. The method of
McClatchey was selected for inclusion in ATRAD because of its
comprehensive treatment of all known atmospheric absorbers, its
accuracy, and its computational economy (only tabular interpola-
tion is required to obtain transmissions).

The method of McClatchey, et.al., as furnished to us in
subroutine LOTRAN (for LOw-resolution TRANsmission functions),
contains separate values of the transmission for: (a) H_2O
vapor; (b) the uniformly mixed gases CO_2, N_2O, CH_4, CO, and O_2;
(c) O_3; (d) the H_2O 8-13μ continuum; and (e) the N_2-N_2 4μ con-
tinuum. In ATRAD, the two continua (d) and (e) have been placed
in subroutines separate from LOTRAN because their transmissions
are simple exponentials (for small enough $\Delta\nu$) and they can be
added to α_ν cont, the continuum part of the absorption coef-
ficient.

LOTRAN furnishes transmissions averaged over 20 cm^{-1}
intervals centered from 350 cm^{-1} to 50,000 cm^{-1}. To obtain
transmissions over larger wavenumber intervals, it follows
rigorously from the definition (4.20) that the 20 cm^{-1} trans-
missions may be averaged; e.g.,

$$T_{400-440} = \frac{1}{2} (T_{400-420} + T_{420-440})$$

Hence ATRAD may use wavenumber intervals which are any multiple
of 20 cm^{-1}, subject to restrictions on the size of $\Delta\nu$ dis-
cussed in the prior semiannual report.[2] For wavenumber in-
tervals centered below 350 cm^{-1}, the Goody random band model
for the H_2O rotational band is used in LOTRAN, on the recom-
mendation of one of McClatchey's colleagues (J.E.A. Selby).

Parameters for this band model were taken from Goody,[35] Table 5.5.

In order to account for atmospheric slant paths along which the pressure p and temperature T, and therefore α_ν^{line}, vary--that is, in order to perform the integration in Eq. (4.19)--LOTRAN employs a version of the scaling (or effective mass) approximation. This approximation is an attempt to sum up z_1, z_2 and the p-T variation of $\alpha_\nu^{line}(z)$ into a single argument u called the 'effective absorber amount.' u is calculated using certain a priori assumptions concerning the pressure and temperature variation of α_ν^{line}, with parameters chosen to best fit the real data. Following Goody,[35] the scaling approximation assumes the following decomposition of α_ν^{line}:

$$\alpha_\nu^{line}(z) = \rho_a(z)\,\alpha_1(\nu)\,\alpha_2(p,T)$$

(the absorber density ρ_a is separated out because the mass absorption coefficient $\alpha_1\alpha_2$, an intrinsic property, is preferred by spectroscopists). The stimulated emission correction has been omitted from explicit consideration, but the effects of stimulated emission are present in the LOTRAN model insofar as certain parameters are determined, at least in part, from measured transmissions*. The absorption optical depth (4.19) then becomes

$$\tau_{\nu,ab}(z_1,z_2) = \alpha_1(\nu)\int_{z_1}^{z_2}\rho_a(z)\,\alpha_2(p,T)\,dz$$

$$= \kappa_\nu\,u(z_1,z_2) \qquad (4.21)$$

. . . .

*McClatchey, private communication.

where

$$k_\nu = \alpha_1(\nu)\alpha_2(p_0,T_0)$$

$$u(z_1,z_2) = \int_{z_1}^{z_2} \rho_a(z) \frac{\alpha_2(p,T)}{\alpha_2(p_0,T_0)} dz \qquad (4.22)$$

and p_0 and T_0 are taken in LOTRAN as STP (1 atm., $273^\circ K$). u is the equivalent absorber amount on the vertical path between z_1 and z_2. The further assumption is then made that α_2 has the form

$$\alpha_2(p,T) = Ap^{\lambda_1}T^{\lambda_2}$$

Different values of γ_1, chosen to give a best fit to line-by-line transmissions, are used in LOTRAN for each category of absorber (a)-(e).

Unfortunately, because of lack of good data on line strengths as a function of temperature, it has not been possible to obtain best values of γ_2 in the same way. An attempt has been made to include the temperature dependence of the line half-width by using $p/T^{\frac{1}{2}}$ instead of p, so that at present $\gamma_2 = -\gamma_1/2$, but it is not at all certain that this leads to less error nor that $T^{-\frac{1}{2}}$ is indeed the correct temperature dependence of the half-width. A prescription for putting temperature dependence into $T_{\Delta\nu}$ has been proposed by Kondratyev and Timofeev.[39] These authors claim that transmission errors of up to .1 - .2 may result if temperature dependence is not accounted for, even if one uses the Curtis-Godson approximation instead of scaling. Therefore more work is needed on this question.

Many IR radiative transfer studies employ the Curtis-Godson approximation (see Armstrong[40] for an excellent discussion) rather than the scaling approximation. Very few comparisons have been made, however, of Curtis-Godson and scaling with exact calculations. Two such comparisons are that of Kondratyev and Timofeev, discussed in the last paragraph, and that of Zdunkowski and Raymond.[41] The first concludes that Curtis-Godson and scaling incur comparable errors. The second concludes that, while Curtis-Godson has the edge in accuracy, the scaling approximation is accurate to at least two decimal places for a wide range of path lengths. Thus it appears to be justified to use the scaling approximation, especially for applications such as the present one in which errors in any one frequency interval are mitigated by the integration over all frequencies.

4.6 SEPARATION OF INTENSITY INTO SOLAR AND DIFFUSE PARTS

Because the solar beam and the specular reflection (if any) of the solar beam are essentially δ-functions in angle, it is customary before solving the radiative transfer equation numerically to eliminate these beams from explicit consideration via the following transformation:

$$i_\nu = \begin{cases} \overline{I}_\nu - \overline{I}_\nu^{spec} & -1 \le \mu < 0 \\ \overline{I}_\nu - \overline{I}_\nu^{solar} & 0 < \mu \le 1 \end{cases} \tag{4.21}$$

i_ν, the diffuse intensity, may be expected to behave 'smoothly' as a function of angle, that is, to be amenable to angular quadrature schemes which assume i_ν can be approximated by a low-order polynomial in μ. The solar intensity $\overline{I}_\nu^{solar}$ and the specularly reflected solar intensity $\overline{I}_\nu^{spec}$ are obtained by considering the incident solar beam to be acted upon only

75

by extinction κ_ν and specular reflection $\rho'_{\nu,s}$:

$$\overline{I}_\nu^{solar} = \frac{S_\nu}{2\pi} e^{-\tau_\nu(z)/\mu} \delta(\mu-\mu_0)$$

$$\overline{I}_\nu^{spec} = \frac{S_\nu}{2\pi} \rho'_{\nu,s}(|\mu|) e^{[2\tau_\nu(z_0)-\tau_\nu(z)]/\mu} \delta(\mu+\mu_0)$$

where

$$\tau_\nu(z) = \int_0^z \kappa_\nu(z')dz' \quad .$$

is the optical depth measured from the top of the atmosphere.

If the transformation (4.21) is applied to the radiative transfer equation (4.6), the boundary conditions (4.10) and (4.14), and the flux equation (4.7), the results are:

$$\mu\frac{\partial i_\nu}{\partial z} + \kappa_\nu i_\nu = \alpha'_\nu B_\nu + \frac{\beta_\nu}{2}\int_{-1}^1 \overline{P}_\nu(z,\mu,\mu')i_\nu(z,\mu')d\mu'$$

$$+ \frac{\beta_\nu S_\nu}{4\pi} \overline{P}_\nu(z,\mu,\mu_0) e^{-\tau_\nu(z)/\mu_0}$$

$$+ \frac{\beta_\nu S_\nu}{4\pi} \rho'_{\nu,s}(\mu_0)\overline{P}_\nu(z,\mu,-\mu_0)e^{-[2\tau_\nu(z_0)-\tau_\nu(z)]/\mu_0}$$

$$\hspace{13cm} (4.22)$$

$$i_\nu(0,\mu) = 0, \hspace{2cm} 0 < \mu \le 1 \hspace{1.5cm} (4.23)$$

$$i_\nu(z_0,\mu) = \varepsilon_\nu'(|\mu|)B_\nu(T_g) + \rho_{\nu,s}'(|\mu|)i_\nu(z_0,|\mu|)$$

$$+ 2\int_0^1 d\mu' \; \overline{\rho}_{\nu,d}''(|\mu|,\mu')i_\nu(z_0,\mu')\mu'$$

$$+ \frac{S_\nu}{\pi}\mu_0\,\overline{\rho}_{\nu,d}''(|\mu|,\mu_0)\,e^{-\tau_\nu(z_0)/\mu_0}, \quad -1 \le \mu < 0$$

$$(4.24)$$

$$F_\nu(z) = 2\pi\int_{-1}^1 \mu i_\nu(z,\mu)d\mu + \mu_0 S_\nu \, e^{-\tau_\nu(z)/\mu_0}$$

$$- \mu_0 S_\nu \rho_{\nu,s}'(\mu_0)\,e^{-[2\tau_\nu(z_0)-\tau_\nu(z)]/\mu_0} \qquad (4.25)$$

These are the equations which are solved numerically in ATRAD.

There are two functions in Eqs. (4.22) and (4.24) which, if they were not smooth functions of angle, could destroy the assumed smoothness of i_ν as a function of μ; they are the phase function $\overline{P}_\nu$ and the diffuse bidirectional reflectivity $\overline{\rho}_{\nu,d}''$. The strongest peak in P_ν is due to forward scattering by aerosol particles; therefore, ATRAD incorporates an approximation wherein this sharp peak is replaced by a δ-function, leaving a truncated phase function which is much smoother (see Section 4.7.5). The same procedure can be applied to a broadened reflection peak in $\rho_{\nu,d}''$, such as might be caused by a slightly disturbed ocean surface. That is, the peak will be approximated by a δ-function and lumped into the specular reflectivity $\rho_{\nu,s}'$, leaving a truncated and much smoother diffuse bidirectional reflectivity $\rho_{\nu,d}''^{(trunc)}$ for use in the boundary condition (4.24).

4.7 SCATTERING TREATMENT

4.7.1 Rayleigh Scattering

The Rayleigh volume scattering coefficient,

$$\beta_{v,R} = \frac{8\pi^3}{3} \frac{(n_s^2-1)^2}{\lambda^4 N_s^2} \left(\frac{6+3\rho_n}{6-7\rho_n}\right) \frac{p}{kT}$$

and the Rayleigh phase function for unpolarized light

$$P_R(\mu_s) = \frac{3(1+\rho_n)}{4+2\rho_n} \left(1 + \frac{1-\rho_n}{1+\rho_n} \mu_s^2\right)$$

are taken from the review article of Penndorf.[42] The various quantities in these equations are:

n_s = index of refraction of air at 760 mm Hg and 15°C

λ = wavelength

N_s = number density of air molecules at 760 mm Hg and 15°C = 2.54743×10^{19} cm^{-3}

ρ_n = depolarization factor

k = Boltzmann's constant

μ_s = cosine of scattering angle

n_s is calculated according to the new empirical formula of Peck and Reeder,[43] which supersedes the older Edlen formula.[42] ρ_n, which is a measure of the anisotropy of the air molecules, is taken as 0.0303 following Gucker, et.al.[44]

4.7.2   Mie Scattering, Single Sphere

Mie scattering of a plane wave of wavelength λ from an aerosol particle of radius a is described rigorously by the following infinite series: [15]

$$\sigma_{ext} = \frac{\lambda^2}{2\pi} \sum_{n=1}^{\infty} (2n+1) \ \mathrm{Re}(a_n + b_n) \tag{4.26}$$

$$\sigma_{sca} = \frac{\lambda^2}{2\pi} \sum_{n=1}^{\infty} (2n+1)(|a_n|^2 + |b_n|^2) \tag{4.27}$$

$$\sigma_{abs} = \sigma_{ext} - \sigma_{sca}$$

$$i_1 = \left| \sum_{n=1}^{\infty} \frac{2n+1}{n(n+1)} \left[a_n(\alpha,m)\,\pi_n(\mu_s) + b_n(\alpha,m)\,\tau_n(\mu_s) \right] \right|^2 \tag{4.28}$$

$$i_2 = \left| \sum_{n=1}^{\infty} \frac{2n+1}{n(n+1)} \left[a_n(\alpha,m)\,\tau_n(\mu_s) + b_n(\alpha,m)\,\pi_n(\mu_s) \right] \right|^2 \tag{4.29}$$

where

$$\alpha = \frac{2\pi a}{\lambda}$$

m = complex index of refraction
$\quad = n_1 - i n_2$

$\beta = m\alpha$

79

$$a_n = \frac{\psi_n(\alpha)\psi_n'(\beta) - m\,\psi_n(\beta)\psi_n'(\alpha)}{\zeta_n(\alpha)\psi_n'(\beta) - m\,\psi_n(\beta)\zeta_n'(\alpha)}$$

$$b_n = \frac{\psi_n(\beta)\psi_n'(\alpha) - m\,\psi_n(\alpha)\psi_n'(\beta)}{\psi_n(\beta)\zeta_n'(\alpha) - m\,\zeta_n(\alpha)\psi_n'(\beta)}$$

$$\pi_n(\mu) = P_n'(\mu)$$

$$\tau_n(\mu) = \mu\pi_n(\mu) - (1-\mu^2)\pi_n'(\mu) \quad .$$

The P_n are Legendre polynomials and the ψ_n, ζ_n are Ricatti-Bessel functions. σ_{ext}, σ_{sca}, and σ_{abs} are the extinction, scattering, and absorption cross sections of the particle. i_1 and i_2 describe the patterns of scattered intensity polarized perpendicular and parallel to the scattering plane (determined by incident and scattered beams), respectively. For the unpolarized light treatment assumed in ATRAD, the pattern of scattered intensity is proportional to $i_1 + i_2$.

It can be shown that σ_{sca} is related to the integral of $i_1 + i_2$ over all scattering angles Ω_s:

$$\sigma_{sca}(\alpha) = \left(\frac{\lambda}{2\pi}\right)^2 \int_{4\pi} [i_1(\alpha,\mu_s) + i_2(\alpha,\mu_s)]d\Omega_s \quad . \qquad (4.30)$$

The numerical evaluation of the infinite series, Eqs. (4.26) through (4.29), while seemingly straightforward, has sources of error which are related to the accumulation of round-off error in recursively calculating ψ_n, ζ_n, π_n, and τ_n. Techniques to eliminate these errors have been discussed by numerous authors. Dave,[45] Kattawar and Plass,[46] and Denman, Heller, and Pangonis[47] are the primary sources of the present ATRAD formulation of the series

80

summation, in subroutine MIESCT. Calculated results were compared with the graphs of Kerker[15] and the tables of Deirmendjian[48] and of Denman, et.al.[47] Agreement was found in all cases with the published results.

The Mie scattering calculation requires the aerosol complex index of refraction $m_\nu(z)$ as a function of frequency and height. This is the least well-known, for the real atmosphere, of all the required aerosol data. Excellent m_ν data are available for water; we have selected the measurements of Irvine and Pollack,[49] Rusk, et.al.,[50] and Robertson and Williams[51] for inclusion in ATRAD (subroutine IOR). Even for water, however, the uncertainty in the real part of m_ν is as high as 5 percent and in the imaginary part as high as 20·25 percent. Somewhat less accurate data are available for ice,[49] aqueous solutions of NaCl,[52] carbonaceous aerosol,[53,54] and quartz,[55] all of which have been included in ATRAD. The above substances have each been studied by several investigators, so at least the data have been measured independently. No such independent evaluation exists for the index of refraction measurements of Volz,[56,57] who studied sea salt, dust, Sahara dust, and several samples of water-soluble aerosol material; nevertheless, these data have also been included in ATRAD.

Aerosol materials, of course, have highly variable compositions and are subject to uncertainties regarding their chemical and physical states.

A large number of transmission spectra have been taken for atmospheric dust and for individual components of atmospheric dust.[58,59,60] These spectra indicate strong dust absorption in the atmospheric window region 8-13μ, which could have a pronounced effect on radiative heating. However,

more data than the transmission spectrum of a substance are needed to deduce the index of refraction. Even less is known about the index of refraction of many other inorganic aerosol constituents. As for the organic aerosol fraction, which is considerable,[61] the lack of data is almost complete.

4.7.3 Mie Scattering, Polydispersion

In reality, the atmospheric aerosol consists of particles with a wide range of radii a. This variation is described by a size distribution function,

$$N_{aer}(z) \, n(a,z) \qquad , \qquad a_{min} \leq a \leq a_{max}$$

where $N_{aer}(z)$ is the total number density of aerosol particles at height z and $n(a,z)$ is the normalized distribution of radii at height z, defined such that

$$n(a,z)\,da = \text{fraction of particles at height z with radii in } (a,a+da)$$

$$\int_{a_{min}}^{a_{max}} n(a,z)\,da = 1 \quad .$$

The separation of N_{aer} from n is convenient because in practical applications we often assume n is independent of z. The volume scattering and absorption coefficients for an aerosol described by such a size distribution are

$$\beta_{\nu,M}(z) = N_{aer}(z) \int_{a_{min}}^{a_{max}} \sigma_{sca}(\alpha) \, n(a,z)\,da \qquad (4.31)$$

$$\alpha_{\nu,M}(z) = N_{aer}(z) \int_{a_{min}}^{a_{max}} \sigma_{abs}(\alpha) \, n(a,z) \, da \quad . \qquad (4.32)$$

The pattern of scattered intensity will be proportional to

$$N_{aer}(z) \int_{a_{min}}^{a_{max}} [i_1(\alpha,\mu_s) + i_2(\alpha,\mu_s)] \, n(a,z) \, da \quad .$$

Normalizing this so that its integral over all scattering direc-tions Ω_s is 4π, we obtain the Mie phase function

$$P_{\nu,M}(z,\mu_s) = 4\pi \frac{\int_{a_{min}}^{a_{max}} [i_1(\alpha,\mu_s) + i_2(\alpha,\mu_s)] \, n(a,z) \, da}{\int_{4\pi} d\Omega_s \int_{a_{min}}^{a_{max}} [i_1(\alpha,\mu_s) + i_2(\alpha,\mu_s)] \, n(a,z) \, da}$$

Inverting the order of integration in the denominator and employing the relationships of Eqs. (4.30) and (4.31),

$$P_{\nu,M}(z,\mu_s) = \frac{\lambda^2 N_{aer}(z)}{\pi \beta_{\nu,M}(z)} \int_{a_{min}}^{a_{max}} [i_1(\alpha,\mu_s) + i_2(\alpha,\mu_s)] \, n(a,z) \, da$$
$$(4.33)$$

Various analytic forms for $n(a,z)$ have been proposed. Perhaps the most popular is the Junge power-law distribution[62] $(ca^{-\gamma})$; in the American literature Derimendjian's modified gamma distribution[63] $(ca^{\gamma} e^{-ba\delta})$ for haze and cloud is also used extensively. Log-normal distributions

83

$$\left(\frac{1}{\sigma\sqrt{2\pi}\,a}\, e^{-\ln^2(r/r_o)/2\sigma^2} \right)$$

are used by some European and Russian aerosol researchers.[64,65] Twomey, et.al.,[66] employ Gaussian distributions, but these are not in general use because most available data indicate an asymmetrical distribution of aerosol sizes. With the exception of the Junge distribution, which is unrealistically monotonic for all a, the data do not favor one size distribution formula over another. All of the above are included as options in ATRAD.

The dependence of $N_{aer}(z)$ on z for the cloudless atmosphere has been investigated extensively;[67,68,69,70,71] certain regularities have been determined. Eltermann,[72] for example, has proposed a clear standard atmosphere with a prescription for $N_{aer}(z)$ which has been included in ATRAD as an option. In clouds, N_{aer} may vary widely,[64] but most models ignore this and assume homogeneous clouds. The variation of N_{aer} (as well as n) near a cloud's upper and lower boundaries may have important consequences for atmospheric heating, however, and should not be ignored. Such variations can be incorporated quite straightforwardly, within the framework of the ATRAD formalism.

A further complication for realistic aerosols is that the size distribution and the index of refraction depend on the relative humidity.[73,74] Hygroscopic aerosols may begin to take up water at a relative humidity as small as 50 percent. Hence it is impossible to specify realistic atmospheric structure data for ATRAD without taking this variable into consideration.

4.7.4   Numerical Integration Over Aerosol Size Distribution

Techniques for performing the numerical integrations over size distribution in Eqs. (4.31) - (4.33) are far from standard. Most investigators use trapezoidal quadrature on the grounds that σ_{sca}, σ_{abs}, i_1, and i_2 oscillate so rapidly and non-uniformly with α that more sophisticated quadrature schemes are less accurate. This, of course, is a tacit admission that their integration meshes are not fine enough to resolve the oscillations. However, the present authors performed several integrations over size in which the oscillations <u>were</u> resolved, and the improvement in accuracy was too small (never more than a few percent) to warrant the additional computing cost — especially in light of uncertainties in the Mie input data for a real aerosol. Therefore, Romberg quadrature,[75] which is based on multiple trapezoidal quadratures, was selected for use in ATRAD.

The comprehensive study of Deirmendjian[63] proved useful in ascertaining suitable integration increments $\Delta\alpha$ for the Romberg quadrature. However, Deirmendjian's $\Delta\alpha$'s were chosen by trial-and-error; he did not determine a universal prescription for selecting $\Delta\alpha$'s small enough to ensure accuracy yet large enough to avoid wasting computer time. Studies by Dave[76,77] indicate the danger of selecting $\Delta\alpha$ too large and show that a $\Delta\alpha$ which is satisfactory for integrating $\beta_{\nu,m}$ and $\alpha_{\nu,m}$, and $P_{\nu,M}$ for small angles, may be unsatisfactory for integrating $P_{\nu,M}$ for larger angles. However, Dave, whose work was restricted to water droplets in the visible spectrum, provides no rule for automatic selection of $\Delta\alpha$.

We have devised an automatic selection scheme for $\Delta\alpha$ which has proven successful in duplicating the extensive

tables of Deirmendjian.[63] It is based on our observations
that:

    (a)   as the upper limit of integration α_{max}
increases, computing expense increases
inordinately, because the number of
terms needed in the Mie series [Eqs. (4.26)
through (4.29)] is proportional to α ;

    (b)   the number of points necessary in the
integration mesh increases more or less
linearly with α_{max} ;

    (c)   the angular interval $\Delta\theta$ needed to re-
solve the forward peak in $P_{\nu,m}$ is in-
versely proportional to α_{max} , but away
from the peak progressively larger angular
steps may be taken.

In light of observations (a) and (b), it was decided
to perform the crudest of the Romberg trapezoidal integrations
with a step size

$$\Delta\alpha_o = \frac{\alpha_{max} - \alpha_{min}}{N_\alpha}$$

where

$$
N_\alpha = \begin{cases} N_{min} & \alpha_{max} \leq N_{min} \\[2ex] N_{min} + B(\alpha_{max} - N_{min}) & N_{min} < \alpha_{max} \leq N_{min} + \dfrac{N_{max} - N_{min}}{B} \\[2ex] N_{max} & \alpha_{max} > N_{min} + \dfrac{N_{max} - N_{min}}{B} \end{cases}
$$

and to terminate this integration (and, therefore, the more refined integrations with $\Delta\alpha = \frac{1}{2}\Delta\alpha_o$, $\Delta\alpha = \frac{1}{4}\Delta\alpha_o$, etc.) whenever the relative changes in $\beta_{\nu,M}$, $\alpha_{\nu,M}$, and $P_{\nu,M}$ resulting from addition of the next term are less than δ_o . The current ATRAD values of these parameters are

$$
N_{min} = 25 \qquad N_{max} = 80 \qquad B = 0.55 \qquad \delta_o = 0.001
$$

which are sufficient to reproduce the tables of Deirmendjian. By terminating the integration in this fashion, unnecessary computation is avoided.

The forward (diffraction) peak in $P_{\nu,M}$ for a particle of size parameter α is proportional to $[\ ]_{\nu,M}$

$$
F(z) = \left(\frac{2\, J_1(z)}{z} \right)^2
$$

where $z = \alpha \sin\theta$, and J_1 is the Bessel function of order one. This quantity is shown in Figure 4.3.

The actual forward peak will be a composite of the peaks for all $\alpha \epsilon [\alpha_{min}, \alpha_{max}]$. The sharpest of the component peaks is due to $\alpha = \alpha_{max}$, and therefore in order to resolve this peak, which varies substantially over $\Delta z \overset{\sim}{=} \alpha_{max} \Delta\theta = 1$, we pick an angular increment
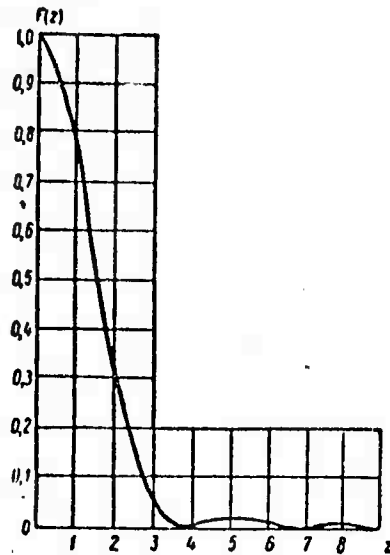
Figure 4.3 — Graph of F(z)

$$\Delta\theta_o = \frac{1}{2\,\alpha_{max}}$$

Actually, because the π_n's and τ_n's entering the Mie series [Eqs. (4.28) and (4.29)] are pre-calculated with a predetermined angular mesh $\Delta\theta_{tab}$, $\Delta\theta_o$ is selected to be the closest multiple of $\Delta\theta_{tab}$ to $1/2\,\alpha_{max}$. $\Delta\theta_o$ is also limited to be less than θ_m (currently 1°). The angular mesh on which $P_{\nu,M}$ is calculated is then taken as a user-supplied (see NSTEP, Appendix A) and even number of steps of $\Delta\theta_o$, then $2\Delta\theta_o$, then $4\Delta\theta_o$, etc., with the restriction that no step is larger than θ_{max} (currently 2.5°). The number of steps of each size is even so that a piecewise Simpson quadrature can be used to integrate $P_{\nu,M}$ in case truncation (Section 4.7.5) or renormalization (Section 4.7.7) is necessary.

4.7.5 Phase Function Truncation

Hansen[78] and Potter[79] have shown that the forward peak of the phase function $P_{\nu,M}$ can be truncated without significantly changing the results of the transport calculation. Thus, for $\theta \epsilon [0,\theta^t]$, where θ^t is the truncation angle, the real phase function $P_\nu(z,\theta)$ is 'replaced' (to within a normalization factor) by a truncated phase function $P_{\nu,M}^t(z,\theta)$ in the manner of Figure 4.4. The logarithm of $P_{\nu,M}^t$ is taken to be a linear function of θ on $[0,\theta^t]$ and the values of $P_{\nu,M}^t$ and its derivative are matched to those of $P_{\nu,M}$ at $\theta = \theta^t$.

Neither Hansen nor Potter propose a general method for selecting θ^t. Therefore we devised the following procedure: If $P_{\nu,M}$ for $\theta = 0$ is less than a prescribed P_{max} (currently 5), $P_{\nu,M}$ is not truncated. Otherwise, truncation is attempted at a succession of θ^t's beginning near $\theta = 0$ until either a successful truncation is achieved (such that $P_{\nu,M}^t(z,0) < P_{max}$) or θ^t exceeds θ^T (currently 20°). If θ^t exceeds θ^T first, $P_{\nu,M}$ is truncated at θ^T without regard to P_{max}, provided only that $P_{\nu,M}^t(z,0) < P_{\nu,M}(z,0)$. If the latter procedure is unsuccessful, $P_{\nu,M}$ is not truncated.

Mathematically, trunction amounts to approximating the forward peak, $P_{\nu,M} - P_{\nu,M}^t$, by a δ-function:

$$P_{\nu,M} = (P_{\nu,M} - P_{\nu,M}^t) + P_{\nu,M}^t$$

$$\simeq 4\pi F\, \delta(\vec{\Omega}' - \vec{\Omega}) + P_{\nu,M}^t$$

where F may be determined by integrating both sides over all scattering angles
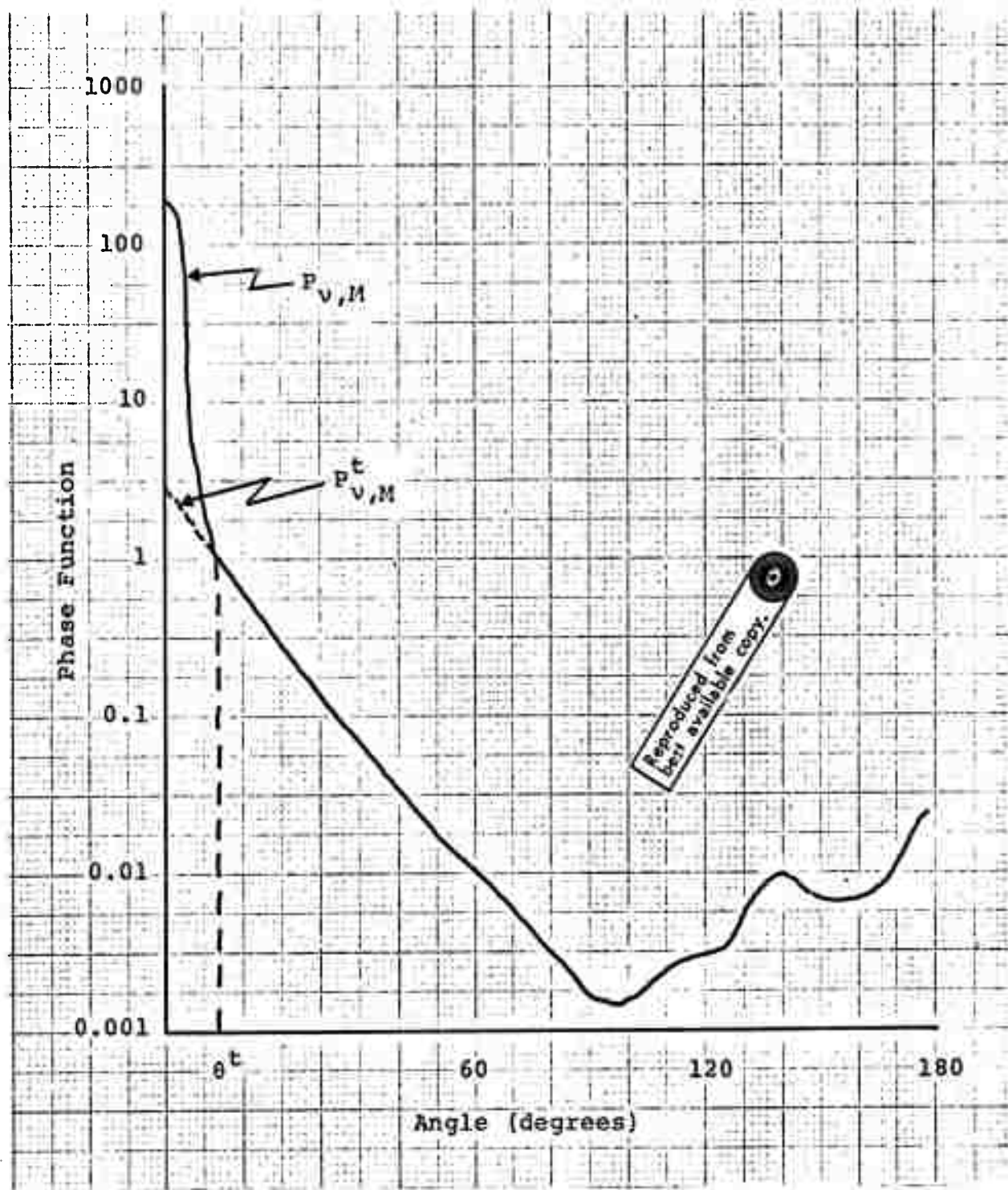
Figure 4.4 — Exact ($P_{\nu,M}$) and Truncated ($P^t_{\nu,M}$) Phase Function

$$F = \frac{1}{4\pi} \int_{4\pi} (P_{\nu,M} - P_{\nu,M}^t) d\Omega'$$

$$= \frac{1}{2} \int_0^\pi [P_{\nu,M}(z,\theta) - P_{\nu,M}^t(z,\theta)] \sin\theta \, d\theta$$

$$= \frac{1}{2} \int_0^{\theta^t} [P_{\nu,M}(z,\theta) - P_{\nu,M}^t(z,\theta)] \sin\theta \, d\theta \qquad (4.34)$$

F is determined numerically (in subroutine TRUNCT) using a Simpson quadrature.

Substituting the δ-function approximation into the scattering terms of the radiative transfer equation (4.6), and eliminating subscripts and unnecessary arguments for brevity,

$$\text{scat. terms} = \frac{\beta}{4\pi} \int P(\vec{\Omega},\vec{\Omega}') I(\vec{\Omega}') d\Omega' - \beta I(\vec{\Omega})$$

$$\simeq \frac{\beta}{4\pi} \int [4\pi F \, \delta(\vec{\Omega}'-\vec{\Omega}) + P^t] I(\vec{\Omega}') d\Omega' - \beta I(\vec{\Omega})$$

$$= \frac{\beta(1-F)}{4\pi} \int \frac{P^t(\vec{\Omega},\vec{\Omega}')}{1-F} I(\vec{\Omega}') d\Omega' - \beta(1-F) I(\vec{\Omega})$$

$$= \frac{\beta'}{4\pi} \int P'(\vec{\Omega},\vec{\Omega}') I(\vec{\Omega}') d\Omega' - \beta' I(\vec{\Omega}) \quad ,$$

where

$$\beta' \equiv (1 - F)\beta \quad ,$$

$$P' \equiv \frac{P^t}{1 - F} \quad .$$

91

Therefore, the scattering terms have their original form, but P and β are replaced by P' and β' defined above.

4.7.6 Azimuthal Integration

The aximuthally-averaged phase function $\overline{P}_\nu$. (Eq. (4.5)), not P_ν itself, is required in the ATRAD formulation of radiative transfer. The azimuthal average of the Rayleigh phase function (Section 4.7.1) is computed analytically in ATRAD, from

$$\overline{P}_R(\mu,\mu') = \frac{c_1}{2\pi} \int_0^{2\pi} (1 + c_2\, \mu_s^2)d\phi$$

$$= \frac{c_1}{2\pi} \int_0^{2\pi} [1+c_2(\mu\mu')^2+2c_2\mu\mu'\sqrt{(1-\mu^2)(1-\mu'^2)}\cos\phi$$

$$+ c_2(1-\mu^2)(1-\mu'^2)\cos^2\phi]d\phi$$

$$= c_1 [1 + c_2(\mu\mu')^2 + \frac{1}{2}c_2(1-\mu^2,(1-\mu'^2)]$$

where

$$c_1 = \frac{3(1 + \rho_n)}{4 + 2\rho_n} \qquad c_2 = \frac{1 - \rho_n}{1 + \rho_n}$$

The azimuthal average of the Mie phase function is computed numerically. The techniques are described in the prior semi-annual report of this contract.[2] The only change is that the quadrature has been changed from trapezoidal to Simpson in order to reduce errors affecting the renormalization procedure (section 4.7.7).

4.7.7 Renormalization of the Phase Function

There are two types of renormalization of the Mie phase function in ATRAD. The first operates on the Mie phase function $P_{\nu,M}$ before azimuthal averaging, and consists in multiplying all values of $P_{\nu,M}$ by the renormalization factor

$$\frac{2}{\int_{-1}^{1} P_{\nu,M}(z,\mu_s)d\mu_s}. \tag{4.35}$$

where the integral in the denominator is computed numerically using Simpson's Rule.

The second type of renormalization operates on the aximuthally averaged phase function $P_{\nu,M}$ and is required by the Grant and Hunt algorithm[2] in order to preserve flux conservation. In terms of the Gaussian angular quadrature mesh $0 < \mu_1 < \ldots < \mu_m \leq 1$ defined in the previous semiannual,[2] the numerical equivalent of the normalization condition

$$\int_{-1}^{1} \overline{P}_{\nu,M}(z,\mu,\mu')d\mu = 2 \tag{4.36}$$

is

$$\sum_{j=1}^{m} c_j \, \rho_{jk} = 2 \qquad (k = 1,\ldots,m) \tag{4.37}$$

where

$$\rho_{jk} = P_{jk}^{++} + P_{jk}^{+-}$$

$$P_{jk}^{++} = \overline{P}_{\nu,M}(z,\mu_j,\mu_k)$$

$$P_{jk}^{+-} = \overline{P}_{\nu,M}(z,\mu_j,-\mu_k)$$

There are several reasons why $\overline{P}_{\nu,M}$ will in general fail to satisfy Eq. (4.37). One is that Gaussian quadrature does not accurately represent Eq. (4.36); that is, $\overline{P}_{\nu,M}$ may not closely approximate a polynomial in μ. Also, errors are introduced in each step of the process by which $\overline{P}_{\nu,M}$ is constructed:

(a) the numerical computation of the Mie series (4.26)-(4.29)

(b) the numerical integration over the aerosol size distribution, Eq. (4.33)

(c) the numerical integration to obtain the truncation factor F, Eq. (4.34)

(d) the numerical integration over azimuth.

Tests have been run to determine ATRAD's errors from each of the four sources (a)-(d); it has been determined that in no case do they exceed 1%. Hence, the necessity for renormalization will be almost entirely due to the inadequacy of Eq. (4.37) as an approximation to Eq. (4.36).

Let us assume that the corrected values ρ_{jk}, satisfying Eq. (4.37), are to be obtained from the calculated values ρ_{jk}^{calc} by applying a multiplicative correction,

$$\rho_{jk} = (1 + \epsilon_{jk}) \, \rho_{jk}^{calc}$$

94

Unfortunately, there are $\frac{m(m-1)}{2}$ unknowns ε_{jk} (the number is reduced from m^2 by the symmetry requirement $\varepsilon_{kj} = \varepsilon_{jk}$) and there are only m equations (Eqs. (4.37)) to determine them. This underspecification can be handled in many ways, no one of which seems much preferable on physical grounds over any other. Grant* corrects only the diagonal elements, $\varepsilon_{jk} = \varepsilon_j \delta_{jk}$, and so has a determinate set of equations for the ε_j. He points out that the phase matrices ρ_{jk} are usually strongly diagonally dominant and that his procedure thus incorporates the entire correction where it makes the smallest relative change.

An alternative procedure has been investigated. Assume

$$\varepsilon_{jk} = \varepsilon_j + \varepsilon_k.$$

Then Eqs. (4.37) become

$$\sum_{j=1}^{m} (c_j \rho_{jk}^{calc} + b_k \delta_{jk}) \varepsilon_j = 2 - b_k \quad (k=1,\ldots,m)$$

where

$$b_k = \sum_{j=1}^{m} c_j \, \rho_{jk}^{calc}$$

and δ_{jk} is the Kronecker delta. This is a determinate set of linear equations for the ε_j.

Both Grant's method and our method of renormalization have been included as options in ATRAD. The effect of our

---

*Private communication.

method is, in practice, similar to Grant's; the largest corrections are made to the diagonal elements of ρ_{jk}. Progressively smaller relative corrections result when an element is farther from the diagonal. However, our method offers the advantage of spreading the correction, while Grant's procedure concentrates it entirely on the diagonal element. In our opinion it is difficult to justify correcting only a subset of the ρ_{jk}'s.

Several test calculations have been run in which the Henyey-Greenstein phase function,

$$\frac{1 - g^2}{(1 + g^2 - 2g\mu_s)^{3/2}}$$

was used for $P_{\nu,M}$, with $g = 0.8$ and $g = 0.95$ so that large forward scattering peaks were being tested. Twelve Gaussian angles (m=6) were used. For these examples, it was found that reasonably large (up to 8% for g=0.8 and up to 20% for g=0.95) renormalization corrections were necessary. The results point up to the importance of truncation to ensure that $\overline{P}_{\nu,M}$ can be treated by low-order Gaussian quadrature.

4.7.8   Total Phase Function

The total phase function $\overline{P}_\nu$ is obtained from $\overline{P}_R$ and $\overline{P}_{\nu,M}$ according to

$$\overline{P}_\nu = \frac{\beta_{\nu,R}\,\overline{P}_R + \beta_{\nu,M}\,\overline{P}_{\nu,M}}{\beta_\nu}$$

where

$$\beta_\nu = \beta_{\nu,R} + \beta_{\nu,M}$$

is the total volume scattering coefficient.

4.8   NUMERICAL SOLUTION OF THE RADIATIVE TRANSFER PROBLEM

The numerical methods employed to solve the radiative transfer problem, Eqs. (4.22)-(4.25), were presented in the previous semiannual.[2] Therefore only changes, improvements, and items omitted from that report are discussed in this section.

4.8.1 Source Doubling

The Planck source doubling scheme has been derived in a computationally more efficient form. The details are given in the paper we presented at the AMS Conference on Atmospheric Radiation (Fort Collins, Colo., Aug 1972); that paper is reproduced in Appendix C.

4.8.2 Treatment of Overlapping Bands

In many frequency groups $\Delta \nu$, more than one atmospheric constituent may contribute to the absorption. ATRAD then fits the transmission function $T_{\Delta\nu}^{(n)}$ of each individual constituent with an exponential sum,

$$T_{\Delta\nu}^{(n)}(u) \simeq \sum_{i=1}^{M^{(n)}} a_i^{(n)} e^{-k_i^{(n)} u^{(n)}}$$

Superscript 1 refers to H_2O, superscript 2 to the uniformly mixed gases CO_2, etc., and superscript 3 to O_3. The product of these individual transmission functions is taken as the total transmission,

$$T_{\Delta\nu} \simeq \sum_{i=1}^{M^{(1)}} \sum_{j=1}^{M^{(2)}} \sum_{\ell=1}^{M^{(3)}} a_i^{(1)} a_j^{(2)} a_\ell^{(3)} e^{-(k_i^{(1)} u^{(1)} + k_j^{(2)} u^{(2)} + k_\ell^{(3)} u^{(3)})}$$

Then $M = M^{(1)}M^{(2)}M^{(3)}$ monochromatic problems are calculated, one for each term of the triple sum, in each of which the optical depth of zone $[z,z']$ is

$$\Delta\tau(z,z') = k_i^{(1)}u^{(1)}(z,z') + k_j^{(2)}u^{(2)}(z,z')$$

$$+ k_\ell^{(3)}u^{(3)}(z,z')$$

and the line absorption coefficient at z is

$$\alpha^{line}(z) = -\frac{\partial}{\partial z}\Delta\tau(z,z')$$

$$= -k_i^{(1)}\frac{\partial}{\partial z}u^{(1)}(z,z') - k_j^{(2)}\frac{\partial}{\partial z}u^{(2)}(z,z')$$

$$- k_\ell^{(3)}\frac{\partial}{\partial z}u^{(3)}(z,z')$$

The z-derivatives of the u's are simply the integrands in the expressions (4.22) defining the u's.

4.8.3 Special Case of No Scattering in the Grant-Hunt Algorithm

In the case of negligible scattering it is not necessary to build up the solution from optically thin layers; simple analytic expressions for the reflection and transmission matrices and Planck source vectors can be derived for zones of arbitrary optical depth. These analytic expressions are obtained from the Grant-Hunt algorithm by taking the limit as the primary-layer thickness $\Delta\tau_p$ goes to zero. For the reflection and transmission matrices of a zone of optical thickness $\Delta\tau$, we obtain

98

$$r_{ij} = 0$$

$$t_{ij} = e^{-\Delta\tau/\mu_i} \delta_{ij}$$

For a Planck source which varies linearly in τ,

$$B_\nu(\tau) = B_\nu(\tau_0) + B_\nu'(\tau - \tau_0)$$

where

$$B_\nu' = \frac{B_\nu(\tau_0 + \Delta\tau) - B_\nu(\tau_0)}{\Delta\tau}$$

we obtain for the jth component of each source vector,

$$\Sigma^+_{plk_j} = B_\nu(\tau_0)(1 - e^{-\Delta\tau/\mu_j}) + \mu_j B_\nu'\left[\frac{\Delta\tau}{\mu_j} - (1 - e^{-\Delta\tau/\mu_j})\right]$$

$$\Sigma^-_{plk_j} = B_\nu(\tau_0)(1 - e^{-\Delta\tau/\mu_j}) + \mu_j B_\nu'\left[1 - (1 + \frac{\Delta\tau}{\mu_j}) e^{-\Delta\tau/\mu_j}\right]$$

These special case results are incorporated in ATRAD.

4.8.4 Exponential-Sum Fitting

The method of Cantor and Evans[80] for exponential-sum fitting is now incorporated into ATRAD, although numerous modifications and simplifications have been introduced in adapting the method to the fitting of transmission functions.

The method is briefly outlined in the following paragraphs.

We desire to fit a transmission function $T_{\Delta\nu}(u)$, whose values $T_{\Delta\nu}(u_n)$ are given at a set of points

$$0 = u_1 < u_2 < \ldots < u_N \quad,$$

with a positively-weighted sum of exponentials,

$$T_{\Delta\nu}(u) \simeq \sum_{i=1}^{M} a_i e^{-k_i u} \quad, \qquad a_i > 0$$

The fit is to be best in the least-squares sense, that is, it is to be such that the residual

$$R = \sum_{n=1}^{N} W_n \left[T_{\Delta\nu}(u_n) - \sum_{i=1}^{M} a_i e^{-k_i u_n} \right]^2$$

is minimized. The quantities W_n are positive weights which may be assigned arbitrarily. In order to ensure that small and large values of the transmission receive equal treatment, the weights have been taken as

$$W_n = 1/[T_{\Delta\nu}(u_n)]^2$$

so that R is in fact a sum of squared relative errors.

The u_n's are selected to be equally spaced,

$$u_n = (n-1)\Delta u$$

(this requirement will be partially relaxed in the near future). Then R may be written

$$R = \sum_{n=1}^{N} W_n \left[T_{\Delta\nu}(u_n) - \sum_{i=1}^{M} a_i \theta_i^{n-1} \right]^2$$

where

$$\theta_i = e^{-k_i \Delta u}$$

Let us presume the following ordering of the θ_i's:

$$0 \leq \theta_1 < \theta_2 < \ldots < \theta_M \leq 1$$

The problem of minimizing R is partly linear (finding $a_1, \ldots, a_M$) and partly nonlinear (finding $\theta_1, \ldots, \theta_M$). The algorithm which we shall describe below treats the linear and non-linear parts of the problem separately, although we shall see that there is some coupling.

Given a set of $\theta_1, \ldots, \theta_M$, we shall call the procedure of finding the $a_1, \ldots, a_M$ which minimize R with no constraints "solving the linear problem." Since the a_i's are unconstrained, solving the linear problem may produce one or more negative a_i's.

The extreme (and well-documented) ill-conditioning of the linear problem is side-stepped, as far as the calculation of the residual is concerned, by the use of divided differences, which is made possible by the use of equally-spaced u_n's . During the iteration between linear and non-linear problems, the a_i are of importance only in determining which exponential factors θ_i are to be dropped because of a negative coefficient.

101

To find the best θ_i's we proceed iteratively. Imagine that to the approximant

$$\sum_{i=1}^{m} a_i \theta_i^{n-1} \quad , \qquad a_i > 0$$

we add a new term with exponential factor θ and coefficient a. We want to see how the residual changes as we increase a from zero; therefore, we evaluate the slope of R at a=0:

$$\left\{ \frac{d}{da} \sum_{n=1}^{N} W_n \left[T_{\Delta\nu}(u_n) - \sum_{i=1}^{m} a_i \theta_i^{n-1} - a\theta^{n-1} \right]^2 \right\}_{a=0}$$

$$= -2 \sum_{n=1}^{N} W_n \left[T_{\Delta\nu}(u_n) - \sum_{i=1}^{m} a_i \theta_i^{n-1} \right] \theta^{n-1} \qquad (4.38)$$

which is simply a polynomial in θ. Since we want to minimize the sum of squares, we pick θ so that this expression is as negative as possible (if it is never negative for $0 \leq \theta \leq 1$, we are already at a best fit). In other words, we find the absolute minimum of the polynomial in (4.38) over $0 \leq \theta \leq 1$. This search was originally done by simply partitioning [0,1] into a large number of points ($\sim 1,000$) and finding the absolute minimum over that set of points. This kind of search proved to be quite expensive computationally, however, since it required evaluating an $(N-1)^{st}$ degree polynomial ($N \sim$ 15-50) at more than 1,000 points, for each iteration of the fitting process, for each molecular species, in every frequency level. Therefore, the search has been improved by taking into account the third derivative of the polynomial.

With this scheme large fractions of [0,1] can be eliminated
from consideration and convergence is accelerated in the
remainder of the interval. The new procedure requires far
fewer polynomial evaluations.

When the new exponential factor θ is added to the
previous ones and the linear problem for the coefficients is
solved we obtain an approximant

$$\sum_{i=1}^{m} b_i \theta_i^{n-1} + c\theta^{n-1}$$

Because the polynomial (4.38) was negative at θ, we know
that $c > 0$; but it may happen that some of the b_i's are
non-positive. In that case, we move on a straight line in
coefficient space from $(a_1,\ldots,a_m,0)$, the point represent-
ing the old coefficients, to $(b_1,\ldots,b_m,c)$, the point repre-
senting the new coefficients. We stop when we encounter the
first zero coefficient and eliminate the corresponding exponential
factor. Then we re-solve the linear problem and repeat the
above process if any of the resulting coefficients are non-
positive. When solving the linear problem finally yields all
positive coefficients, we are ready to solve the nonlinear
problem again.

In moving toward a solution of the linear problem, we
constantly diminish the residual as we proceed.

A diagram summarizing the algorithm follows:

Start with approximant = 0

Add new exponential factor $\theta \epsilon [0,1]$
which minimizes polynomial (4.38)

Solve linear problem for best coef-
ficients in least squares sense,
eliminating exponential factors as
needed to obtain positive coefficients.
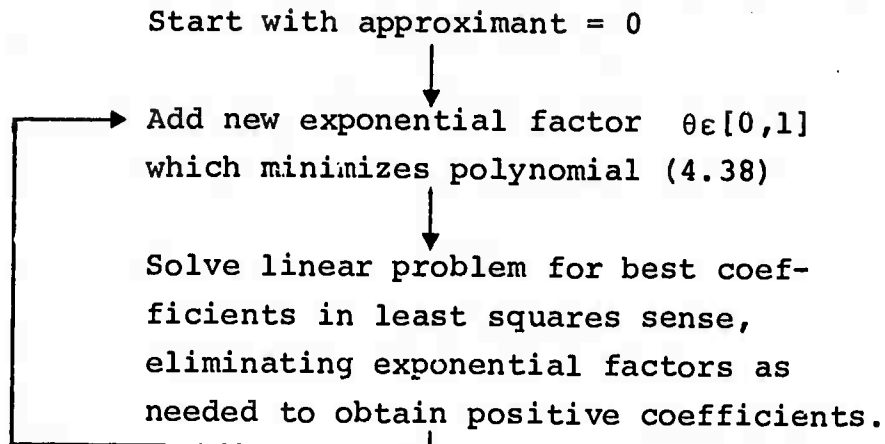
The algorithm is terminated when the residual R increases
from the preceding iteration or when its relative decrease is
at the noise level. Either situation indicates that a best
fit has been obtained and that the algorithm is "spinning its
wheels" due to round-off.

For the purposes of the radiation code, two clean-up
steps have been added to the algorithm for the sake of com-
putational efficiency.

First, it is often the case that the exponential factors
θ_i occur in very close pairs. Since every extra θ_i means
extra monochromatic problems to solve, it seemed reasonable to
replace each close pair (θ_i, θ_{i+1}) by a single θ_i with a
new coefficient. This procedure causes essentially no loss
in accuracy in the radiation computation.

Secondly, all coefficients which are small, $a_i \leq \epsilon$,
have the corresponding terms dropped from the approximant.
The remaining coefficients are renormalized so that they sum
to unity, in order to preserve flux conservation. Currently
we take $\epsilon = .005$, in view of inaccuracies in our transmission
functions of roughly 1%.

The polynomial (4.38) plays an important role in this
theory. Based on its minimum value for a given approximant,

104

a bound can be derived on the "distance" (in the least squares sense) between the best approximant and the given approximant. Also, a lower bound on the amount of improvement that will result from the next iterative step can be derived. Taken together, these bounds guarantee the convergence of the algorithm.

If the best fit is not perfect, then it can be shown that the exponential factors and coefficients of the best approximant are unique. In fact, the exponential factors will all be from among the roots between zero and one of the final polynomial (4.38).

4.9   ATRAD FLOW DIAGRAM

A simplified flow diagram of ATRAD is presented in Figure 4.5. The various boxes are self-explanatory. More detailed flow diagrams of the transmission function fitting and scattering boxes are presented in Figures 4.6 and 4.7.

In Figure 4.7, subroutine SETPAR either sets the parameters for one of the analytic aerosol size distributions in SIZDIS or reads size distribution data from cards. Subroutine IOR supplies index of refraction data. The dashed box refers to an option which is discussed in Section 4.10 and which has not yet been programmed.

Figure 4.5 — ATRAP Code Organization

LOOP OVER SPECIES (H_2O, CO_2+, O_3)

LOTRAN
(McClatchey)

GENERATE TRANSMISSION
FUNCTION DATA

FIT WITH SUM OF
EXPONENTIALS (Evans)

$$T_{\Delta v}^{(N)} = \sum A_I^{(N)} \varepsilon^{-K_I^{(N)} u}$$

END LOOP OVER SPECIES
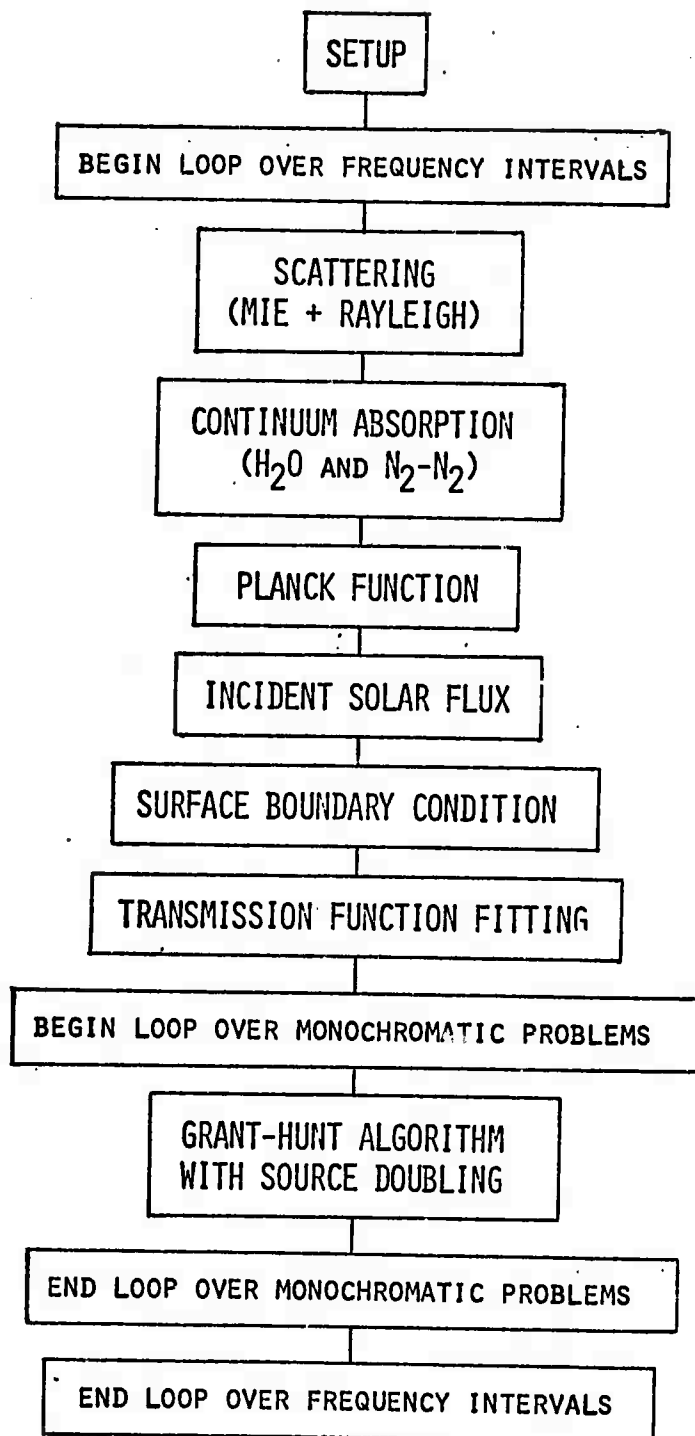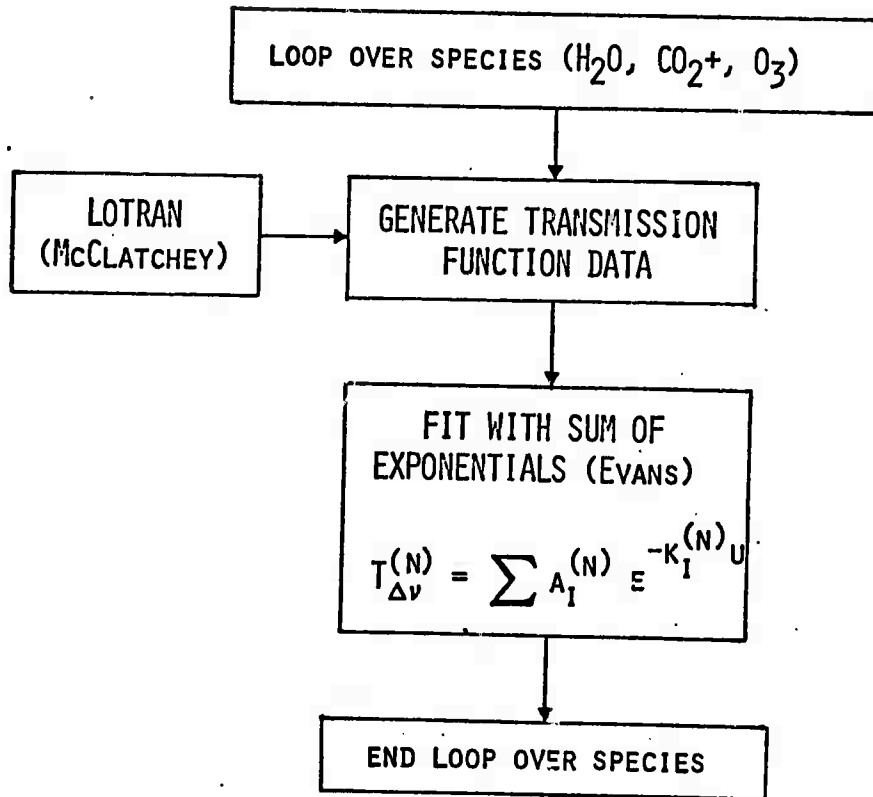
Figure 4.6 — Transmission Function Fitting
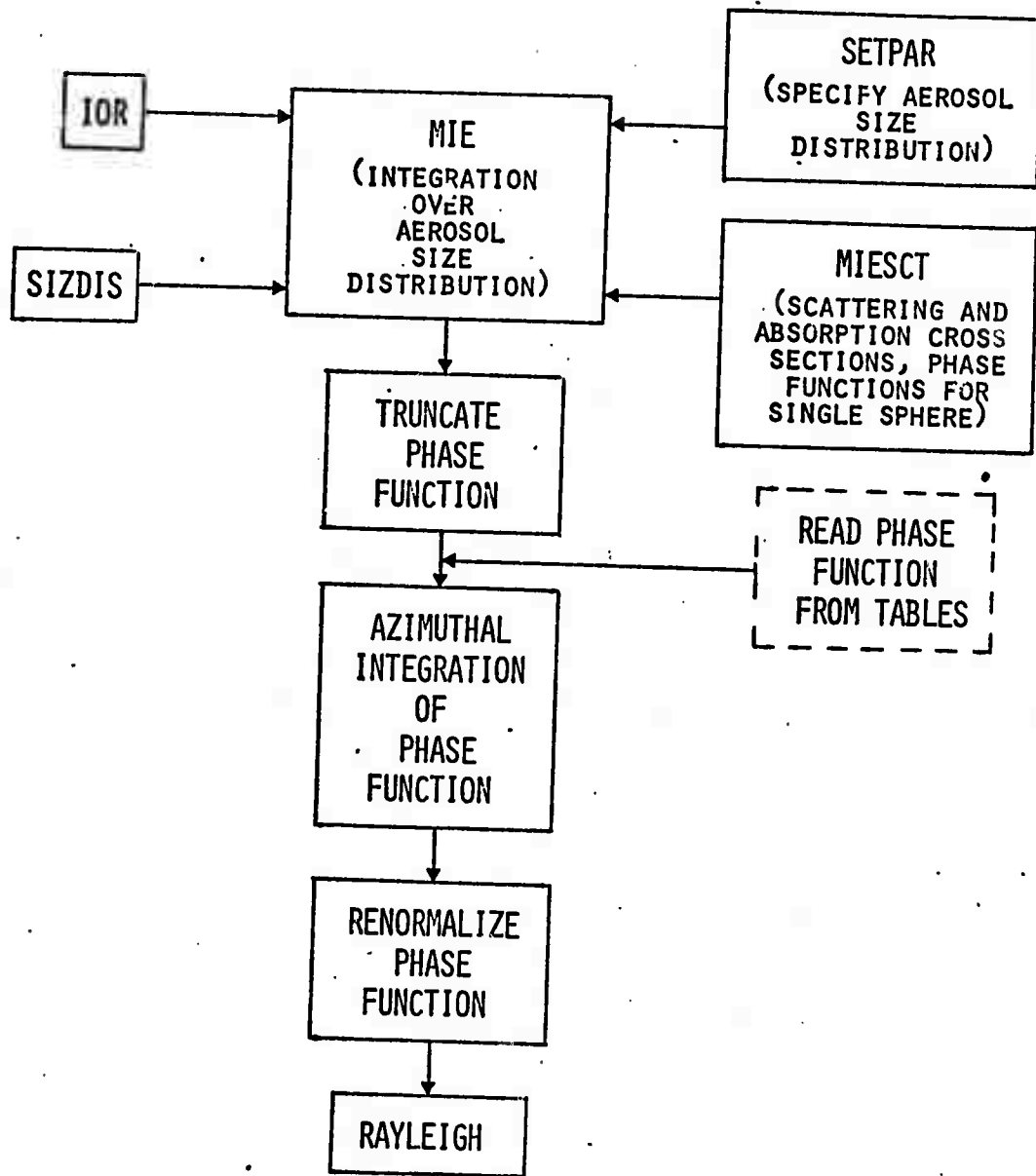
Figure 4.7 – Scattering Treatment

4.10 ATRAD COMPUTATIONAL COST; POSSIBLE IMPROVEMENTS IN EFFICIENCY

Two major realistic test problems, reported in Chapter 5, have now been calculated with ATRAD; numerous more idealized calculations have also been completed. From these calculations we have obtained a quite accurate estimate of how much computer time will be required for any particular problem and of the pacing items in the computation.

The average amount of UNIVAC 1108 computer time required for a complete run of ATRAD without aerosols is about .8 hour, or 48 minutes. With cloud aerosol included, the computing time may approximately double, although for haze aerosol the increase may be smaller. Therefore we are devoting considerable thought to improving the efficiency of the aerosol computation.

In spite of any improvements which we may make in the calculation of the Mie series (4.26)-(4.29), there is a certain irreducible amount of computation involved in forming the products $a_n \pi_n$, $b_n \tau_n$, $a_n \tau_n$, and $b_n \pi_n$. These four multiplications must be performed for every n, for every size parameter α, for every angle at which $F_{\nu,M}$ is tabulated, for every level at which aerosol is present, and for every frequency group. Making generous estimates of each of these factors, we obtain 5×10^8 multiplications for a complete problem. At roughly 5 μsec per multiplication, this amounts to 2,500 sec or about .7 hours.

We have two ideas on reducing the computing time in the Mie calculation. The first is simply to use a much coarser frequency group structure for the Mie calculation than for the problem itself, with some sort of extrapolation or interpolation to obtain Mie quantities on the finer mesh.

The frequency group structure of the problem is determined by the necessity to resolve rapidly varying quantities such as the solar flux S_ν, Rayleigh scattering coefficient $\beta_{\nu,R}$, Planck function B_ν, etc. The Mie quantities in general vary much more slowly with frequency.

The second approach is to calculate large tables of Mie quantities, store them on disc or fast drum, and then merely interpolate in these tables in subsequent ATRAD runs. New tabular entries could be made as new index of refraction data, size distribution data, etc., became available. This approach will probably be implemented in the near future.

A further pacing item in ATRAD is the matrix inversion subroutine used for doubling and for the foward pass of the Grant-Hunt algorithm. This routine was obtained from Bell Labs[81] and is unquestionably the best general matrix inverter available today. However, the matrices we are inverting have a special form which is not being exploited. We intend to consult with a few of the leading experts in linear algebra to determine if improvement can be achieved in the inversion of this particular matrix.

5. RADIATION IN THE EARTH'S ATMOSPHERE: ATRAD APPLICATIONS

This chapter presents the results of comparisons between the ATRAD code and the radiation subroutine of the Mintz-Arakawa global circulation code. The Mintz-Arakawa treatment is discussed in Section 5.1. The test problem results are presented in Section 5.2.

5.1 THE MINTZ-ARAKAWA RADIATION SUBROUTINE

The calculation of radiation heating and cooling in the Mintz-Arakawa (M/A) global circulation model (GCM) is necessarily a considerably simplified one in order to keep the computational work within practicality. In order to determine the size of the errors which result from this simplified radiative treatment, a series of comparisons of fluxes and heating rates calculated with the first-principles radiative transfer code, ATRAD, and those from the Mintz-Arakawa two-level GCM are being made. The results of the first two comparison cases corresponding to cloud-free conditions over land are reported in Section 5.2. In order to make these comparisons we performed calculations of radiative quantities with the M/A radiative subroutine corresponding to a particular epoch in a standard global circulation calculation. (We are indebted to A. B. Kahle of RAND for the M/A computer code and for input data for it.) In the

following section we outline the features of the M/A radiative model and describe how the input data for it are transcribed to the ATRAD code.

The M/A treatment as employed in the climate dynamics program of the RAND Corporation is described by Gates, et.al.[11], who give a definitive description of the formulation and code. We outline the principal features of the code here; however, we are particularly interested in specifying how the M/A atmosphere is constituted in order that we may provide a proper initialization for ATRAD.

The M/A radiative subroutine determines the radiative heating rate in two layers of the atmosphere and the radiative flux into the surface. Each of the layers contains one-half of the mass of the atmosphere lying below the 200 mb level. The part of the atmosphere above 200 mb is not explicitly contained in the M/A calculation but is included in ATRAD. The relevant radiative quantities to determine atmospheric heating are completely specified by giving the net radiative fluxes at the boundaries of these levels; in terms of the variable σ denoting the fraction of the atmosphere below 200 mb these are $F(\sigma = 0)$ at the 200 mb level, $F(\sigma = 0.5)$ in the middle of the atmosphere, and $F(\sigma = 1.0)$ at the lower boundary of the atmosphere. These three altitudes are included among the zone boundaries of ATRAD for which radiative fluxes are calculated.

The radiative model of the M/A code distinguishes three spectral regions in which different radiative calculations are performed. Taking advantage of the fact that there is little overlap between the solar and thermal radiative sources, the major frequency division is between long-wave and short-wave radiation. The frequency dividing these regions is not specified in the M/A code but is chosen to be at

4μ for the purposes of editing data from ATRAD. In the long-wave region the M/A code takes account only of thermal emission and absorption by the atmosphere and the ground. In the short-wave case where thermal emission is neglected the spectrum is divided at 0.9μ into two parts; in the near IR region the solar radiation is assumed to be absorbed but unscattered, while in the remaining spectral interval it is assumed to be unabsorbed but Rayleigh scattered. Using these spectral intervals, the results of the M/A calculation can be presented as a matrix of nine net fluxes, corresponding to the three spectral intervals and the three altitudes.

The most important atmospheric absorber for typical atmospheric conditions is water vapor. The M/A calculation takes account principally of the effect of water vapor, incorporating empirical corrections for the effect of CO_2. Based on a single value Q_3 of the water vapor mixing ratio at $\sigma = 3/4$, and an assumed saturated vapor pressure above 120 mb in the stratosphere, the code interpolates a profile of water vapor density. The vertical profile, Q, as a function of pressure, p, in mb is given by

$$Q = Q_3 \left(\frac{p}{p_3} \right)^k \quad , \qquad p \geq 120 \text{ mb} \quad ,$$

$$Q = \frac{2.06255 \times 10^{-4}}{p} \quad , \qquad p < 120 \text{ mb} \quad . \tag{5.1}$$

p_3 is the pressure at $\sigma = 3/4$ and the constant k is determined by matching the values of Q at 120 mb:

$$k = \frac{\ln(Q_3/1.7188 \times 10^{-6})}{\ln(p_3/120 \text{ mb})} \quad .$$

Using this profile the effective water vapor amount, including a factor for the pressure broadening of the absorption lines, is calculated between altitude levels. This quantity is subsequently used to form the absorptivity of each layer for the near IR short-wave radiation and the transmissivity of each layer for the IR radiation.

Equation (5.1) is also used to form the water vapor density input data for the ATRAD code. In addition, it is necessary to interpolate and extrapolate the temperature. The M/A code makes use of the calculated values of temperature T_1 in the upper layer and T_3 in the lower layer. From these values the temperatures at the 200 mb level and at the boundary between the upper and lower layer are found by invoking the following functional dependence of temperature on pressure:

$$T = \frac{\theta_3 - \theta_1}{p_3^\kappa - p_1^\kappa} (p^\kappa)^2 + \frac{\theta_1 p_3^\kappa - \theta_3 p_1^\kappa}{p_3^\kappa - p_1^\kappa} p^\kappa \quad , \tag{5.2}$$

where $\kappa = R/C_p$ and

$$\theta = T/p^\kappa$$

is proportional to potential temperature. Equation (5.2) insures that the prescribed values of temperature at p_1 ($\sigma = 1/4$) and p_3 ($\sigma = 3/4$) are recovered and in addition, the temperature becomes zero at $p = 0$. In addition, the air temperature near the ground at the top of the boundary layer, T_4, is also calculated in the M/A code from a consideration of

114

the fluxes of static energy between the ground and level 3 (σ = 3/4). Subsequent adjustments of the original input temperatures may take place from convection. In order to specify the initial temperature profile for the ATRAD code, we use Eq. (5.2) from σ = 0 to σ = 3/4. To determine temperatures from σ = 0.75 to σ = 1.0, we use the same expression adjusted to match T_3 and T_4:

$$T = \frac{\theta_4 - \theta_3}{p_4^K - p_3^K} (p^K)^2 + \frac{\theta_3 p_4^K - \theta_4 p_3^K}{p_4^K - p_3^K} p^K \quad , \quad P_3 \leq P \leq P_4 \quad . \quad (5.3)$$

Finally, in the region above 200 mb, where the M/A code gives no guidance, we provide a rough simulation of the stratospheric temperature rise, using an expression which is continuous with T_o at p_o = 200 mb .

$$T = T_o \frac{(p_o + k_1)}{(p + k_1)} \quad , \quad 0 \leq P \leq P_o \quad . \quad (5.4)$$

Having specified the relation between temperature and pressure throughout the atmosphere, we can proceed to the determination of the altitude by using the hydrostatic relationship,

$$Z - Z_4 = \frac{R}{g} \int_p^{P_4} \frac{T}{p} \, dp \quad ,$$

where Z_4 is the altitude of the surface and we have neglected the effect of water vapor in the atmosphere. In view of the several analytic forms given above for the temperature-pressure relationship, we have approximated it by linear expressions, $T = A + Bp$, within each of the ATRAD zones which are of the order of 25 mb thick. The altitude of zone I becomes

$$Z(I) = Z(I-1) + \frac{R}{g}\left[A \ln \frac{P(I-1)}{P(I)} + B\left(P(I-1) - P(I)\right)\right] \quad , \qquad (5.5)$$

where

$$A = \frac{T(I-1)\ P(I) - T(I)\ P(I-1)}{P(I) - P(I-1)}$$

and

$$B = \frac{T(I) - T(I-1)}{P(I) - P(I-1)} \quad .$$

We have chosen $Z(1) = 0$, thereby measuring the altitude relative to the surface.

5.2   TEST PROBLEMS

Two different locations on the Earth's surface were chosen for comparison calculations. The criteria for choosing these locations were first, that they be the centers of grid squares in the M/A code, second, that the M/A code predict no clouds for the chosen points, and third, that the chosen points have substantially different water vapor profiles. Two such locations were found in the M/A run that was furnished to us. The first (Problem 1) was at 14°N, 20°E, in Chad (in the Sahara desert). The second (Problem 2) was at 18°S, 65°W, in Bolivia. Temperature profiles and water vapor profiles for the two problems, as extracted from M/A by the methods of the previous section, are shown in Figures 5.1 and 5.2, respectively. Since M/A does not calculate ozone profiles, an analytic ozone profile taken from Green,[82]
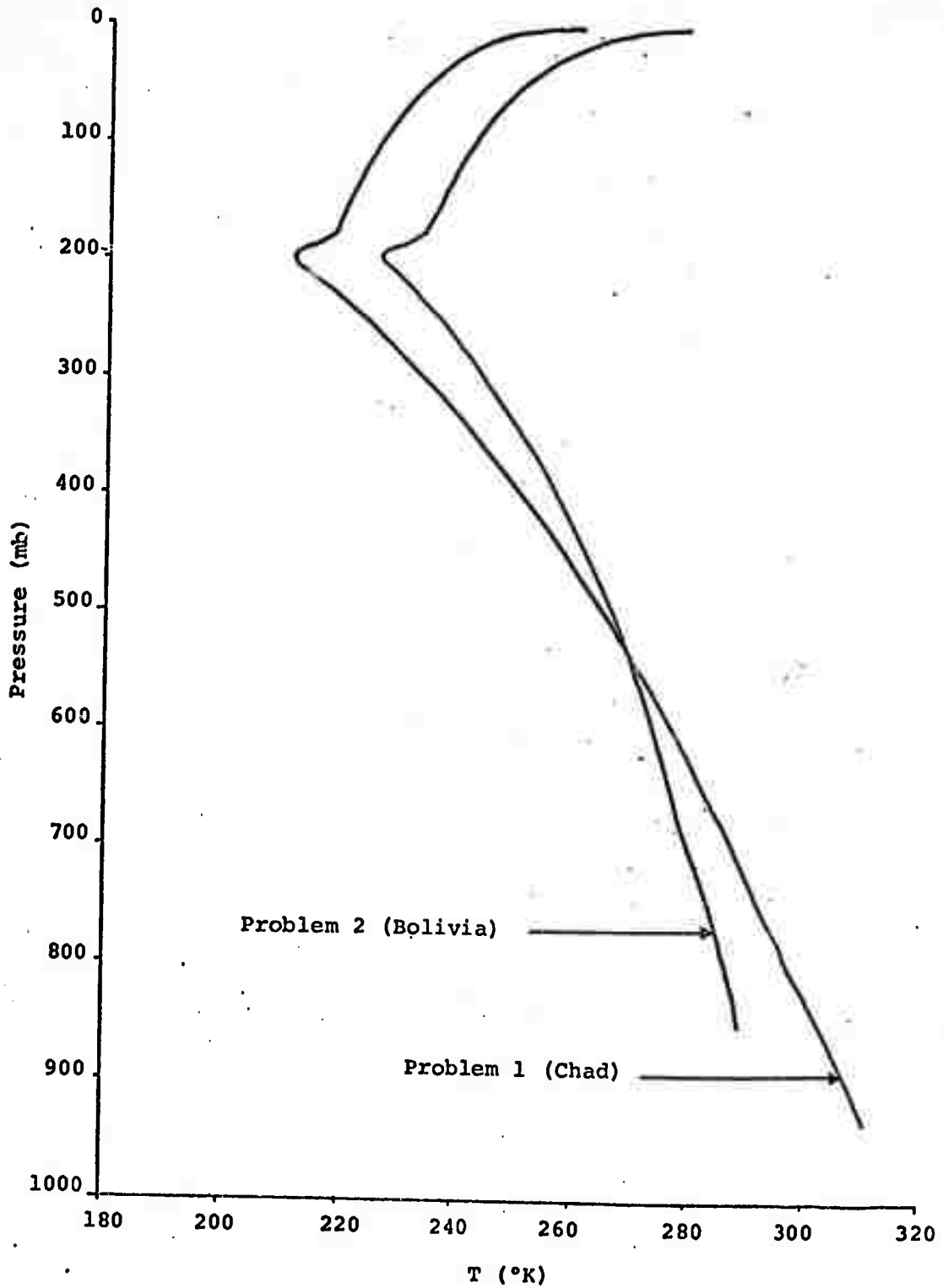
Figure 5.1 — Test Problem Temperature Profiles.

117
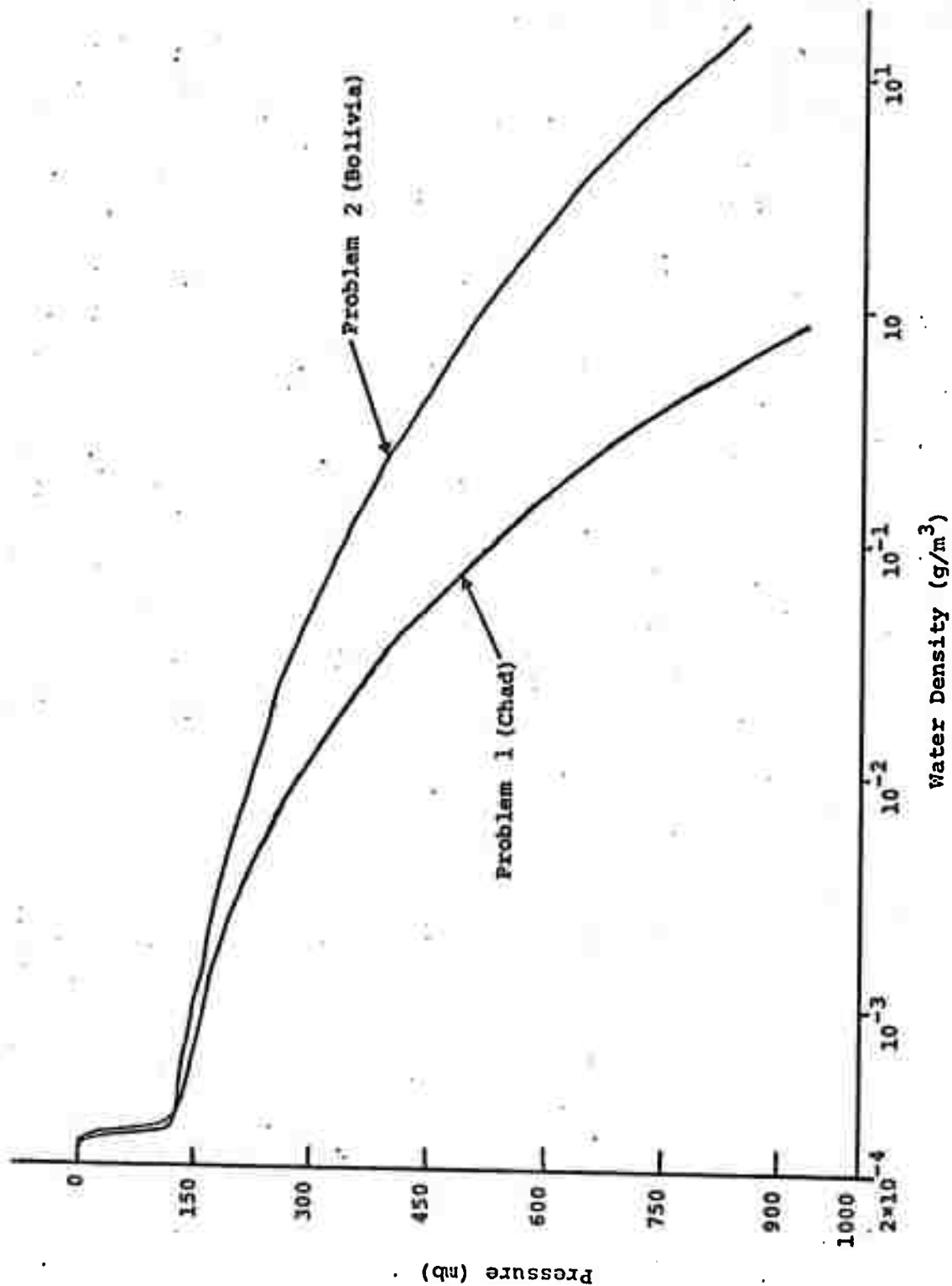
Figure 5.2 — Test Problem Water Vapor Density Profiles

$$\rho_{O_3}(Z) = \frac{We^{(Z-Z_o)/h}}{h\left[1 + e^{(Z-Z_o)/h}\right]^2}$$

was used with parameters $W = 0.218$ atm-cm (total ozone), $h = 4.5$ km (ozone layer half-width), and $Z_o = 23.25$ km (ozone maximum). This profile is shown in Figure 5.3.

The cosine of the solar zenith angle, ground temperature, T_g, and surface albedo for each problem were also taken directly from the M/A code. For Problem 1 they are

$$\mu_o = 0.84641818$$

$$T_g = 343.26°K$$

$$\rho_\nu = \begin{cases} 0 & \nu < 2500 \text{ cm}^{-1} \\ 0.2 & \nu > 2500 \text{ cm}^{-1} \end{cases}$$

and for Problem 2,

$$\mu_o = 0.454845$$

$$T_g = 304.19°K$$

$$\rho_\nu = \begin{cases} 0 & \nu \leq 2500 \text{ cm}^{-1} \\ 0.09 & \nu > 2500 \text{ cm}^{-1} \end{cases}$$

Note from Figure 5.1 that in both problems there is a temperature slip at the ground, of magnitude 31.5°K for Problem 1, and of magnitude 15°K for Problem 2.

Both problems were run with 39 zones, extending from the surface to 2 mb. A total of 116 frequency groups were

119
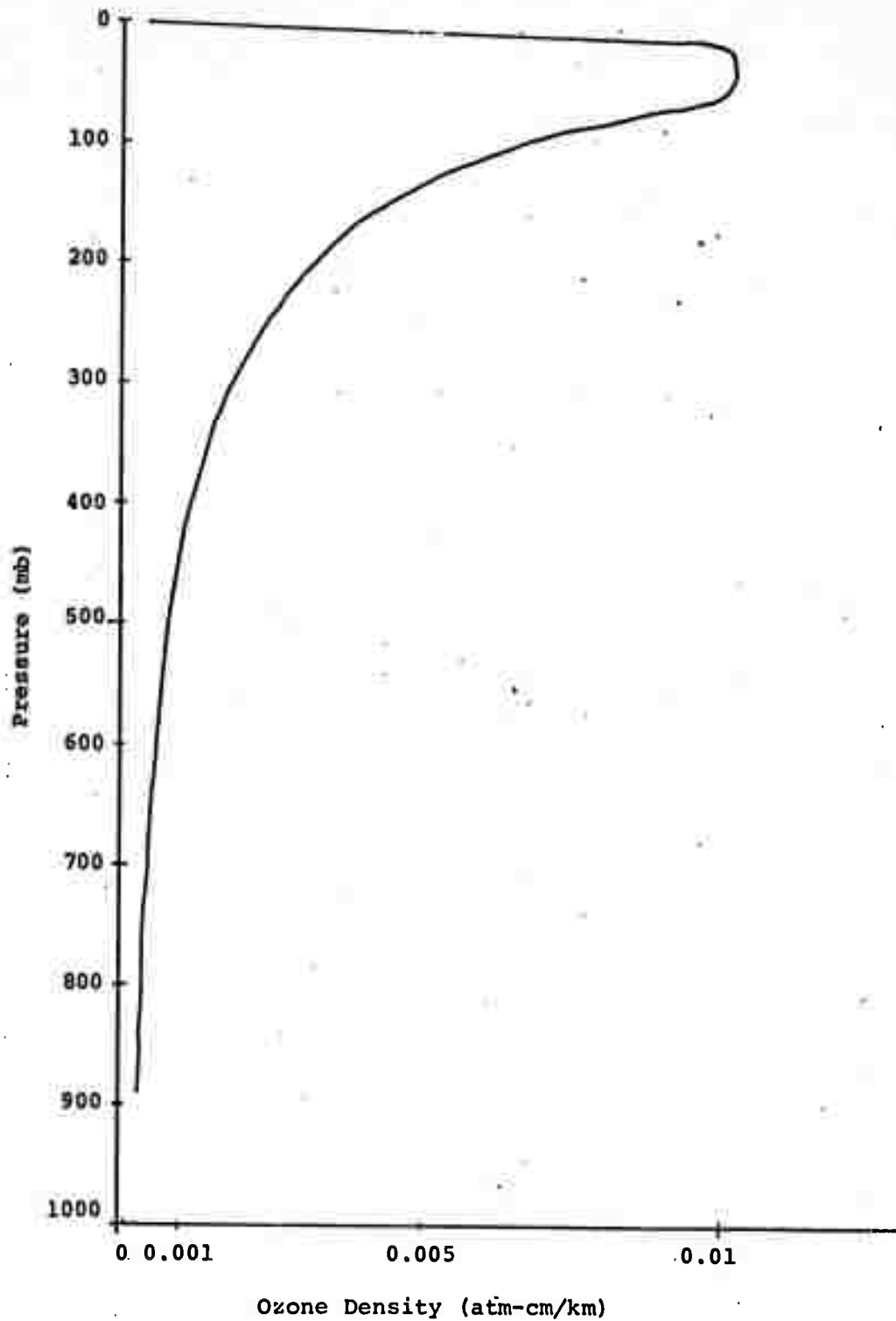
Figure 5.3 — Test Problem Ozone Density Profile

used, 32 in the IR (60-2500 cm^{-1}) 29 in the near IR (2500-11,000 cm^{-1}) and 55 in the "visible" (11,000-50,000 cm^{-1}). A variable number of Gaussian angles was used: 6 between 60 and 800 cm^{-1}, 10 between 800 and 1400 cm^{-1}, 8 between 1400 and 2500 cm^{-1}, and 10 between 2500 and 50,000 cm^{-1}. Fewer angles were used in the strong water vapor and CO_2 absorption bands, based on sample calculations showing a high degree of hemispherical isotropy in the intensity in these bands. Test calculations were run with more angles in selected frequency groups to determine if the number of angles being used was sufficient; in no case did the fluxes vary by more than a percent upon using more angles.

Test calculations were also performed to ascertain if the fluxes were sensitive to variations in the exponential fitting process. As we pointed out in the previous report,[2] the exponents and coefficients resulting from this process are highly sensitive to perturbations in the transmission function data, but the conjecture was made that the fluxes and intensities would be insensitive to variations in the fit. In the test calculations, various small perturbations in the transmission function data, which produced large perturbations in the exponential fits, nevertheless produced only small perturbations (always less than 1 percent) in the fluxes. Hence, our previous conjecture has been borne out remarkably well.

The ATRAD frequency-integrated radiative flux F(z) for Problem 1 is given in Figure 5.4 as a function of pressure p(z). (NOTE: positive fluxes are downward directed, negative fluxes are upward directed.) The Problem 1 atmosphere is very dry, which is manifested in the near constancy of F throughout most of the atmosphere. The large change in F near the surface can be explained in terms of the large temperature slip

121
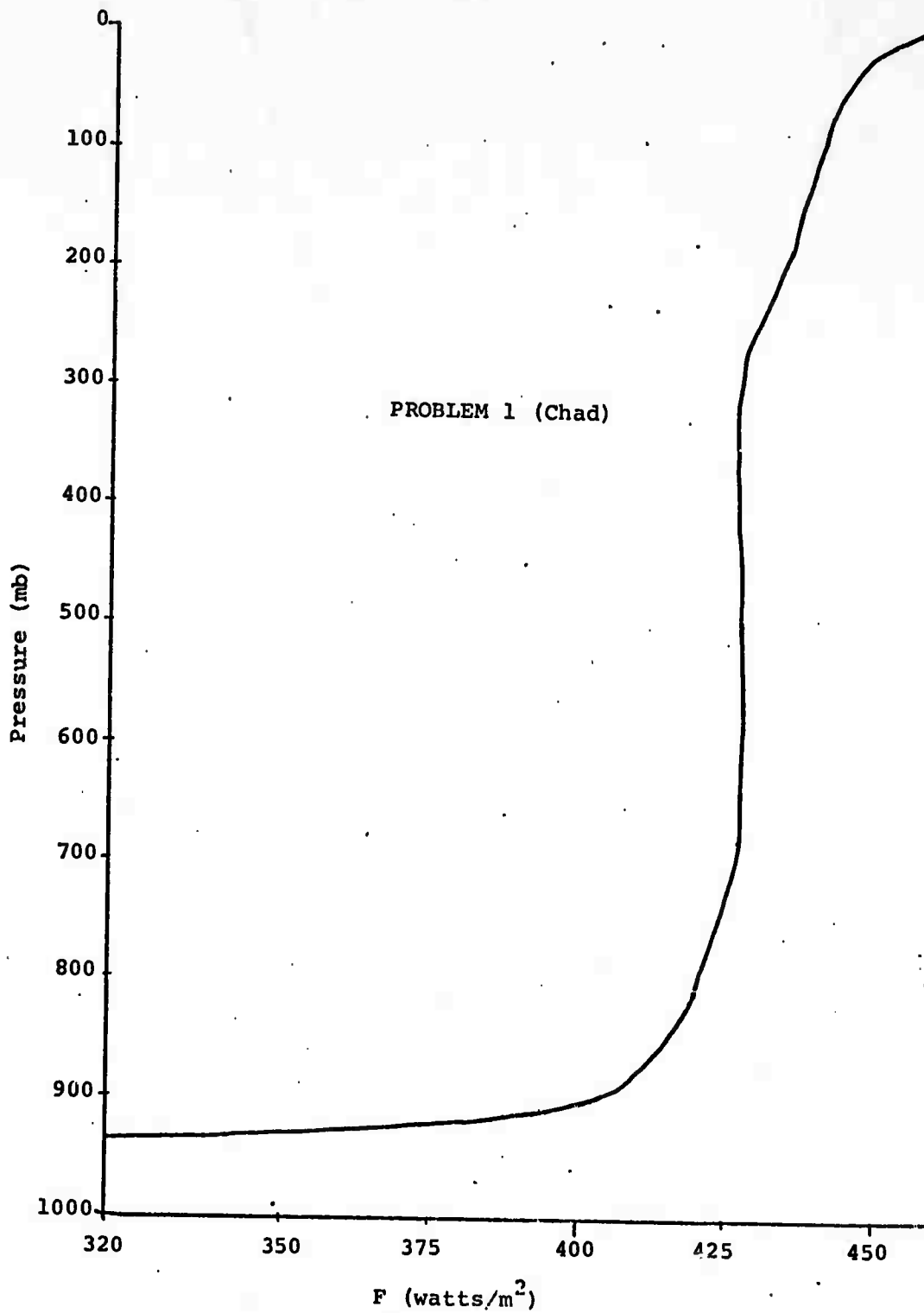
Figure 5.4 — Total (frequency-integrated) radiative
flux profile from ATRAD, Problem 1

(31.5°) at the surface; this slip produces a large upward blackbody flux which decreases the downward flux and which penetrates several hundred meters upward before absorption and re-emission by water vapor can produce a cancelling downward flux.

The Problem 1 flux spectrum $F_\nu(z)$ for $z = 0$ (top of the atmosphere) and $z = z_0$ (surface) is plotted as a function of wavenumber ν in Figure 5.5. Actually, because of the logarithmic wavenumber scale, νF_ν rather than F_ν is plotted; the relationship

$$\int \nu F \, d(\ln \nu) = \int F \, d\nu$$

then insures that the area between the curve and the horizontal axis in any wavenumber interval is really the integrated flux. Prominent absorption features due to CO_2 around 700 cm^{-1} (15μ band), O_3 around 1000 cm^{-1} (9.6μ band), H_2O in the near IR (5 strong bands between 2500 and 12,000 cm^{-1}), and O_3 in the ultraviolet (35,000-50,000 cm^{-1}) are all visible in this spectrum.

Comparisons between ATRAD's and Mintz-Arakawa's radiative fluxes and "heating rates" are presented in Table 5.1 for Problem 1. The "heating rate" table simply contains flux differences from the flux table above it. The error in the M/A net heating rate is quite large for this problem – it is too small by about a factor of 2 for the lower level, and too large by a factor of 4 and of the wrong sign for the upper level. The M/A flux into the ground is too large by almost 100 watts/m^2, or about 31 percent. The M/A fluxes are in general considerably more accurate than the M/A heating rates.
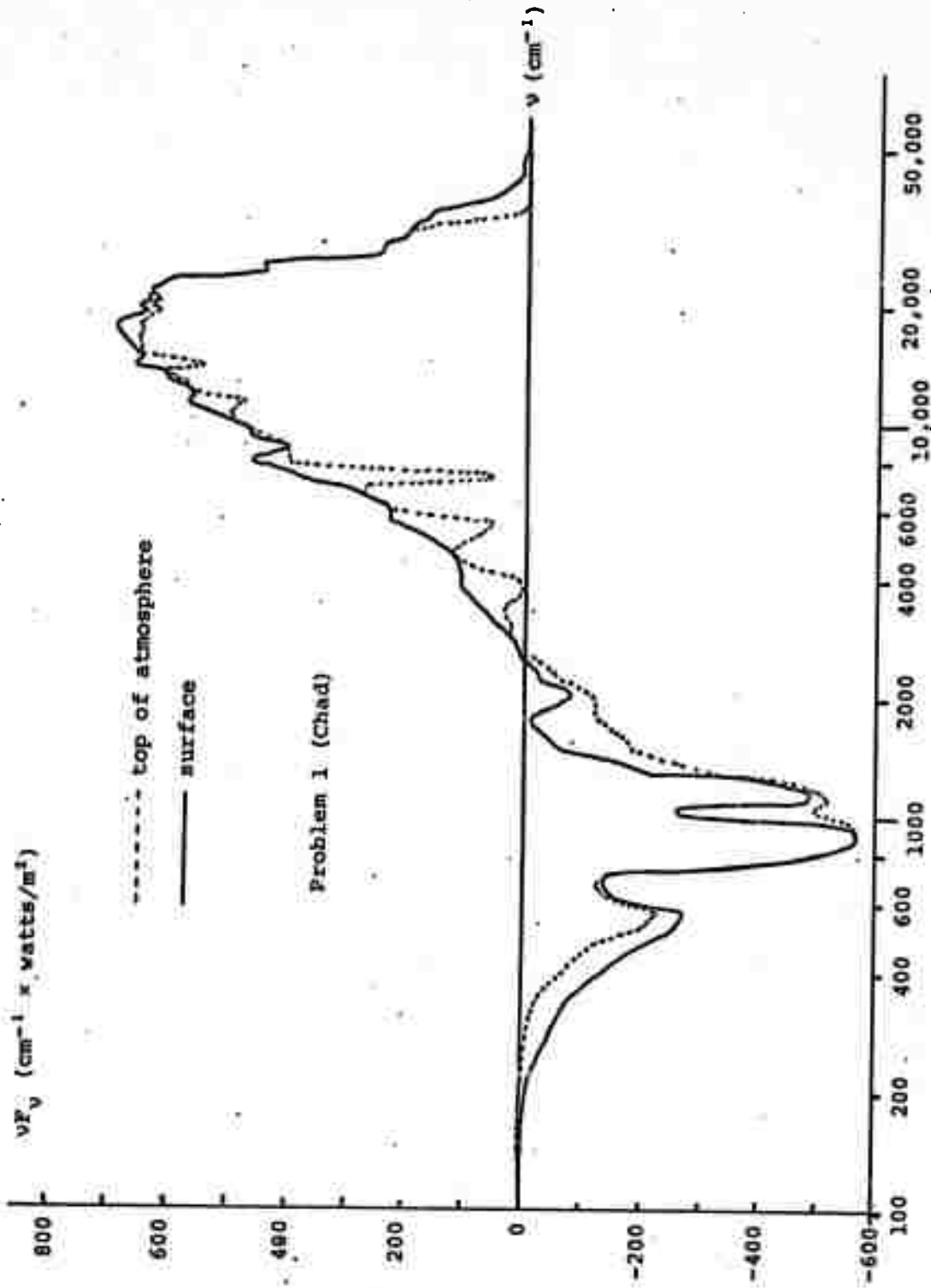
Figure 5.5 — Radiative flux spectrum at the surface and at the top of the atmosphere from ATRAD, Problem 1

TABLE 5.1

Comparison between ATRAD and Mintz-Arakawa (in parentheses)
fluxes and heating rates, Problem 1

FLUX (WATTS/M²)

	σ = 0 (200 MB)	σ = 0.5 (567 MB)	σ = 1.0 (934 MB)
IR (60 - 2,500 CM⁻¹)	-452.3 (-471.8)	-425.7 (-422.3)	-484.2 (-438.0)
NEAR IR (2,500 - 11,000 CM⁻¹)	337.2 (343.6)	307.3 (319.0)	261.9 (283.1)
VISIBLE (11,000 - 50,000 CM⁻¹)	548.1 (572.2)	545.4 (572.2)	542.3 (572.3)
VISIBLE + NEAR IR	885.3 (915.9)	852.6 (891.3)	804.2 (855.3)
NET	433.0 (444.1)	426.9 (469.0)	319.9 (417.3)

HEATING RATES (WATTS/M²)

	σ = 0.25	σ = 0.75	SURFACE
IR	-26.6 (-49.5)	58.5 (15.8)	-484.2 (-438.0)
NEAR IR	30.0 (24.6)	45.4 (35.9)	261.9 (283.1)
VISIBLE	2.7 (0)	3.1 (0)	542.3 (572.3)
NET	6.1 (-24.9)	107.0 (51.7)	319.9 (417.3)

σ = dimensionless pressures

$= \dfrac{P - P_{reference}}{P_{surface} - P_{reference}}$

= 1.0 at surface

= 0 at p = 200 mb

125

This illustrates the fact that crude models to obtain radia-
tive fluxes perform reasonably well in practice but flux
differences obtained from such models can be grossly in error.
It is necessary to have quite an accurate flux computation if
flux differences are desired, for in the process of differenc-
ing one or even two significant figures of accuracy may be
lost.

The ATRAD frequency-integrated flux $F(z)$ for Problem 2
is given in Figure 5.6. The Problem 2 atmosphere has con-
siderably more water vapor at all levels than the Problem 1
atmosphere — a factor of 12 more in total water content and a
factor of 19 more at the surface — which explains the slow de-
crease of F with altitude (the higher in the atmosphere one
is, the stronger the upward flux due to water vapor emission
becomes, which cancels more of the downward solar flux). As
in Problem 1, the sharp flux change near the surface is as-
cribed to the temperature slip (15°). The change is much
more abrupt in Figure 5.6 than in Figure 5.4 because the air
near the surface is so much wetter, causing the water vapor
emission to cancel the temperature slip flux a very short
distance above the surface.

The Problem 2 flux spectrum $F_\nu(z)$ is given in Figure
5.7 for $z = 0$ and $z = z_o$. For the same reasons as in Figure
5.5, νF_ν rather than F_ν is plotted. Note that the near IR
H_2O absorption features are enhanced, and that the CO_2 15μ
and O_3 9.6μ features are more washed out, with respect to
Problem 1. This is because of the increased amount of water
vapor in Problem 2.

The comparison of ATRAD with M/A for Problem 2 is pre-
sented in Table 5.2. The M/A and ATRAD fluxes agree much more
closely for Problem 2 than they did for Problem 1. The M/A
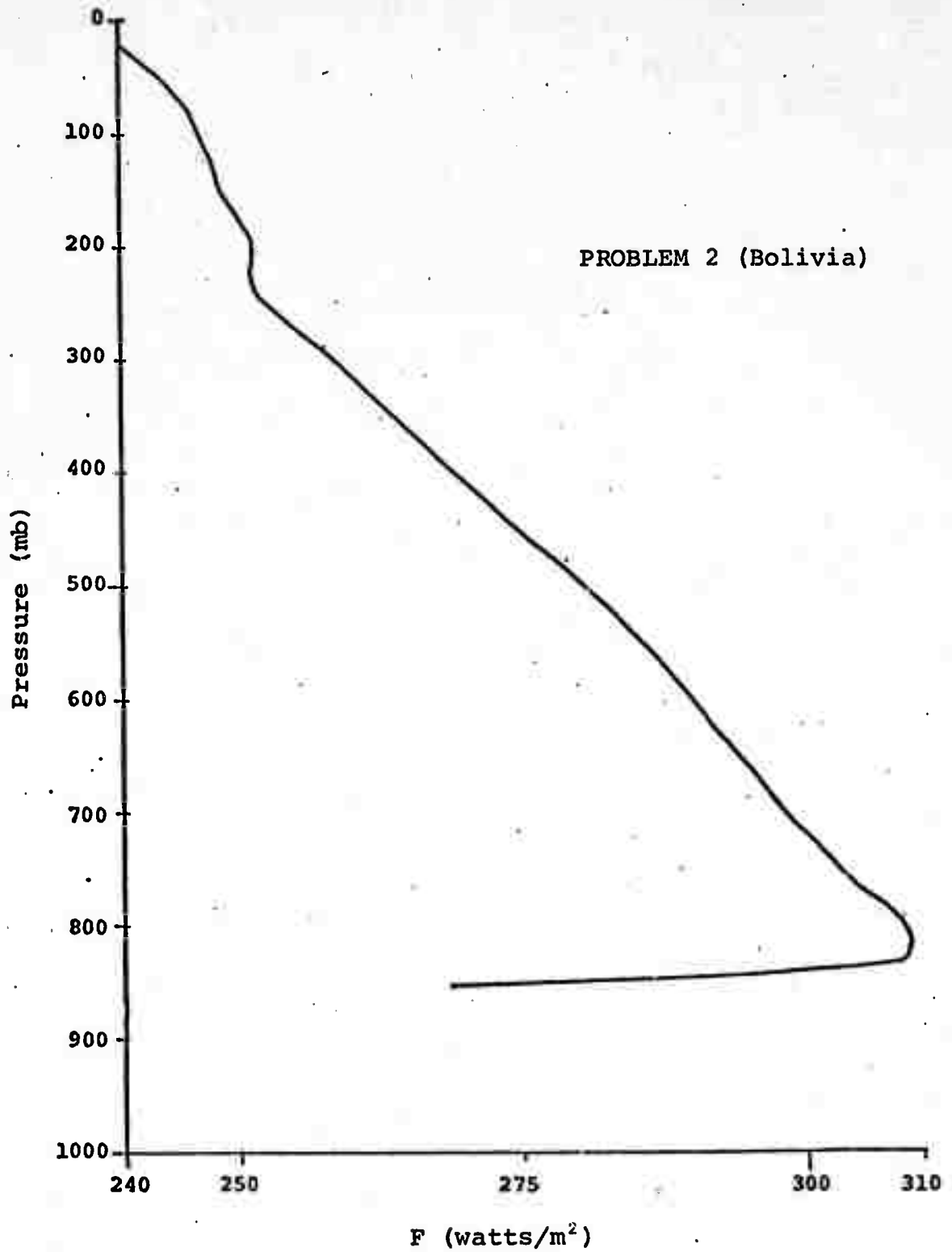
Figure 5.6 — Total (frequency-integrated) radiative
flux profile, Problem 2
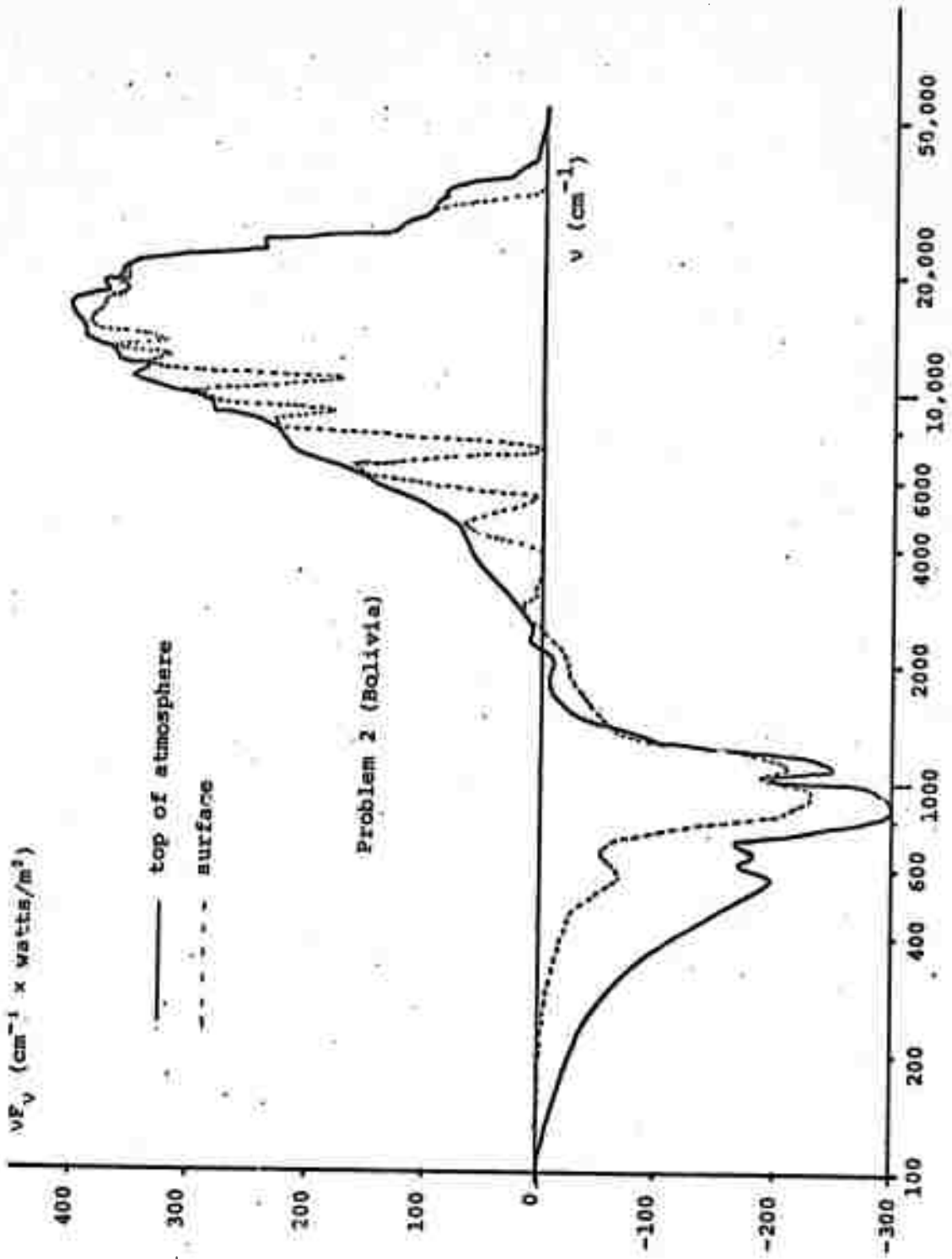
Figure 5.7 — Radiative flux spectrum at the surface and at the top of the atmosphere, Problem 2

TABLE 5.2

Comparison between ATRAD and Mintz-Arakawa (in parentheses)
fluxes and heating rates, Problem 2

FLUX (WATTS/M²)

	σ = 0 (200 MB)	σ = 0.5 (526 MB)	σ = 1.0 (852 MB)
IR (60 - 2,500 CM⁻¹)	-266.3 (-271.8)	-195.9 (-208.2)	-161.9 (-181.5)
NEAR IR (2,500 - 11,000 CM⁻¹)	203.1 (209.2)	166.2 (179.3)	123.7 (121.2)
VISIBLE (11,000 - 50,000 CM⁻¹)	314.5 (318.0)	312.4 (318.0)	306.6 (318.0)
VISIBLE + NEAR IR	517.6 (527.2)	478.6 (497.3)	430.3 (439.2)
NET	251.4 (255.5)	282.7 (289.2)	268.4 (257.7)

HEATING RATE (WATTS/M²)

	σ = 0.25	σ = 0.75	SURFACE
IR	-70.4 (-63.6)	-34.0 (-26.6)	-161.9 (-181.5)
NEAR IR	36.9 (29.9)	42.5 (58.1)	123.7 (121.2)
VISIBLE	2.2 (0)	5.7 (0)	306.6 (318.0)
NET	-31.3 (-33.7)	14.3 (31.4)	268.4 (257.7)

σ = dimensionless pressures

$= \dfrac{P - P_{reference}}{P_{surface} - P_{reference}}$

= 1.0 at surface

= 0 at p = 200 mb

net flux errors are 1.6 percent for $\sigma = 0$, 2.3 percent for $\sigma = 0.5$, and 4 percent for $\sigma = 1.0$. Again, however, because of loss of significance in subtraction, the heating rate errors are substantially larger. The M/A heating rate in the lower level is too large by more than a factor of 2, and in the upper level is in error by 7.7 percent. The M/A surface flux ($\sigma = 1$), which determines the heating of the ground, is in error by 4 percent. Thus, the M/A radiation model makes very good predictions of fluxes and heating of the lower level. It is not surprising that the M/A radiation model performs substantially better on Problem 2 than it did on Problem 1, for it devotes a great deal of attention to water vapor absorption, and Problem 2 is much more dominated by water vapor absorption than Problem 1.

It is clear that the M/A radiation model incurs substantial error in the case of dry atmospheres. However, no definitive conclusions with respect to the usefulness of the M/A radiation model for global climate calculations can be drawn from just these two problems. Many more test calculations, including cases with clouds, cases with realistic aerosol distributions, cases with high albedo (such as in the Arctic), and nighttime cases, need to be performed in order to obtain a more complete picture.

Even when this picture is obtained, other factors need to be considered. For example, the magnitude of the error in the total heating rate, including latent heating, adiabatic heating, etc., produced by errors in the radiative contribution must be ascertained. Also, it might be the case that a radiation model whose averaged (zonally, diurnally, etc.) predictions are correct is sufficient for climate dynamics calculations. In that case, it would be the average of many ATRAD calculations which would have to be compared with

the average of many M/A radiation calculations. The questions raised in this paragraph will have to be addressed before the amount of improvement necessary in the M/A radiation model can be ascertained.

6. FUTURE CONSIDERATIONS

6.1 OROGRAPHIC EFFECTS ON VERTICAL MOMENTUM FLUX IN THE ATMOSPHERE

The main emphasis of the next contract period will be the development of three dimensional transient and steady state codes. The parameterization effort will also continue attempting to understand the relationship between the steady state and transient results and in arriving at simplified expressions capable of being used in the global circulation model.

One important question which will be addressed during the parameterization studies is the desirability of using an expression derived from either the steady state or transient results as neither properly expresses the results truly representative of the GCM calculations. The changing wind patterns rule out to a certain degree the steady state results and the transient results calculated to this date have not been carried out late enough in time to determine if they are respentative of the situation. Certainly, it seems worth while to pursue this question on at least a semi-quantitative basis.

6.2 RADIATIVE HEATING IN THE ATMOSPHERE

In order to perform a large number of comparison calculations between ATRAD and the M/A radiation model, especially

with the Mie part of ATRAD turned on (as it was not for the problems of Chapter 5), substantial effort will have to be devoted to improving the running time of ATRAD. Some of our ideas for doing so were discussed in Section 4.10. The main methods by which we intend to improve ATRAD's running time are:

(1) replace the Mie calculation with tabular interpolation in large tables of Mie quantities;

(2) replace the exponential fitting calculation with tables of coefficients a_i and exponents k_i;

(3) look for a faster matrix inversion subroutine;

(4) code some frequently performed calculations in assembly language for greater efficiency.

Once these improvements are completed, we intend to perform many more comparisons between ATRAD and M/A, sufficient to obtain a spatially and temporally complete picture of the accuracy of the M/A radiation model. Concurrently with this effort, methods will be sought to improve the M/A code, especially the treatment of absorbers other than H_2O and its crude frequency resolution. Comparisons will also be made with the radiation subroutines of other Global Circulation Codes (it is likely that the GCM of the National Center for Atmospheric Research will be first). These calculations will provide a basis for intercomparison of different GCM radiation subroutines. Subsequently, a more comprehensive assessment of radiative subroutine accuracy and efficiency can be made.

REFERENCES

1. "The Effects of Meso-Scale and Small-Scale Interactions on Global Climate," Report No. 3SR-795 (30 September 1971), Systems, Science and Software, La Jolla, Calif.

2. "The Effects of Meso-Scale and Small-Scale Interactions on Global Climate," Report No. 3SR-1034 (31 March 1972), Systems, Science and Software, La Jolla, Calif.

3. F. P. Bretherton, "Momentum Transport by Gravity Waves," Qtrly. J. R. Met. Soc. (April 1969), Vol. 95.

4. P. D. Thompson, Numerical Weather Analysis and Prediction, The MacMillan Co., New York (1961).

5. T. H. Gawain and J. W. Pritchett, "A Unified Heuristic Model of Fluid Turbulence," J. Computational Phys. (June 1970), Vol. 5.

6. E. F. Danielsen and R. Bleck, "Tropospheric and Stratospheric Ducting of Stationary Mountain Lee Waves," J. Atmos. Sci. (August 1970), Vol. 27.

7. R. S. Scorer, "Theory of Waves in the Lee of Mountains," Qtrly J. R. Met. Soc. (1949), Vol. 76.

8. A. Eliassen and E. Palm, On the Transfer of Energy in Stationary Mountain Waves, Geof. Publ., Oslo (1960), Vol. 22.

9. B. Carnahan, et. al., Applied Numerical Methods, John Wiley & Sons, New York (1969).

10. E. Palm and A. Foldoik, "Contribution to the Theory of Two-Dimensional Mountain Waves," Geofysiske Publekaszoner Geophysica Norvegica (1959), Vol. 6.

11. W. L. Gates, et. al., "A Documentation of the Mintz-Arakawa Two-Level Atmospheric General Circulation Model," Report R-877-ARPA, Rand (December 1971).

12. W. Wiscombe and B. Freeman, A Detailed Radiation Model for Climate Studies; Comparisons with a General Circulation Model Radiation Subroutine, Conference on Atmospheric Radiation, American Meteorological Society, Boston, Mass., Preprint Volume (August 1972).

13. H. Howell and H. Jacobowitz, "Matrix Method Applied to Multiple Scattering of Polarized Light," J. Atmos. Sci. (1970), Vol. 27, p. 1195.

14. J. Dave, "Subroutines for Computing the Parameters of the Electromagnetic Radiation Scattered by a Sphere, IBM Program 360D - 17.4.002 (Decemb. 1968).

15. M. Kerker, The Scattering of Light and Other Electromagnetic Radiation, Academic Press, New York (1969).

16. F. Hodkinson, Proceedings of Inter-disciplinary Conference on Electromagnetic Scattering, Potsdam, N.Y., 1962, Pergamon Press, London (1963).

17. J. Ellison, Proc. Phys. Soc. B, (1957), Vol. 10, p. 102.

18. A. Holland and G. Gagne, "The Scattering of Polarized Light by Polydisperse Systems of Irregular Particles," Appl. Opt. (1970), Vol. 9, p. 1113.

19. F. Hall, Appl. Opt. (1968), Vol. 7, p. 891.

20. J. Houghton and G. Hunt, "The Detection of Ice Clouds From Remote Measurements of Their Emission in the Far Infrared," Qtrly. J. R. Met. Soc. (1971), Vol. 97, p. 1.

21. H. Jacobowitz, "A Method for Computing the Transfer of Solar Radiation Through Clouds of Hexagonal Ice Crystals, JQSRT (1971), Vol. 11, 691.

22. K. Kondrat'yev, Radiation in the Atmosphere, Academic Press, New York (1969).

23. G. Hoover, et.al., "Infrared Absorption by Overlapping Bands of Atmospheric Gases," Appl. Opt. (1967), Vol. 6, p. 481.

24. E. A. Milne, Thermodynamics of the Stars, in Selected Papers on the Transfer of Radiation, D. Menzel, Editor, Dover, New York (1966).

25. R. Siegel and J. Howell, "Thermal Radiation Heat Transfer, Vol. III," SP-164, NASA (1971).

26. H. Woolf, "On the Computation of Solar Elevation Angles and the Determination of Sunrise and Sunset Times," TM-X-1646, NASA (1968)

27. M. Thekaekara, et.al., "The Solar Constant and the solar Spectrum Measured From a Research Aircraft," Technical Report TR-R-351, NASA (1970).

28. R. Siegel and J. Howell, "Thermal Radiation Heat Transfer, Vol. I," Special Publication SP-164, NASA (1968).

29. C. Cox and W. Munk, "Slopes of the Sea Surface Deduced From Photographs of Sun Glitter," Bull. Scripps Inst. Oceanog., Vol. 6 (1956), p. 401.

30. A. Boileau and J. Gordon, "Atmospheric Properties and Reflectances of Ocean Water and Other Surfaces for a Low Sun," Appl. Opt., Vol. 5 (1966), p. 803.

31. D. McStravick, "The Effect of Surface Roughness on the Reflected and Emitted Energy From a Rough Surface," Ph.D. Thesis, Rice University, Texas (1972).

32. T. Paltridge, J. Geophys. Res., Vol. 76 (1971), p. 2857.

33. D. Earing and J. Smith, "Target Signatures, Analysis Center: Data Compilation," Willow Run Labs., Institute of Science and Techn., Univ. of Mich., Ann Arbor (1966).

34. T. Kyle, "Calculations of Atmospheric Transmittance From 1.7 to 20 μ," JQSRT, Vol. 9 (1969), p. 1477.

35. R. Goody, Atmospheric Radiation, Oxford Univ. Press, London (1964).

36. P. Wyatt, et.al., Appl. Opt., Vol. 3 (1964), p. 229.

37. W. Smith, "A Polynomial Representation of CO_2 and H_2O Vapor Transmission," ESSA Tech. Report NESC-47, National Environmental Satellite Service, Washington, D.C. (1969).

38. R. McClatchey, et.al., "Optical Properties of the Atmosphere," AFCRL-70-0527, Air Force Cambridge Research Labs., Cambridge, Mass. (1970).

39. K. Ya. Kondratyev and Yu. M. Timofeev, "Numerical Experiments on Studying Transmission Functions of Atmospheric Gases," in Radiation Including Satellite Techniques, Proceedings of WMO/IUGG Symposium, WMO Tech. Note 104 (1968).

40. B. Armstrong, "Analysis of the Curtis-Godson Approximation and Radiation Transmission Through Inhomogeneous Atmospheres," J. Atmos. Sci., Vol. 25 (1968), p. 312.

41. W. Zdunkowski and W. Raymond, "Exact and Approximate Transmission Calculations for Homogeneous and Non-Homogeneous Atmospheres," Beitr zur Phys. der Atmos., Vol. 43 (1970), p. 185.

42. R. Penndorf, "Tables of the Refractive Index for Standard Air and the Rayleigh Scattering Coefficient for the Spectral Region Between .2 and 20 μ," J. Opt. Soc., Amer. Vol. 47 (1957), p. 176.

43. E. Peck and K. Reeder, "Dispersion of Air," J. Opt. Soc., Amer., Vol. 62 (1972), p. 958.

44. F. Gucker, et.al., "Intensity and Polarization of Light Scattered by Some Permanent Gases and Vapors," J. Chem. Phys., Vol. 50 (1969), p. 2526.

45. J. Dave, Subroutines for Computing the Parameters of the Electromagnetic Radiation Scattered by a Sphere, IBM Program 360D-17.4002, IBM Scientific Center, Palo Alto, Calif. (1968).

46. G. Kattawar and G. Plass, "Electromagnetic Scattering From Absorbing Spheres," Appl. Opt., Vol. 6 (1967), p. 1377.

47. H. Denman, W. Heller, and W. Pangonis, Angular Scattering Functions for Spheres, Wayne State Univ. Press, Detroit (1966).

48. Deirmendjian, "Tables of Mie Scattering Cross Sections and Amplitudes, Rand Report R-407-PR, Rand Corp., Santa Monica, Calif. (1963).

49. W. Irvine and J. Pollack, "Infrared Optical Properties of Water and Ice Spheres," Icarus, Vol. 8 (1968), p. 324.

50. A. Rusk, D. Williams and M. Querry, "Optical Constants of Water in the Infrared," J. Opt. Soc., Amer., Vol. 61 (1971), p. 895.

51. C. Robertson and D. Williams, "Lambert Absorption Co-efficients of Water in the Infrared," J. Opt. Soc., Amer., Vol. 61 (1971), p. 1316.

52. M. Que-ry, et.al., "Optical Constants in the Infrared for Aqueous Solutions of NaCl," J. Opt. Soc., Amer., Vol. 62 (1972), p. 849.

53. J. Twitty and J. Weinman, "Radiative Properties of Carbonaceous Aerosols," J. Appl. Met., Vol. 10 (1971), p. 725.

54. W. Dalzell and A. Sarofim, "Optical Constants of Soot and Their Application to Heat-Flux Calculations," J. Heat Transfer, (February 1969), p. 100.

55. W. Spitzer and D. Kleinman, "Infrared Lattice Bands of Quartz," Phys. Rev., Vol. 121 (1961), p. 1324.

56. F. Volz, "Infrared Absorption by Atmospheric Aerosol Substances," JGR, Vol. 77 (1972), p. 1017.

57. F. Volz, "Infrared Refractive Index of Atmospheric Aerosol Substances, Appl. Opt., Vol. 11 (1972), p. 755.

58. A. Blanco and G. Hoidale, "Infrared Absorption Spectra of Atmospheric Dust," ECOM-5193, 1968, Atmospheric Sciences Lab, White Sands Missile Range, New Mexico.

59 D. Flanigan and H. DeLong, "Spectral Absorption Characteristics of the Major Components of Dust Clouds," EATR-4430, 1970, Edgewood Arsenal, Maryland.

60. J. Hunt, M. Wisherd, and L. Bonham, "Infrared Absorption Spectra of Minerals and Other Inorganic Compounds," Anal. Chem., Vol. 22 (1950), p. 1478.

61. F. Went, "On the Nature of Aitken Condensation Nuclei," Tellus, XVIII (1966), p. 549.

62. C. E. Junge, Air Chemistry and Radioactivity, Academic Press, New York (1963).

63. D. Deirmendjian, Electromagnetic Scattering on Spherical Polydispersions, Elsevier, New York (1969).

64. Khrgian, ed., Cloud Physics, Israel Program for Scientific Translations, Jerusalem (1963), p. 83.

65. O. A. Germogenova, "Atmospheric Haze: A Review," Report 1821, Bolt Beranek and Newman, Cambridge, Mass. (1970).

66. S. Twomey, H. Jacobowitz, and H. Howell, "Light Scattering by Cloud Layers, J. Atmos. Sci., Vol. 24 (1967), p. 70.

67. I. H. Blifford, "Tropospheric Aerosols," JGR, Vol. 75 (1970), p. 3099.

68. D. Chang and R. Wexler, "Meteorological Relationships to Tropospheric and Stratospheric Turbidity Profiles," AFCRL-70-0197, Air Force Cambridge Research Labs., Cambridge, Mass. (1970).

69. K. Ya. Kondratyev, et.al., "Aerosol Structure of the Troposphere and Stratosphere," WMO Technical Note No. 104, Radiation Including Satellite Techniques (1968).

70. L. Dufour, "The Atmospheric Aerosol," translated at Atmospheric Sciences Laboratory, White Sands Missile Range, New Mexico (1969)

71. E.S. Selezneva, Atmospheric Aerosols, translated and published for ESSA (now NOAA) by Indian National Scientific Documentation Center, New Delhi, India (1970).

72. L. Eltermann, "Parameters for Attenuation in the Atmospheric Windows for Fifteen Wavelengths," Appl. Opt. (1964), Vol. 3, 745.

73. A. Meszaros, "On the Variation of the Size Distribution of Large and Giant Atmospheric Particles as a Function of the Relative Humidity," Tellus (1971), XXIII, 436.

74. G. Hanel, "The Real Part of the Mean Complex Refractive Index and the Mean Density of Samples of Atmospheric Aerosol Particles," Tellus (1968), XX, 371.

75. A. Ralston and H. Wilf, eds., Mathematical Methods for Digital Computers (1967), Vol. II, Wiley, New York.

76. J. Dave, "Effect of Coarseness of the Integration Increment on the Calculation of the Radiation Scattered by Polydispersed Aerosols," Appl. Opt. (1969), Vol. 8, 1161.

77. J. Dave, "Effect of Varying Integration Increment on the Computed Polarization Characteristics of the Radiation Scattered by Polydispersed Aerosols," Appl. Opt. (1969), Vol. 8, 2153.

78. J. Hansen, J. Atm. Sci. (1969), Vol. 26, 478.

79. J. Potter, "The Delta Function Approximation in Radiative Transfer Theory," J. Atm. Sci. (1970), Vol. 27, 943.

80. D. Cantor and J. Evans, "On Approximation by Positive Sums of Powers," SIAM J. Appl. Math, (1970), Vol. 18, 380.

81. P.A. Businger, "MIDAS — Solution of Linear Algebraic Equations," Computing Science Research Center, Bell Labs, Murray Hill, New Jersey (January 1970).

82. A. Green, Appl. Opt., Vol. 3 (1964), p. 203.

APPENDIX A — ATRAD INPUT

The input for ATRAD consists entirely of FORTRAN NAMELIST's, which are the most convenient and versatile way of performing data input in the FORTRAN language. NAMELIST's also have the advantage of being exceptionally easy for even non-programmers to use, so that the code could be exercised by personnel with a minimal amount of instruction.

There are two possible deck set-ups for running ATRAD. The first (the "normal" mode) is used for setting-up and starting a problem ab initio, and is illustrated in Figure A.1. The second (the "restart" mode) is used for restarting a problem from a dump tape at a predetermined frequency group, and is illustrated in Figure A.2.

The variables required by each NAMELIST are described below. If the variable is not specified in the NAMELIST, it will assume a default value which is given in parentheses at the end of the description of the quantity. The subscript convention employed is as follows:

I is a level index,
J is an angular index, and
NU is a frequency index.

140

WISCOM NAMELIST

    Input Control Parameters
    (listed in Section A.1)

END

LEVELS NAMELIST

    Z, NZ, IBD, NBD   Only if
    (listed in A.2)   PRSETZ = TRUE

END

FREQS NAMELIST

    WAVNUM, NNU   Only if
    (listed in A.3)   PRSETF = TRUE

END

STRUCT NAMELIST

    P, T, H2ODEN, O3DEN,
    AERDEN, NAER, NMAT   Only if NOPT = 0
    (listed in A.4)

END

AEROS NAMELIST

    RAD, AERNUM, NDAT   Only if NAER(I) = 0
    (listed in A.5)   or -1 for at least
                         one I.

END

Figure A.1   Input Deck Set-up for a Normal Run of ATRAD.

141

RSTART NAMELIST

        NUSTRT, INPT   }
        (listed in A.6)

END

WISCOM NAMELIST

        Input Data   }   Only if INPT > 0
        (listed in A.1)

END

AEROS NAMELIST

        RAD, AERNUM, NDAT   }   Only if NUSTRT = 1
        (listed in A.5)   and NAER(I) = 0 or
                                -1 for at least
                                one I.

END

Figure A.2   Input Deck Set-up for Restarting
                 ATRAD from Dump Tape at Frequency
                 Group NUSTRT.

A.1   WISCOM NAMELIST

Variable	Type	Description
PR1	Logical	If TRUE, atmospheric structure (P, T, etc.) is edited. (FALSE)
PR2	Logical	If TRUE, edits frequency-integrated fluxes, heating rates, and intensities, as well as the flux spectrum at the upper and lower boundaries of the atmosphere. (TRUE)
PR3	Logical	If TRUE, edits fluxes, heating rates, intensities, incident solar flux, and earth-atmosphere albedo for each frequency group. (FALSE)
PR4	Logical	If TRUE, edits solar flux, Planck function, scattering coefficient, and continuum absorption coefficient for both the current and previous frequency group, and the percent change of each quantity from the previous frequency group. Also edits the continuum part of the optical depth of each zone, and various surface quantities such as the directional emissivity $\varepsilon(\mu)$ and reflection matrix $r_G(\mu,\mu')$. (FALSE)
SCTPRT	Logical	If TRUE, edits truncation information, Mie scattering and absorption coefficients, Mie phase function

143

Variable	Type	Description
SCTPRT (cont.)	Logical	both before and after renormalization, Rayleigh and total scattering coefficients, and total phase function. (FALSE)
MIEPR(1)	Logical	If TRUE, edits on each call to MIESCT the real and imaginary parts of A_n, a_n, and b_n, which are coefficients in the Mie series. This edit is primarily useful when the Mie package is being driven separately; it should never be turned on for a normal radiation calculation, as it would produce a vast amount of printing. (FALSE)
MIEPR(2)	Logical	If TRUE, edits from each call to MIESCT the Mie phase function and the efficiency factors and cross-sections for scattering, absorption, and extinction. Same comments apply as for MIEPR(1). (FALSE)
MIEPR(3)	Logical	If TRUE, edits information relevant to integration over aerosol size distribution in MIE and prints Mie phase function and corss-sections for absorption and scattering resulting from that integration. (FALSE)

144

Variable	Type	Description
FITPRT	Logical	If TRUE, edits for each frequency group and for each molecular species (H_2O, CO_2+, O_3) the transmission function, its exponential-sum approximant, and the percent error. Also edits the coefficients a_i and exponents k_i of the approximant. (FALSE)
FITPR2	Logical	If TRUE, edits the exponential-sum fitting, including the coefficients a_i and exponential factors θ_i, the residual, and the polynomial (4.38), for each iteration. Also edits information about pairs of exponential factors which are combined. (FALSE)
TPR1	Logical	If TRUE, performs a "short" edit for each call to TRNPRT (Grant-Hunt algorithm), including the single-scattering albedo, line absorption coefficient, optical depth, doubling parameters, source vectors, and resultant (diffuse) intensities for each zone. (FALSE)
TPR2	Logical	If TRUE, performs all of the edits of TPR1 plus the Planck and solar source vectors, the reflection and transmission matrices for each zone, and the various vectors and matrices (E, V_1, etc.) used in the Grant-Hunt algorithm. (FALSE)

145

A-6

Variable	Type	Description
PRSETZ	Logical	If TRUE, the user intends to input the zone structure through the "LEVELS" NAMELIST. If FALSE, user intends to set OZONE, TROPO, NCLOUD, CLDBAS, CLDTOP, NZONES, and EXPAN (see below) with which the code will calculate the zone structure. (FALSE)
OZONE	Logical	If TRUE, place the uppermost level at 50 km altitude. If FALSE, take the uppermost level at TROPO km (the tropopause or some level just below the ozone layer). In the latter case, the incident solar flux will be truncated at O3CUT. (TRUE)
TROPO	Real	If OZONE = FALSE, the height in km of the uppermost level in the problem is set to TROPO. This level should be reasonably close to the bottom of the ozone layer. (15.0)
NCLOUD	Integer	The number of cloud layers (only 0, 1, or 2 are allowed). (0)
CLDBAS(1,2)	Real	Heights in km of bases of lower (1) and upper (2) cloud. (2*0.)
CLDTOP(1,2)	Real	Heights in km of tops of lower (1) and upper (2) cloud. (2*0.)

146

Variable	Type	Description
NZONES(1-5)	Real	Number of zones in each of the sub-regions into which the clouds partition the atmosphere. E.g., NZONES(1) is the number of zones from the surface to the first cloud base, or, if NCLOUD = 0, is the total number of zones. NZONES(2) is the number of zones in cloud 1, etc. (20,4*0.)
EXPAN(1-5)	Real	Expansion factors for each sub-region. E.g., in sub-region 1, each zone has a geometrical width EXPAN(1) times the width of the zone below it. This enables one to generate zones of more or less constant mass, increasing mass, etc. (1.1,4*0.)
PRSETF	Logical	If TRUE, user intends to input frequency group structure through "FREQS" NAMELIST. If FALSE, user intends to set NWAV, WAV, DWAV or NGRPS, IWV (see below) and let the code calculate the frequency group structure. (FALSE)
NWAV	Integer	Number of frequency "regions." (12)
WAV(1-15)	Integer	Wavenumber boundaries in cm^{-1} for each frequency "region." E.g., WAV(1) < WAV(2) are the wavenumbers bounding frequency region 1. Each value must be an integer multiple

147

Variable	Type	Description
WAV(1-15) (cont.)	Integer	of 20 cm^{-1}. (60, 600, 760, 1300, 1800, 2500, 3200, 4400, 7400, 9000, 32000, 35000, 50000)
DWAV(1-14)	Integer	Frequency group width in cm^{-1} for all of the groups within a frequency "region" defined above. Each value must be an integer multiple of 20 cm^{-1}. E.g., between WAV(1) and WAV(2) all frequency groups are of size DWAV(1). (60, 40, 60, 100, 140, 140, 200, 300, 400, 500, 1000, 1500)
NGRPS	Integer	If $15 \geq$ NGRPS > 0, it overrides the WAV, DWAV option. The NGRPS option allows one to do NGRPS disjoint frequency groups with boundaries IWV (see below); it can be used to sample the spectrum. (0)
IWV(1-30)	Integer	Used when NGRPS > 0. Successive pairs of IWV values define the frequency boundaries (cm^{-1}) of the frequency groups being sampled. E.g., if NGRPS $= 2$, the first group is [IWV(1),IWV(2)] and the second group is [IWV(3),IWV(4)]. (30*0)
IWVANG(1-15)	Integer	Wavenumber boundaries in cm^{-1} delineating regions in which the number of quadrature angles is constant. This allows one to use fewer angles in frequency regions where the

148

Variable	Type	Description
IWVANG(1-15) (cont.)	Integer	intensity is more nearly isotropic (in each hemisphere separately). (50, 50000, 13*0)
NUMANG(1-14)	Integer	Number of quadrature angles used in each hemisphere in the corresponding frequency region delineated by IWVANG. E.g., the number of quadrature angles between IWVANG(1) and IWVANG(2) is NUMANG(1). (6, 13*0)
NUMANG(15)	Integer	Number of wavenumber regions delineated by IWVANG. (1)
RADOW(1-14)	Logical	If RADOW(K) = TRUE, then use Radau quadrature in wavenumber interval [IWVANG(K),IWVANG(K+1)]. Otherwise, Gaussian quadrature. (14*FALSE)
NOPT	Integer	Atmostpheric structure flag.

NOPT continued:

= 0 Input atmospheric structure through "STRUCT" NAMELIST.

= 6 Calculate structure from user-supplied analytic forms contained in subroutines TEMPER, SPFHUM, O3D, AERD, NMATL, NAERO (default forms of these subroutines are used if user does not intervene.)

= 7 Restart. Read in structure from dump tape.

149

Variable	Type	Description
NOPT (cont.)	Integer	Otherwise, use one of the following standard atmospheres: = 1 Tropical = 2 Mid-latitude summer = 3 Mid-latitude winter = 4 Sub-arctic summer = 5 Sub-arctic winter
NOPT1	Integer	Phase function renormalization flag. = 1 Use Grant method. = 2 Use Wiscombe method. (2)
NOPT2	Integer	If >0, stop calculation just before entering frequency loop. This allows user to check that his problem set-up is correct before doing a full run of the code. (0)
P0	Real	Surface pressure in mb for case NOPT = 6. (1013.)
DAY	Real	Day of the year, January 1 being day 1. (1.)
TIME	Real	Greenwich time, in hours. (0).
LONG	Real	Longitude, in degrees, counted positive west of Greenwich. (117.)
LAT	Real	Latitude, in degrees. (33.)
CUTPLK	Real	Wavenumber in cm^{-1} above which Planck function is set to zero. (3333.)

150

Variable	Type	Description
CUTSOL	Real	Wavenumber in cm^{-1} below which incident solar flux is set to zero. (1666.)
CUTRAY	Real	Wavelength in microns above which Rayleigh scattering is neglected. (3.)
O3CUT	Real	Wavenumber in cm^{-1} above which incident solar flux is set to zero in case OZONE = FALSE. (33333.)
NMATG	Integer	Surface material flag. (1)
TG	Real	Surface temperature in °K. (300.)
WNSURF(1-11)	Real	Frequency boundaries in cm^{-1} specifying regions within which the surface boundary condition is calculated according to the corresponding value of NSURF. (50.,50000.,9*0.)
NSURF(1-10)	Integer	Between WNSURF(K) and WNSURF(K+1), the surface boundary condition is flagged by NSURF(K). The options are: NSURF = 1 Hemispherical reflectivity or hemispherical emissivity supplied by user as function of wavelength, in subroutine SURF1. Diffuse emission and reflection assumed.

151

A-12

Variable	Type	Description
NSURF(1-10) (cont.)	Integer	= 2 Directional emissivity or directional-hemispherical reflectivity supplied by user as a function of angle and wavelength, in subroutine SURF2. Diffuse reflection assumed.
		= 3 Azimuthally-averaged bidirectional reflectivity supplied by user as a function of angle of incidence, angle of reflection, and wavelength, in subroutine SURF3. (1,9*0)
NSURF(11)	Integer	Number of non-zero WNSURF entries. (2)
DEL0	Real	Convergence criterion for aerosol size integration in MIE. (0.001)
NOTHG(I)	Logical	If NOTHG(I) = TRUE, use the normal procedure to calculate the Mie phase function for zone I. If NOTHG(I) = FALSE, calculate the Mie phase function only at 0°, calculate the parameter g such that the Henyey-Greenstein phase function matches that value, and use the HG phase function at all other angles. (40*FALSE)

152

Variable	Type	Description
NSTEP(1-6)	Integer	Used in the determination of the angular mesh on which Mie phase function is calculated. $\Delta\theta$ is calculated in MIE, and from it the angular mesh is calculated as follows: NSTEP(1) steps of $\Delta\theta$, NSTEP(2) steps of $2\Delta\theta$, ..., NSTEP(K) steps of $2^{K-1}\Delta\theta$, ... All values of NSTEP must be even. (16,3*10,2*0)
NDOUB	Integer	Number of non-zero entries in NSTEP. (4)
DANGLO	Real	Lower boundary on $\Delta\theta$ in degrees (see NSTEP). Must be a multiple of $\Delta\theta_{tab}$, the interval for which π_n, τ_n are tabulated. (0.1)
DANGHI	Real	Upper boundary on $\Delta\theta$ in degrees. Must be a multiple of $\Delta\theta_{tab}$ (see DANGLO). (1.0)
DANGMX	Real	If at any point in the NSTEP procedure described above, $2^{K-1}\Delta\theta >$ DANGMX, then the NSTEP procedure is terminated and the rest of the steps to 90° are taken with an increment $\Delta\theta_m$ which is as close as possible to DANGMX, is a multiple of $\Delta\theta_{tab}$ (see DANGLO), and yet allows an even number of steps (as required by the Simpson-rule integration used to renormalize the Mie phase function in MIE and to truncate it in TRUNCT). (2.5)

153

Variable	Type	Description
ANGMAX	Real	The maximum allowed angle, in degrees, at which the Mie phase function may be truncated (TRUNCT chooses progressively larger angles in attempting to perform a satisfactory truncation). (20.)
CUTMIN	Real	The maximum allowed value at 0° of the truncated Mie phase function (if the TRUNCT search reaches ANGMAX without satisfying the CUTMIN criterion, the default truncation at ANGMAX may produce a P_ν^t (0°) > CUTMIN). (5.)
NPTS	Integer	The maximum number of transmission function data points to be used in the exponential fitting procedure. (50)
MINPTS	Integer	The minimum number of transmission function data points to be used in the exponential fitting procedure. (10)
THMN, THMX	Double Precision	The lower and upper limits, θ_{min} and θ_{max}, on the search interval used to find a new exponential factor θ in the exponential-sum fitting iteration. These limits are imposed because $\theta = 0$ and $\theta = 1$ correspond to unphysical values of the exponent k (∞ and 9, respectively). (1.D-8,.99999999D0)

154

Variable	Type	Description
TRMIN	Real	The smallest value of the transmission function to be used as a data point for exponential fitting. (.005)
TRMAX	Real	If the transmission through the entire vertical mesh on a slant path specified by SLANT is > TRMAX for a given molecular species, then the transmission for that species is taken to be unity and no fitting is done. (.99)
NSRCH	Integer	The maximum number of search points taken on $[\theta_{min}, \theta_{max}]$ in locating a new exponential factor θ in the exponential fitting iteration. (1001)
NSRCH2	Integer	The number of search points taken in intervals $[\theta_i - \Delta\theta, \theta_i + \Delta\theta]$ around each of the old exponential factors θ_i in the process of finding a new exponential factor θ (since exponential factors often occur in close pairs, these intervals should be subjected to a more refined search). (21)
COALES	Double Precision	The criterion for whether or not to coalesce a close pair of exponential factors θ_i, θ_{i+1}. If

$$2 \left| \frac{\ln \theta_{i+1} - \ln \theta_i}{\ln \theta_{i+1} + \ln \theta_i} \right| \leq COALES$$

155

A-16

Variable	Type	Description
COALES (cont.)	Double Precision	then θ_i, θ_{i+1} are replaced by a single exponential factor. (.05)
CTEST	Double Precision	If any coefficient a_i in an exponential-sum fit is < CTEST, the corresponding term in the fit is dropped. This number should not be much larger than the estimated error in the transmission function data. (.001)
RTEST	Double Precision	The exponential fitting iteration is stopped when $$\left\| \frac{R_{new} - R_{old}}{R_{new}} \right\| < RTEST$$ where R is the residual and 'old' and 'new' refer to the previous and current iterations. (1.D-16)
ITMAX	Integer	The maximum allowed number of iterations in the exponential-sum fitting procedure. (150)
ISEC1	Integer	Maximum number of iterations of secant method used in pair-coalescence procedure in FITTRN. (10)
SLANT	Real	If u_v is the vertical absorber amount of a given molecular species, then the smallest value of the transmission function $T_{\Delta\nu}(u)$ used in

156

Variable	Type	Description
SLANT (cont.)	Real	fitting is $$T_{\Delta\nu}(SLANT*u_\nu)$$ provided this value is > TRMIN. (2.0)
CHGMAX	Real	If > 0, overrides the normal surface boundary condition flags NSURF and WNSURF and sets the albedo = CHGMAX (for zero albedo, input CHGMAX = 10^{-30}). (0.)
FACT	Real	The fraction of the maximum primary layer optical depth, $\Delta\tau_{max}$, which is actually used as a doubling interval in the Grant-Hunt algorithm in TRNPRT. (0.5)
SCTMIN	Real	If the single-scattering albedo ω < SCTMIN, then the part of subroutine TRNPRT which neglects scattering entirely (involving considerably less calculation) is used. (1.E-5)

A.2   LEVELS NAMELIST

Variable	Type	Description
Z(I)	Real	The heights above the surface of the various levels in the vertical mesh, starting from the surface [Z(1)], in km.
NZ	Integer	The number of levels.

157

A-18

Variable	Type	Description
IBD(1-5)	Integer	The indices of the levels which divide the mesh into sub-regions. E.g., Z(IBD(1)) is the height of the lower cloud base, and Z(IBD(2)) is the height of the lower cloud top. If there are no clouds, IBD(1) = NZ.
NBD	Integer	The number of sub-regions required by the presence of clouds (NBD = 2 × # clouds + 1).

A.3 FREQS NAMELIST

Variable	Type	Description
WAVNUM(NU)	Integer	The frequencies in cm^{-1} bounding the frequency groups, in increasing order (WAVNUM(1) is the smallest.)
NNU	Integer	The number of non-zero WAVNUM's (or one plus the number of frequency groups.)

A.4 STRUCT NAMELIST

Variable	Type	Description
P(I)	Real	Pressures in mb corresponding to Z(I). (P(1) is the surface pressure.)
T(I)	Real	Temperatures in degrees Kelvin. T(1) is the temperature of the air immediately above the ground, and may be different from TG, the ground temperature.
H2ODEN(I)	Real	Water vapor density in g/m^3.

158

Variable	Type	Description
O3DEN(I)	Real	Ozone density in atm-cm/km.
AERDEN(I)	Real	Aerosol number density in particles/cm^3.
NAER(I)	Integer	Flag specifying aerosol size distribution:

= -2	Use size distribution from level above.	
= -1	Card input, histogram form	
= 0	Card input, pointwise form	
= 1	Deirmendjian Haze M	
= 2	Deirmendjian Haze L	
= 3	Deirmendjian Haze H	
= 4	Deirmendjian Cloud C.1	
= 5	Deirmendjian Cloud C.2	
= 6	Deirmendjian Cloud C.3	
= 7-15	Various Gaussians	
= 16-20	Various log-normals	

Variable	Type	Description
NMAT(I)	Integer	Flag specifying aerosol material:

= 1	Water
= 2	Sahara dust (Volz)
= 3	Dust, γ (Volz)
= 4	Sea-salt (Volz)
= 5	Water solubles, B1 (Volz)
= 6	Water solubles, M (Volz)
= 7	Water solubles, T2 (Volz)
= 8	Soot
= 9	Ice

159

A-20

A.5 AEROS NAMELIST

Variable	Type	Description
RAD(K,I)	Real	Finite mesh of aerosol radii, in microns, K = 1 to NDAT(I), on which aerosol size distribution AERNUM is specified (level I).
NDAT(I)	Integer	Number of values of RAD for level I.
AERNUM(K,I)	Real	Aerosol number density distribution in particles/cm^3/micron (level I). NAER(I) = 0: Pointwise data, (RAD(K,I), AERNUM(K,I)), K = 1 to NDAT(I). NAER(I) = -1: Histogram data, value of distribution = AERNUM(K,I) between RAD(K,I) and RAD(K+1,I).

A.6 RSTART NAMELIST

NUSTRT	Integer	The number of the frequency group with which the calculation is to begin (if NUSTRT = 1, this saves the expense of setting up a problem again, but otherwise does the problem from scratch).
INPT	Integer	If > 0, WISCOM NAMELIST follows immediately containing changes to one or more input variables. If = 0, WISCOM is edited only. If < 0, none of the above.

160

APPENDIX B — ATRAD OUTPUT

In order to illustrate the output of ATRAD, a sample calculation has been performed for frequency group 29,000-29,800 cm^{-1}. A Dejrmendjian Hase M water droplet aerosol was used at one level only (the surface level); no aerosol was assumed at any other levels. Selections from the printed output (there is also tape output) are presented in the following pages and described below in order of appearance:

B.1 EDITS DONE BEFORE LOOP OVER FREQUENCIES

(a) The input parameters in NAMELIST WISCOM (see Appendix A, Section A.1);

(b) The atmospheric structure (see Appendix A, Section A.4);

(c) The quantities F, DU, and UMAX, which are respectively the integrands in the expressions (4.22) as a function of level, the effective absorber amounts Δu for each zone (integrals of the F's), and the sum of all the Δu's . All these quantities are given as a function of absorbing species using the LOTRAN prescriptions.

(d) The solar zenith angle (MUSUN) and earth-sun distance (RSUN);

161

B.2   <u>FREQUENCY GROUP 29,000-29,800 cm^{-1}</u>

(e)   The quadrature angles (MU(J)) and weights (WT(J));

(f)   Edits from the integration over aerosol sizes in subroutine MIE. Successive Romberg results for SGSCT (proportional to $\beta_{\nu,M}$) and SGEXT (proportional to $\beta_{\nu,M} + \alpha_{\nu,M}$) and $P_{\nu,M}(0°)$ ($P_{\nu,M}$ is filled in at other angles with the Henyey-Greenstein phase function) are followed by an edit of $P_{\nu,M}$ (PHASEM) for all ANGL(θ) and XMU($\cos\theta$), and by the integrals of $n(a,z)$ times each of σ_{sca}, σ_{abs}, and σ_{ext} (average cross-sections). Finally the renormalization factor (4.35) is printed.

(g)   Mie phase function truncation information, including value of $P_{\nu,M}^{t}(0°)$ (AX) and factor F (FTRUNK).

(h)   BETASC ($\beta_{\nu,M}$), BETABS ($\alpha_{\nu,M}$), vectors SOURC1 and SOURC2 ($\overline{P}_{\nu}(z,\mu_i,\mu_o)$ and $\overline{P}_{\nu,M}(z,-\mu_i,-\mu_o)$), and matrices PHFCN1 and PHFCN2 ($\overline{P}_{\nu,M}(z,\mu_i,\mu_j)$ and $\overline{P}_{\nu,M}(z,\mu_i,-\mu_j)$) before and after renormalization by the methods of Section 4.7.7.

(i)   The results of the transmission function fitting process for O_3, the only active absorber. Only the special case of a 1-term fit is used because the total optical depth of O_3 is small.

(j)   A "short" edit of the single pass (because of the single term exponential fit) through the Grant-Hunt algorithm.

(k)   The Planck function B_{ν} (B), scattering coefficient β_{ν} (BETASC), continuum absorption coefficient α_{ν}^{cont} (BETABS), and solar flux (SOLFLX) for the current and previous frequency group. Also the optical depth DTAU(CONT) of each zone due to α_{ν}^{cont} .

(1)   Boundary condition information: emissivity ε'_ν (EPS), $\varepsilon'_\nu B_\nu (T_g)$ (W), $\bar{\rho}''_\nu (\mu_i, \mu_o) \mu_o S_\nu / \pi$ (Wl), and matrix $r_G = 2\mu_j c_j \bar{\rho}''_\nu (\mu_i, \mu_j)$ (RG).

(m)   Fluxes and intensities for each level and heating rates for each zone.

B.3   SUMMARY PRINTS

The summary prints contain:

(1)   the frequency-integrated flux $F(z)$ at each level and the frequency-integrated heating rate in each zone.

(2)   the flux spectrum, F_ν , as a function of frequency group, at the upper boundary of the problem and at the surface.

163

```
AXOT    ATRAE=
PR1     =  T
PR2     =  T
PR3     =  T
PR4     =  T
PR5     =  F
SCTPOT  =  T
MIEPR   =  F,    F,    T
FITPRI  =  T
FITPR2  =  T
TPP1    =  T
TPP2    =  F
PRSETZ  =  F
OZONE   =  T
TRPPO   =  .150000000E+02
NCLOUD  =  .00000000E+00    .00000000E+00
CLOBAS  =  .00000000E+00    .00000000E+00
CLOTOP  =  +16.             +12.             +10.
NZONES  =  +0
EXPAN   =  .11000000E-01    .00000000E+00    .00000000E+00
PRSETF  =  .00000000E+00
NWAV    =  F
WAV     =
CWEV    =  +7      +3200.   +4400.   +7400.
           +2500.  +32000.  +35000.  +50000.
           +9000.  +16500.  +22500.  +31500.
           +8500.  +0       +0
           +49500.
           +140.   +200.    +300.    +400.
           +500.   +1000.   +1500.   +600.
           +300.   +1200.   +1800.   +3000.
NGRDS   =  +0
IWV     =  +2      +720.    +2900.   +29800.
           +700.   +0.      +0.      +0.
           +0.     +0.      +0.      +0.
           +0.     +0.      +0.      +0.
           +0.     +0.      +0.      +0.
           +0.     +0.
PACCW   =  F, F, F, F, F, F, F, F, F, F
INWANG  =  +20     +320.    +1400.   +2500.
           +50000. +0.      +0.      +0.
           +0.     +0.      +0.      +0.
NUMANG  =  +7      +5.      +4.      +5.
```

```
NOPT3  =  0
NOPT4  =  0
NOPT5  =  0
PO     =  .10130000E+04
DAY    =  .52000000E+02
TIME   =  .12000000E+02
LONG   = -.20000000E+02
LAT    =  .14000000E+02
CUTPLK =  .33720000E+04
CUTSOL =  .30000000E+04
CUTRAY =  .30000000E+01
O3CUT  =  .33333000E+05
NMATS  =  1
TG     =  .34326000E+03
NSURF  =  1.           1.          1.
                       1.          1.
                       1.          2.
WNSURF =  .50000000E+00   .41000000E+05   .00000000E+00
          .00000000E+00   .00000000E+00   .00000000E+00
          .00000000E+00   .00000000E+00   .00000000E+00
DELO   =  .10000000E-57
NOTHS  =  F. F. F. F. F.   F. F. F. F. F.   F. F. F. F. F.
          F. F. F. F. F.   F. F. F. F. F.   F. F. F. F. F.
NSTEP  =  .10           .10.         10.
          0             0
NCHUN  =  4
RANGLO =  .12500000E+00
CANGHT =  .10000000E+01
CAVEMX =  .25000000E+01
ANGVAR =  .20000000E+02
CUTMIN =  .50000000E+01
NOFF   =  50
WINDTE =  10
TMAX   = -.99999999999997D-008
EMX    = -.99999999999999D-000
TPMIN  =  .10000000E-01
TDMAX  =  .99000000E+00
NSRCHE =  1001
CORLEE =  21
CTEST  =  .50000000000000D-001
RTEST  =  .50000000000000D-002
ITMAX  =  .99999999999997D-016
ISEC1  =  150
TSEC2  =  21
SLANT  =  10
CHSMIN =  .20000000E+01
FACT   =  .50000000E+00
```

I N P U T   D A T A

I	NAED	NPAT	AER DEN	O3DEN	H2ODEN	TEMP	PRESS	ZDN	ACT	I

SSS-R-72-1255

	H20	CO2+	O3	O3 O-4	N2 CONT	H20 CENT
1	1.03972-07	1.87646-05	3.63953-05	4.35287-04	3.35321-06	2.81359-10
2	9.86436-07	2.42102-03	2.33466-03	1.05808-02	4.41250-04	3.19662-09
3	1.83501-06	4.56904-03	2.41532-03	1.14586-02	1.67594-03	5.25784-09
4	2.57548-06	9.26227-03	3.40617-03	1.01741-02	3.75212-03	9.40218-09
5	3.54287-06	1.54057-02	3.11691-03	4.25581-03	6.70461-03	1.25116-08
6	4.74916-06	4.34916-02	2.79512-03	6.76265-03	1.00528-02	1.59705-08
7	5.39301-06	7.18211-02	2.50522-03	5.53774-03	1.51366-02	1.99424-08
8	1.15204-05	4.20162-02	2.25967-03	4.77551-03	2.10571-02	4.31220-08
9	2.23059-05	5.24925-02	2.05232-03	4.10806-03	2.77172-02	8.42550-08
10	3.98981-05	6.62456-02	1.87756-03	3.58704-03	3.53925-02	1.62220-07
11	8.47415-05	7.29011-02	1.74229-03	3.16900-03	4.56075-02	2.65321-07
12	1.23975-04	1.21129-01	1.53720-03	2.65986-03	5.75957-02	5.23769-07
13	2.35471-04	1.20675-01	1.36668-03	2.26335-03	7.06216-02	9.90737-07
14	3.00140-04	1.41022-01	1.22249-03	1.54807-03	8.83145-02	1.61870-06
15	6.19743-04	1.62224-01	1.09954-03	1.49155-03	9.91585-02	2.66059-06
16	9.79564-04	1.84414-01	9.94190-04	1.48403-03	1.14861-01	4.03456-06
17	1.35896-03	2.07372-01	9.03079-04	1.10746-03	1.31060-01	6.02697-06
18	1.52272-03	2.31121-01	8.23712-04	1.16001-03	1.45607-01	8.73115-06
19	2.86909-03	2.55530-01	7.54205-04	1.03674-03	1.67032-01	1.23421-05
20	3.61103-03	2.80873-01	6.93065-04	9.15666-04	1.85896-01	1.75661-05
21	4.81103-03	3.06305-01	6.38959-04	8.19765-04	2.05902-01	2.31553-05
22	6.29161-03	3.33470-01	5.90809-04	7.50250-04	2.27673-01	3.03000-05
23	8.10547-03	3.60756-01	5.47791-04	6.71173-04	2.48955-01	4.05371-05
24	8.71672-03	3.81069-01	5.18466-04	6.41815-04	2.66710-01	5.96784-05
25	1.15711-02	4.02929-01	4.91376-04	6.01323-04	2.83536-01	5.88623-05
26	1.76969-02	4.24540-01	4.66228-04	5.65169-04	3.01170-01	7.19362-05
27	1.60996-02	4.46494-01	4.47033-04	5.10712-04	3.19227-01	7.19362-05
28	1.84262-02	4.68760-01	4.21405-04	4.58392-04	3.37752-01	8.59818-05
29	7.13072-02	4.91410-01	4.01307-04	4.09092-04	3.56581-01	1.02637-04
30	2.65971-02	5.14210-01	3.82548-04	4.27141-04	3.76450-01	1.22940-04
31	2.92405-02	5.37632-01	3.65930-04	4.17399-04	3.95596-01	1.42518-04
32	3.34926-02	5.60051-01	3.48525-04	3.98336-04	4.18758-01	1.57192-04
33	3.72221-02	5.82707-01	3.33043-04	3.73054-04	4.35249-01	1.92502-04
34	4.94162-02	6.05598-01	3.18503-04	3.58720-04	4.54262-01	2.25409-04
35	4.51079-02	6.28719-01	3.04370-04	3.34067-04	4.74125-01	2.62612-04
36	5.54858-02	6.52066-01	2.91958-04	3.17881-04	4.94563-01	3.05575-04
37	6.24239-02	6.75634-01	2.79827-04	3.01952-04	5.15403-01	3.49628-04
38	7.00450-02	6.99421-01	2.68302-04	2.87031-04	5.36472-01	4.01556-04
39	7.83459-02	7.23422-01	2.57573-04	2.73180-04	5.57846-01	5.25648-04

	H20	CO2+	O3	CU	N2 CONT	H20 CENT
1	6.97697-06	5.83048-03	9.82527-03	5.65051-02	1.59209-03	2.13552-08
2	6.19217-06	1.22204-02	1.24726-02	5.09210-02	4.19612-03	2.06611-08
3	5.94617-06	1.77180-02	9.10172-03	2.93119-02	6.87148-03	2.05000-08
4	5.79279-06	2.27449-02	5.14100-03	1.72514-02	9.53120-03	2.05869-08
5	5.68750-06	2.74636-02	4.28582-03	1.06568-02	1.23162-02	2.05776-08
6	5.71388-06	3.19569-02	3.11305-03	7.28423-03	1.50719-02	2.09946-08

167

#						
7	7.98603-06	3.62744-02	2.35421-03	5.13686-03	1.78451-02	2.97224-08
8	1.38253-05	4.04491-02	1.83352-03	3.77522-03	2.05337-02	5.22549-08
9	2.25905-05	4.45041-02	1.46517-03	2.86450-03	2.34361-02	8.57665-08
10	3.50806-05	4.87217-02	1.18570-03	2.20960-03	2.64384-02	1.33541-07
11	6.01916-05	8.24028-02	1.46871-03	2.60698-03	4.60908-02	3.41025-07
12	1.95053-04	8.99073-02	1.17808-03	1.99554-03	5.17907-02	5.81732-07
13	2.47616-04	9.71278-02	9.62006-04	1.56766-03	5.73968-02	9.32926-07
14	3.39559-04	1.04032-01	7.97419-04	1.24915-03	5.29288-02	1.42507-06
15	8.67272-04	1.10794-01	6.69472-04	1.01427-03	6.83556-02	2.09289-06
16	5.77706-04	1.17306-01	5.62254-04	8.35064-04	7.30041-02	2.97574-06
17	9.18762-04	1.22635-01	4.87254-04	6.95831-04	7.91604-02	4.11803-06
18	1.21653-03	1.29024-01	4.20088-04	5.85931-04	8.44592-02	5.56958-06
19	1.58009-03	1.35028-01	3.66402-04	4.97979-04	8.97246-02	7.38632-06
20	2.02227-03	1.41719-01	3.21247-04	4.26729-04	9.49600-02	9.63081-06
21	2.54270-03	1.47489-01	2.83293-04	3.68380-04	1.00149-01	1.23772-05
22	3.16103-03	1.53147-01	2.51185-04	3.20130-04	1.05303-01	1.56913-05
23	2.03052-03	1.18517-01	1.70211-04	2.13316-04	8.23449-02	1.43429-05
24	3.23204-03	1.21500-01	1.56510-04	1.93475-04	8.52133-02	1.69952-05
25	3.79502-03	1.24644-01	1.44257-04	1.75491-04	8.80693-02	1.97945-05
26	4.45879-03	1.27652-01	1.33264-04	1.60525-04	9.04178-02	2.30856-05
27	4.97528-03	1.30624-01	1.23371-04	1.46793-04	9.37472-02	2.68001-05
28	5.65054-03	1.33563-01	1.14440-04	1.34561-04	9.65702-02	3.09322-05
29	6.40117-03	1.36470-01	1.06557-04	1.23628-04	9.93627-02	3.55798-05
30	7.22436-03	1.39347-01	9.94223-05	1.13828-04	1.02185-01	4.09439-05
31	8.11277-03	1.42152-01	9.24033-05	1.05095-04	1.04938-01	4.68290-05
32	9.07763-03	1.44839-01	8.64119-05	9.72862-05	1.07640-01	5.33972-05
33	1.01251-02	1.47598-01	8.09241-05	9.02122-05	1.10221-01	6.07128-05
34	1.12590-02	1.50279-01	7.58877-05	8.37892-05	1.13211-01	6.88456-05
35	1.24866-02	1.52923-01	7.12569-05	7.79447-05	1.15681-01	7.78755-05
36	1.38057-02	1.55563-01	6.69915-05	7.26156-05	1.18740-01	8.78829-05
37	1.52277-02	1.58167-01	6.30556-05	6.77466-05	1.20989-01	9.39587-05
38	1.67604-02	1.50748-01	5.94131-05	6.32895-05	1.23629-01	1.11201-04

UMAX

2.97799-01	7.93180+00	1.23217-01	4.00589-01	5.41033+03	1.75556-03

MUSUN = .84642+00   PSUN = 1.4890+00

STARTING AT FREQ GROUP   1   CODE USES   3   ANGLES
WHICH ARE: 83.5290   60.0000   27.4647
MU(J):   1.1270-01   5.0000-01   8.6730-01
WT(J):   2.7778-01   4.4444-01   2.7778-01

ALPHA-MIN = 1.4775-01   ALPHA-MAX = 1.3852+02
REVISED ALPHA-MAX = 1.2468+02

TRAPEZOIDAL RESULTS (FOR ROMBERG SCHEME)

SGSCT: 1.0287+03   1.0286+03   1.0300+03   1.0278+03
SGEXT: 1.0287+03   1.0286+03   1.0300+03   1.0278+03

ANGLE	PHASE FUNCTION			
.0000	2.2101+02	2.2101+02	2.2080+02	2.1983+02

MIE PHASE FUNCTION AND CROSS SECTIONS, LEVEL 39

LAMDA = .3402   NAER = 1   NMAT = 1   IOR = 1.3510 + 1.3469-08 I

I	ANGL(I)	XMU(I)	PHASE(I)
1	.0000	1.00000+000	2.19056+02
2	.2406	9.99991-001	2.18454+02
3	.4812	9.99965-001	2.16663+02
4	.7218	9.99921-001	2.13733+02
5	.9625	9.99859-001	2.09741+02
6	1.2031	9.99780-001	2.04788+02
7	1.4437	9.99683-001	1.98993+02
8	1.6843	9.99568-001	1.92491+02
9	1.9249	9.99436-001	1.85416+02
10	2.1655	9.99286-001	1.77908+02
11	2.4061	9.99118-001	1.70100+02
12	2.6467	9.98933-001	1.62112+02
13	2.8874	9.98730-001	1.54058+02
14	3.1280	9.98510-001	1.46034+02
15	3.3686	9.98272-001	1.38122+02
16	3.6092	9.98017-001	1.30390+02
17	3.8498	9.97743-001	1.22893+02
18	4.0904	9.97144-001	1.15753+02
19	4.3310	9.96475-001	9.59024+01
20	4.8173	9.95735-001	8.44059+01
21	5.2935	9.94925-001	7.42367+01
22	5.7747	9.94045-001	6.53125+01
23	6.2559	9.93095-001	5.75526+01
24	6.7272	9.92074-001	5.07449+01
25	7.2184	9.90984-001	4.46579+01
26	7.5956	9.89824-001	3.97473+01
27	8.1808	9.88594-001	3.53091+01
28	8.6621	9.85925-001	2.80907+01
29	9.5245	9.82000-001	2.25964+01
30	10.5870	9.76251-001	1.83762+01
31	11.5494	9.72474-001	1.51016+01
32	12.5119	3.68423-001	1.25339+01
33	13.4743	9.64009-001	1.04996+01
34	14.4358	9.59503-001	8.87150+00
35	15.3992	9.54635-001	7.55405+00
36	16.3517		6.48350+00

IP	ANGLE	PHASE(IP)
69	90.0000	7.23243-02
70	92.3847	6.80536-02
71	94.7695	6.41937-02
72	97.1542	6.06969-02
73	99.5390	5.75223-02
74	101.9237	5.46346-02
75	104.3085	5.20029-02
76	106.6932	4.96005-02
77	109.0780	4.74042-02
78	111.4627	4.53934-02
79	113.8474	4.35502-02
80	116.2322	4.18588-02
81	118.6169	4.03053-02
82	121.0017	3.88774-02
83	123.3864	3.75647-02
84	125.7712	3.63559-02
85	128.1559	3.52440-02
86	130.5406	3.42208-02
87	132.9254	3.32795-02
88	135.3101	3.24140-02
89	137.6949	3.16188-02
90	140.0796	3.08891-02
91	142.4644	3.02205-02
92	144.3693	2.97227-02
93	146.3142	2.92603-02
94	148.2391	2.88317-02
95	150.1640	2.84353-02
96	152.0889	2.80697-02
97	154.0138	2.77336-02
98	155.9387	2.74260-02
99	157.8636	2.71457-02
100	159.7885	2.68918-02
101	161.7134	2.66625-02
102	162.6759	2.65587-02
103	163.6383	2.64601-02
104	164.6004	2.63675-02

37	18.2865	9.49448-001	105	165.5632	2.62809-02
38	20.2115	3.36424-001	106	166.5257	2.52001-02
39	22.1174	9.26789-001	107	167.4881	2.51252-02
40	24.0523	3.13110-001	108	168.4506	2.60561-02
41	25.9062	2.62373+00	109	169.4130	2.59926-02
42	27.9111	8.38830-001	110	170.3755	2.59351-02
43	29.8760	8.43675-001	111	171.3379	2.58830-02
44	31.7509	8.67453-001	112	172.3004	2.58590-02
45	33.6808	8.50252-001	113	173.2628	2.58365-02
46	35.6107	1.19897+00	114	174.2253	2.58151-02
47	37.6355	1.01492+00	115	175.1877	2.57956-02
48	39.9204	8.12992-001	116	176.1502	2.57772-02
49	42.3051	8.57168-001	117	174.2253	2.57602-02
50	44.5299	7.47200-001	118	174.7065	2.57645-02
51	47.0746	6.27934-001	119	175.1877	2.5737-02
52	49.N504	5.33701-001	120	175.6690	2.57173-02
53	51.8041	5.57254-001	121	176.1502	2.57058-02
54	54.2298	5.95840-001	122	176.3908	2.57005-02
55	56.6130	6.45987-001	123	176.6314	2.56956-02
56	58.9983	6.17003-001	124	176.8720	2.56910-02
57	61.3821	5.84743-001	125	177.1126	2.56868-02
58	63.7678	5.50283-001	126	177.3533	2.56879-02
59	66.152E	5.15063-001	127	177.5939	2.56793-02
60	68.5373	4.78951-001	128	177.8345	2.56751-02
61	70.9220	4.42010-001	129	178.0751	2.56712-02
62	73.3058	4.04303-001	130	178.3157	2.56707-02
63	75.6915	3.65095-001	131	178.5563	2.56665-02
64	78.0763	3.26654-001	132	178.7569	2.56666-02
65	80.4510	2.87247-001	133	178.0375	2.56651-02
66	82.8458	2.47142-001	134	179.2782	2.56639-02
67	85.2305	2.05603-001	135	179.5188	2.56631-02
68	87.6153	1.65715-001	136	179.7594	2.56625-02
69	90.0000	1.24541-001	137	180.0000	2.56624-02
		8.31472-002			
		4.16097-002			
		0.00000			

AVG CROSS-SECTION PER PARTICLE (IN SQ MICRONS)?
RENORMALIZATION FACTOR = 1.0000+00

SCAT	APS	EXT
1.024110+00	4.321337-07	1.024111+00

ITRUNC = 37   TRUNCATION ANGLE = 18.2866   WHERE PHASEM = 5.602+00   AX = 9.0135+01   BX = -1.5193-01   FTRUNK = .28895

MIE RESULTS, LEVEL 39:   BETASC = 7.2819-02   BETABS = 4.3213-08
SOURC1: 1.5197227-01 2.31572319-01 5.93137026-01 4.64253336+00 3.22295123+00
SOURC2: 1.27346013-01 9.45695052-02 6.65618284-02 5.00652543-02 4.23339847-02

PHFCN1
4.8015677+00
1.94531003+00 4.93067920+00
4.4311003-01 1.09702592+00 5.54735881+00

```
             1.93263798-01   2.99925905-01   9.56897311-01   7.55519748+00
             2.20123814-01   1.69873880-01   3.47819265-01   1.41574211+00   1.53326333+01

PHFCN2
             3.32270595+00   4.40911409-01
             1.08939624+00   1.90716876-01   1.16605511-01
             3.17589626-01   1.08122575-01   7.35861873-02   5.41126295-02
             1.50584241-01   7.99668664-02   5.86622871-02   4.52407510-02   3.87962307-02
             1.03369725-01

AFTER RENORMALIZATION
SOURC1:      1.68081529-01   2.56077234-01   6.55902617-01   5.13380492+00   3.56400302+00
SOURC2:      1.40821731-01   1.04576823-01   7.36053819-02   5.53631452-02   4.68137548-02

PHFCN1
             4.91647291+00   4.62534082+00
             1.90235357+00   9.88254346-01   4.79082990+00
             4.18197136-01   2.63484590-01   8.05012688-01   6.28713349+00
             1.69559292-01   1.47365741-01   2.88785920-01   1.14381497+00   1.30159329+01
             1.09364251-01

PHFCN2
             3.40222082+00   4.13607430-01
             1.06870018+00   1.71207045-01   9.5521283-02
             2.99733840-01   1.3875453-01   6.13061356-02   4.43141377-02
             1.3875453-01   2.49855580-02   4.8622499-02   3.65511822-02   3.09178028-02
             0.41108353-02   6.93713278-02
```

RAYLEIGH + MIE RESULTS, LEVEL 1: RAY. SCATT. COEFF. =   1.8522-04   TOTAL SCATT. COEFF. =   1.8522-04
SOURC1, ETC. SAME AS FOR LEVEL 38

RAYLEIGH + MIE RESULTS, LEVEL 2: RAY. SCATT. COEFF. =   2.1632-03   TOTAL SCATT. COEFF. =   2.1632-03
SOURC1, ETC. SAME AS FOR LEVEL 38

RAYLEIGH + MIE RESULTS, LEVEL 3: RAY. SCATT. COEFF. =   4.2409-03   TOTAL SCATT. COEFF. =   4.2409-03
SOURC1, ETC. SAME AS FOR LEVEL 38

RAYLEIGH + MIE RESULTS, LEVEL 4: RAY. SCATT. COEFF. =   6.3757-03   TOTAL SCATT. COEFF. =   6.3757-03
SOURC1, ETC. SAME AS FOR LEVEL 38

RAYLEIGH + MIE RESULTS, LEVEL 5: RAY. SCATT. COEFF. =   8.5532-03   TOTAL SCATT. COEFF. =   8.5532-03
SOURC1, ETC. SAME AS FOR LEVEL 38

RAYLEIGH + MIE RESULTS, LEVEL 6: RAY. SCATT. COEFF. =   1.0766-02   TOTAL SCATT. COEFF. =   1.0766-02
SOURC1, ETC. SAME AS FOR LEVEL 38

RAYLEIGH + MIE RESULTS, LEVEL 7: RAY. SCATT. COEFF. =   1.3008-02   TOTAL SCATT. COEFF. =   1.3008-02

171

SOURC1. ETC. SAME AS FOR LEVEL 38

RAYLEIGH + MIE RESULTS, LEVEL 8: RAY. SCATT. COEFF. = 1.5276-02 TOTAL SCATT. COEFF. = 1.5276-02
SOURC1. ETC. SAME AS FOR LEVEL 38

RAYLEIGH + MIE RESULTS, LEVEL 9: RAY. SCATT. COEFF. = 1.7567-02 TOTAL SCATT. COEFF. = 1.7567-02
SOURC1. ETC. SAME AS FOR LEVEL 38

RAYLEIGH + MIE RESULTS, LEVEL 10: RAY. SCATT. COEFF. = 1.9880-02 TOTAL SCATT. COEFF. = 1.9880-02
SOURC1. ETC. SAME AS FOR LEVEL 38

RAYLEIGH + MIE RESULTS, LEVEL 11: RAY. SCATT. COEFF. = 2.2758-02 TOTAL SCATT. COEFF. = 2.2758-02
SOURC1. ETC. SAME AS FOR LEVEL 38

RAYLEIGH + MIE RESULTS, LEVEL 12: RAY. SCATT. COEFF. = 2.5313-02 TOTAL SCATT. COEFF. = 2.5313-02
SOURC1. ETC. SAME AS FOR LEVEL 38

RAYLEIGH + MIE RESULTS, LEVEL 13: RAY. SCATT. COEFF. = 2.7789-02 TOTAL SCATT. COEFF. = 2.7789-02
SOURC1. ETC. SAME AS FOR LEVEL 38

RAYLEIGH + MIE RESULTS, LEVEL 14: RAY. SCATT. COEFF. = 3.0197-02 TOTAL SCATT. COEFF. = 3.0197-02
SOURC1. ETC. SAME AS FOR LEVEL 38

RAYLEIGH + MIE RESULTS, LEVEL 15: RAY. SCATT. COEFF. = 3.2547-02 TOTAL SCATT. COEFF. = 3.2547-02
SOURC1. ETC. SAME AS FOR LEVEL 38

RAYLEIGH + MIE RESULTS, LEVEL 16: RAY. SCATT. COEFF. = 3.4845-02 TOTAL SCATT. COEFF. = 3.4845-02
SOURC1. ETC. SAME AS FOR LEVEL 38

RAYLEIGH + MIE RESULTS, LEVEL 17: RAY. SCATT. COEFF. = 3.7099-02 TOTAL SCATT. COEFF. = 3.7099-02
SOURC1. ETC. SAME AS FOR LEVEL 38

RAYLEIGH + MIE RESULTS, LEVEL 18: RAY. SCATT. COEFF. = 3.9311-02 TOTAL SCATT. COEFF. = 3.9311-02
SOURC1. ETC. SAME AS FOR LEVEL 38

RAYLEIGH + MIE RESULTS, LEVEL 19: RAY. SCATT. COEFF. = 4.1486-02 TOTAL SCATT. COEFF. = 4.1486-02
SOURC1. ETC. SAME AS FOR LEVEL 38

RAYLEIGH + MIE RESULTS, LEVEL 20: RAY. SCATT. COEFF. = 4.3628-02 TOTAL SCATT. COEFF. = 4.3628-02
SOURC1. ETC. SAME AS FOR LEVEL 38

172

RAYLEIGH + MIE RESULTS, LEVEL 21: RAY. SCATT. COEFF. = 4.5740-02 TOTAL SCATT. COEFF. = 4.5740-02
SOURC1. ETC. SAME AS FOR LEVEL 38

RAYLEIGH + MIE RESULTS, LEVEL 22: RAY. SCATT. COEFF. = 4.7823-02 TOTAL SCATT. COEFF. = 4.7823-02
SOURC1. ETC. SAME AS FOR LEVEL 38

RAYLEIGH + MIE RESULTS, LEVEL 23: RAY. SCATT. COEFF. = 4.9879-02 TOTAL SCATT. COEFF. = 4.9879-02
SOURC1. ETC. SAME AS FOR LEVEL 38

RAYLEIGH + MIE RESULTS, LEVEL 24: RAY. SCATT. COEFF. = 5.1406-02 TOTAL SCATT. COEFF. = 5.1406-02
SOURC1. ETC. SAME AS FOR LEVEL 38

RAYLEIGH + MIE RESULTS, LEVEL 25: RAY. SCATT. COEFF. = 5.2920-02 TOTAL SCATT. COEFF. = 5.2920-02
SOURC1. ETC. SAME AS FOR LEVEL 38

RAYLEIGH + MIE RESULTS, LEVEL 26: RAY. SCATT. COEFF. = 5.4421-02 TOTAL SCATT. COEFF. = 5.4421-02
SOURC1. ETC. SAME AS FOR LEVEL 38

RAYLEIGH + MIE RESULTS, LEVEL 27: RAY. SCATT. COEFF. = 5.5910-02 TOTAL SCATT. COEFF. = 5.5910-02
SOURC1. ETC. SAME AS FOR LEVEL 38

RAYLEIGH + MIE RESULTS, LEVEL 28: RAY. SCATT. COEFF. = 5.7388-02 TOTAL SCATT. COEFF. = 5.7388-02
SOURC1. ETC. SAME AS FOR LEVEL 38

RAYLEIGH + MIE RESULTS, LEVEL 29: RAY. SCATT. COEFF. = 5.8856-02 TOTAL SCATT. COEFF. = 5.8856-02
SOURC1. ETC. SAME AS FOR LEVEL 38

RAYLEIGH + MIE RESULTS, LEVEL 30: RAY. SCATT. COEFF. = 6.0313-02 TOTAL SCATT. COEFF. = 6.0313-02
SOURC1. ETC. SAME AS FOR LEVEL 38

RAYLEIGH + MIE RESULTS, LEVEL 31: RAY. SCATT. COEFF. = 6.1761-02 TOTAL SCATT. COEFF. = 6.1761-02
SOURC1. ETC. SAME AS FOR LEVEL 38

RAYLEIGH + MIE RESULTS, LEVEL 32: RAY. SCATT. COEFF. = 6.3103-02 TOTAL SCATT. COEFF. = 6.3103-02
SOURC1. ETC. SAME AS FOR LEVEL 38

RAYLEIGH + MIE RESULTS, LEVEL 33: RAY. SCATT. COEFF. = 6.4434-02 TOTAL SCATT. COEFF. = 6.4434-02
SOURC1. ETC. SAME AS FOR LEVEL 38

RAYLEIGH + MIE RESULTS, LEVEL 34: RAY. SCATT. COEFF. = 6.5754-02 TOTAL SCATT. COEFF. = 6.5754-02

173

```
SOURC1. ETC. SAME AS FOR LEVEL 38

RAYLEIGH + MIE RESULTS, LEVEL 35:   RAY. SCATT. COEFF. =   5.7063-02   TOTAL SCATT. COEFF. =   6.7063-02
SOURC1. ETC. SAME AS FOR LEVEL 38

RAYLEIGH + MIE RESULTS, LEVEL 36:   RAY. SCATT. COEFF. =   6.8362-02   TOTAL SCATT. COEFF. =   6.8362-02
SOURC1. ETC. SAME AS FOR LEVEL 38

RAYLEIGH + MIE RESULTS, LEVEL 37:   RAY. SCATT. COEFF. =   6.9652-02   TOTAL SCATT. COEFF. =   6.9652-02
SOURC1. ETC. SAME AS FOR LEVEL 38

RAYLEIGH + MIE RESULTS, LEVEL 38:   RAY. SCATT. COEFF. =   7.0931-02   TOTAL SCATT. COEFF. =   7.0931-02
SOURC1:   8.64552917-01   9.65938337-01   1.10561362+00   1.23504445+00
SOURC2:   8.64652917-01   8.65938337-01   1.10561362+00   1.23504445+00

PHFCN1
1.11699025+00
1.09995337+00
1.02944189+00   1.00740936+00   1.07123475+00
9.08710450-01   9.77025911-01   1.15853389+00   1.35281914+00
7.96833999-01   9.48870942-01

PHFCN2
1.11699025+00
1.09995337+00
1.02944189+00   1.00740936+00   1.07123475+00
9.08710450-01   9.77025911-01   1.15853389+00   1.35281914+00
7.96833999-01   9.48870942-01

RAYLEIGH + MIE RESULTS, LEVEL 39:   RAY. SCATT. COEFF. =   7.2202-02   TOTAL SCATT. COEFF. =   1.4502-01
SOURC1:   5.14885232-01   8.10260855-01   3.12827945+00   2.40447870+00
SOURC2:   5.01977371-01   5.17873377-01   5.78253910-01   6.38401576-01

PHFCN1
5.02481514+00
1.50537549+00   2.85205408+00
7.22519062-01   1.00650054+00   2.90716901+00
5.37537172-01   5.91732055-01   8.90653327-01   3.64006841+00
4.51636497-01   6.17424063-01   1.15114310+00   7.20918977+00

PHFCN2
2.26446745+00
1.02376241+00   7.47226715-01
5.63035378-01   5.96539870-01   5.49525350-01
5.22093326-01   5.07240051-01   5.17519057-01   5.55589609-01
4.43977337-01   4.47149772-01   4.95831577-01   5.95155455-01   6.89056061-01
```

TRANS. FCN. FITTING FOR FREQ GROUP STARTING AT 29000 CM**-1 AND CONSISTING OF 40 20 CM**-1 SUBGROUPS

FOR O3.

	TRANSMISSION FCN	EXPONENTIAL APPROX	PERCENT ERROR
1	1.00000000+00	1.00000000+00	0.00000000
2	9.90380021-01	9.8959836-01	-7.9893581-02
3	9.80886621-01	9.79304492-01	-1.6133966-01

	COEFFICIENTS	EXPONENTS
1	1.00000000+00	5.22037300-02

175

B-15

ZONE

1 OMEG = 8.4360-01 ABCD(ILINE) = 2.2721-05 CTAU(TOT) = 1.7271-02 TAU = 1.7271-02 FL = 9.7980-01
   DTMAX = 2.4760-02 CTAUPP = 1.7271-02 NCBL = 0 NOSCT = NOPLK = T NOSOL = F

2 OMEG = 8.3435-01 ABCD(ILINE) = 5.5283-04 CTAU(TOT) = 1.6651-02 TAU = 1.3922-02 FL = 9.6072-01
   DTMAX = 2.4760-02 CTAUPP = 1.6651-02 NCBL = 0 NOSCT = NOPLK = T NOSOL = F

3 OMEG = 8.9705-01 ABCD(ILINE) = 6.2115-04 CTAU(TOT) = 1.5498-02 TAU = 9.9520-02 FL = 9.4328-01
   DTMAX = 2.4851-02 CTAUPP = 1.5498-02 NCBL = 0 NOSCT = NOPLK = T NOSOL = F

4 OMEG = 9.3774-01 ABCD(ILINE) = 5.2851-04 CTAU(TOT) = 1.4661-02 TAU = 6.4281-02 FL = 9.2687-01
   DTMAX = 2.4981-02 CTAUPP = 1.4861-02 NCBL = 0 NOSCT = NOPLK = T NOSOL = F

5 OMEG = 9.6012-01 ABCD(ILINE) = 4.3098-04 CTAU(TOT) = 1.4524-02 TAU = 7.0806-02 FL = 9.1110-01
   DTMAX = 2.5012-02 CTAUPP = 1.4524-02 NCBL = 0 NOSCT = NOPLK = T NOSOL = F

6 OMEG = 9.7705-01 ABCD(ILINE) = 1.5535-04 CTAU(TOT) = 1.4336-02 TAU = 9.1141-02 FL = 8.9580-01
   DTMAX = 2.5060-02 CTAUPP = 1.4336-02 NCBL = 0 NOSCT = NOPLK = T NOSOL = F

7 OMEG = 9.0091-01 ABCD(ILINE) = 2.9431-04 CTAU(TOT) = 1.4222-02 TAU = 1.0736-01 FL = 8.8097-01
   DTMAX = 2.5077-02 CTAUPP = 1.4222-02 NCBL = 0 NOSCT = NOPLK = T NOSOL = F

8 OMEG = 9.8294-01 ABCD(ILINE) = 2.6930-04 CTAU(TOT) = 1.4150-02 TAU = 1.2151-01 FL = 8.6527-01
   DTMAX = 2.5080-02 CTAUPP = 1.4150-02 NCBL = 0 NOSCT = NOPLK = T NOSOL = F

9 OMEG = 9.8531-01 ABCD(ILINE) = 2.1495-04 CTAU(TOT) = 1.4102-02 TAU = 1.3552-01 FL = 8.5195-01
   DTMAX = 2.5095-02 CTAUPP = 1.4102-02 NCBL = 0 NOSCT = NOPLK = T NOSOL = F

10 OMEG = 9.9674-01 ABCD(ILINE) = 1.8705-04 CTAU(TOT) = 1.4076-02 TAU = 1.4969-01 FL = 8.3790-01
   DTMAX = 2.5104-02 CTAUPP = 1.4076-02 NCBL = 0 NOSCT = NOPLK = T NOSOL = F

11 OMEG = 9.9767-01 ABCD(ILINE) = 1.6527-04 CTAU(TOT) = 2.1657-02 TAU = 1.7118-01 FL = 8.1671-01
   DTMAX = 2.5104-02 CTAUPP = 2.1657-02 NCBL = 0 NOSCT = NOPLK = T NOSOL = F

12 OMEG = 9.5767-01 ABCD(ILINE) = 1.1295-02 CTAU(TOT) = 2.1657-02 TAU = 1.9305-01 FL = 7.9508-01
   DTMAX = 2.5107-02 CTAUPP = 2.1657-02 NCBL = 0 NOSCT = NOPLK = T NOSOL = F

13 OMEG = 9.9620-01 ABCD(ILINE) = 2.163F-02 CTAU(TOT) = 2.1636-02 TAU = 2.1457-01 FL = 7.7598-01
   DTMAX = 2.5105-02 CTAUPP = 2.1636-02 NCBL = 0 NOSCT = NOPLK = T NOSOL = F

```
14  SIGM   = .315542-03     .857124-04         .230825-04         .221935-04
    OMEG   = 9.9597-01   ABCO(ILINE) = 1.0170-04   CTAU(TOT) =         TAU = 2.3629-01   FL = 7.5641-01
    CTMAX  = 2.5114-02     CTAUPR = 2.1622-02   NCBL =  0            NOPLK = T   NOSOL = F
    SIGP   = .30770N-03     .640597-04         .322505-04         .216324-04
                                                                    .215324-04

15  SIGM   = .30770N-03     .640597-04         .322505-04         .239939-04
    OMEG   = 9.9754-01   ABCO(ILINE) = 4.8317-05   CTAU(TOT) =         TAU = 2.5790-01   FL = 7.3735-01
    CTMAX  = 2.5114-02     CTAUPR = 2.1610-02   NCBL =  0            NOPLK = T   NOSOL = F
    SIGP   = .299951-03     .624481-04         .233903-04         .210882-04
                                                                    .210882-04

16  SIGM   = .299961-03     .624481-04         .714382-04         .233903-04
    OMEG   = 9.9797-01   ABCO(ILINE) = 7.7157-05   CTAU(TOT) =         TAU = 2.7950-01   FL = 7.1876-01
    CTMAX  = 2.5114-02     CTAUPR = 2.1602-02   NCBL =  0            NOPLK = T   NOSOL = F
    SIGP   = .292415-03     .608769-04         .305481-04         .205575-04
                                                                    .205575-04

17  SIGM   = .292415-03     .608769-04         .706981-04         .228018-04
    OMEG   = 9.9821-01   ABCO(ILINE) = 6.8254-05   CTAU(TOT) =         TAU = 3.0110-01   FL = 7.0066-01
    CTMAX  = 2.5114-02     CTAUPR = 2.1595-02   NCBL =  0            NOPLK = T   NOSOL = F
    SIGP   = .285058-03     .593752-04         .222281-04         .200404-04
                                                                    .200404-04

18  SIGM   = .285058-03     .593752-04         .691842-04         .222281-04
    OMEG   = 9.9856-01   ABCO(ILINE) = 6.8254-05   CTAU(TOT) =         TAU = 3.2269-01   FL = 6.8301-01
    CTMAX  = 2.5114-02     CTAUPR = 2.1590-02   NCBL =  0            NOPLK = T   NOSOL = F
    SIGP   = .277805-03     .578519-04         .216688-04         .195361-04
                                                                    .195361-04

19  SIGM   = .277805-03     .578519-04         .676519-04         .216688-04
    OMEG   = 9.9879-01   ABCO(ILINE) = 5.4122-05   CTAU(TOT) =         TAU = 3.4428-01   FL = 6.6581-01
    CTMAX  = 2.5114-02     CTAUPR = 2.1586-02   NCBL =  0            NOPLK = T   NOSOL = F
    SIGP   = .270393-03     .563263-04         .211236-04         .190446-04
                                                                    .190446-04

20  SIGM   = .270393-03     .563263-04         .667963-04         .211236-04
    OMEG   = 9.9897-01   ABCO(ILINE) = 4.9584-05   CTAU(TOT) =         TAU = 3.6585-01   FL = 6.4905-01
    CTMAX  = 2.5115-02     CTAUPR = 2.1583-02   NCBL =  0            NOPLK = T   NOSOL = F
    SIGP   = .264077-03     .549772-04         .205920-04         .185654-04
                                                                    .185654-04

21  SIGM   = .264077-03     .549772-04         .652777-04         .205920-04
    OMEG   = 9.9911-01   ABCO(ILINE) = 4.3818-05   CTAU(TOT) =         TAU = 3.8744-01   FL = 6.3271-01
    CTMAX  = 2.5115-02     CTAUPR = 2.1580-02   NCBL =  0            NOPLK = T   NOSOL = F
    SIGP   = .257433-03     .535933-04         .200739-04         .180982-04
                                                                    .180962-04

22  SIGM   = .257433-03     .535933-04         .639029-04         .200739-04
    OMEG   = 9.9922-01   ABCO(ILINE) = 1.9688-05   CTAU(TOT) =         TAU = 4.0902-01   FL = 6.1679-01
    CTMAX  = 2.5115-02     CTAUPR = 2.1578-02   NCBL =  0            NOPLK = T   NOSOL = F
    SIGP   = .250956-03     .522355-04         .195689-04         .176429-04
                                                                    .176429-04

23  SIGM   = .250956-03     .522355-04         .622485-04         .195689-04
    OMEG   = 9.9931-01   ABCO(ILINE) = 3.5087-05   CTAU(TOT) =         TAU = 4.2520-01   FL = 6.0511-01
    CTMAX  = 2.5116-02     CTAUPR = 2.1587-02   NCBL =  0            NOPLK = T   NOSOL = F
    SIGP   = .184072-03     .383215-04         .192328-04         .143515-04
                                                                    .143515-04

24  SIGM   = .184073-03     .383215-04         .507615-04         .192328-04
    OMEG   = 9.9930-01   ABCO(ILINE) = 3.3362-05   CTAU(TOT) =         TAU = 4.4138-01   FL = 5.9365-01
    CTMAX  = 2.5116-02     CTAUPR = 2.1582-02   NCBL =  0            NOPLK = T   NOSOL = F
    SIGP   = .180743-03     .375960-04         .189275-04         .140818-04
                                                                    .140818-04

25  SIGM   = .180743-03     .375960-04         .522355-04         .189275-04
    OMEG   = 9.9943-01   ABCO(ILINE) = 1.1435-05   CTAU(TOT) =         TAU = 4.5755-01   FL = 5.8241-01
    CTMAX  = 2.5116-02     CTAUPR = 2.1581-02   NCBL =  0            NOPLK = T   NOSOL = F
    SIGP   = .177169-03     .368042-04         .185592-04         .138157-04
                                                                    .138157-04

26  SIGM   = .177169-03     .368042-04         .507563-04         .185592-04
    OMEG   = 9.9948-01   ABCO(ILINE) = 1.6180-02   CTAU(TOT) =         TAU = 4.7374-01   FL = 5.7138-01
    CTMAX  = 2.5116-02     CTAUPR = 1.6180-02   NCBL =  0            NOPLK = T   NOSOL = F
    SIGP   = .172815-03     .351659-04         .182176-04         .135536-04
                                                                    .135536-04

27  SIGM   = .172815-03     .361659-04     ABCO(ILINE) = 2.7684-05   CTAU(TOT) = 1.6179-02   TAU = 4.8992-01   FL = 5.6056-01
```

INTENSITIES FROM BACKWARD PASS

ZONE						
1	IP	0.0000	0.0000	0.0000	0.0000	0.0000
	I4	1.4122-03	1.5274-03	1.3405-03	1.2057-03	1.1497-03
	IP	4.8021-04	9.8864-05	4.7848-05	3.3606-05	2.8997-05

3	IM	1.4750-03	1.5961-03	1.3385-03	1.2000-03	1.1413-03
	IP	7.8116-04	1.8868-04	9.2889-05	6.5503-05	5.6502-05
4	IM	1.5559-03	1.8537-03	1.3755-03	1.1932-03	1.1331-03
	IP	1.0038-03	2.7480-03	1.3760-03	9.7198-05	8.3832-05
5	IM	1.5255-03	1.5660-03	1.3330-03	1.1891-03	1.1231-03
	IP	1.1717-03	3.5710-04	1.8158-04	1.1734-03	1.1054-04
6	IM	1.6350-03	1.6667-03	1.3215-03	1.2862-03	1.1121-03
	IP	3.2035-03	4.2606-04	2.2478-04	1.4734-03	1.3776-04
7	IM	1.6556-03	1.5639-03	2.3112-03	1.5958-04	1.1003-03
	IP	1.4023-03	6.1096-04	2.6711-04	1.1619-03	1.6425-04
8	IM	1.4772-03	1.9587-03	2.6791-04	1.9032-04	1.08A1-03
	IP	1.5720-03	6.0208-04	3.2097-03	1.1497-03	1.9036-04
9	IM	1.5340-03	1.5510-03	1.2493-03	2.2069-04	1.2756-03
	IP	1.5206-03	6.4923-03	3.9609-04	1.1370-03	2.1609-04
10	IM	1.5767-03	1.5434-03	1.2741-03	1.6015-03	1.0524-04
	IP	1.5077-03	7.1259-04	3.8826-04	2.7975-04	2.4141-04
11	IM	1.6077-03	1.5339-03	1.2606-03	1.1106-03	1.0492-03
	IP	1.6623-03	7.7302-04	6.2660-04	3.0708-04	2.6637-04
12	IM	1.6418-03	7.7362-04	5.2464-04	1.0270-03	1.0267-03
	IP	1.6427-03	1.5233-03	5.2417-04	1.5087-04	3.0192-04
13	IM	1.5813-03	8.5971-04	5.2937-04	1.1035-03	1.0162-03
	IP	1.6027-03	1.5056-04	5.2858-04	1.9270-04	3.A047-04
14	IM	1.5813-03	6.1833-04	5.7653-04	3.9270-04	9.9531-04
	IP	1.6734-03	1.4856-04	1.2006-03	1.0536-01	3.7695-04
15	IM	1.5787-03	1.6095-04	5.9678-04	4.4305-04	3.7622-04
	IP	1.6769-03	1.0736-03	1.1754-03	1.0712-03	3.1035-04
16	IM	1.6652-03	1.4390-03	4.6045-04	4.7199-04	9.5291-04
	IP	1.6776-03	1.1311-03	1.1433-03	1.0094-04	4.4755-04
17	IM	1.6558-03	1.4141-03	6.8751-04	7.8531-04	9.3142-04
	IP	1.6730-03	1.1825-03	1.1735-03	9.2541-04	4.7285-04
18	IM	1.6730-03	1.3867-03	7.3232-04	5.4566-04	9.0978-04
	IP	1.6446-03	1.2281-03	1.0956-03	3.6189-03	5.0F8C-04
19	IM	1.6618-03	1.3574-03	7.7960-04	9.8541-04	8.8402-04
	IP	1.6594-03	1.2664-03	7.7960-04	3.3818-04	5.3696-04
20	IM	1.5177-03	1.2533-03	8.1650-03	9.3818-04	8.6615-04
	IP	1.6461-03	1.2472-03	8.5205-04	6.1370-04	6.6586-04
21	IM	1.6221-03	1.2932-03	1.0114-03	6.4562-04	8.4821-04
	IP	1.6361-03	1.1394-03	8.8731-04	8.9007-04	5.93CC-04
22	IM	1.6226-03	1.2984-03	9.9170-04	8.7615-04	8.2222-04
	IP	1.5554-03	1.2215-03	1.0532-04	8.6572-04	6.2036-04
23	IM	1.6076-03	1.3876-03	9.5166-04	7.0579-04	0.4019-04
	IP	1.5471-03	1.1826-03	9.5163-04	8.4121-04	6.459H-04
24	IM	1.5972-03	1.1826-03	9.2006-04	7.9306-04	6.6447-04
	IP	1.6712-03	1.3973-03	9.7260-04	8.1956-04	6.4208-04
25	IM	1.1855-03	1.1521-03	9.0725-04	7.9251-04	7.5262-04
	IP	1.4029-03	1.4075-03	8.3926-04	7.7215-04	6.P23C-04
26	IM	1.1205-03	1.1394-03	8.7735-04	7.7940-04	7.9510-04
	IP	1.5727-03	1.0126-03	1.0126-03	7.9055-04	8.9464-04
27	IM	1.4963-03	1.0876-03	1.0950-04	7.6075-04	7.2860-04
	IP	1.5589-03	1.4284-03	1.0207-03	8.0641-04	7.1632-04
28	IM	1.4771-03	1.0534-03	8.2539-03	7.4208-04	7.1219-04
	IP	1.5443-03	1.4351-03	1.0478-03	8.2511-04	7.3239-04
29	IM	1.4564-03	1.0170-03	8.0094-04	7.2339-04	6.9571-04
	IP	1.5288-03	1.4422-03	1.0635-03	8.4177-04	7.4786-04

179

30	IM	1.4338-03	9.8091-04	7.7626-04	7.0470-04	6.7934-04
	IP	1.5125-03	1.4437-03	1.0784-03	8.5668-04	7.6271-04
31	IM	1.4267-03	9.4256-04	7.5138-04	6.8602-04	6.6303-04
	IP	1.4856-03	1.4456-03	1.0521-03	8.7135-04	7.7700-04
32	IM	1.3801-03	9.0273-04	7.2630-04	6.6737-04	6.4679-04
	IP	1.4775-03	1.4460-03	1.1047-03	8.8528-04	7.2067-04
33	IM	1.3468-03	8.6130-04	7.0105-04	6.4875-04	6.1064-04
	IP	1.4587-03	1.4449-03	1.1162-03	8.9847-04	8.0573-04
34	IM	1.4068-03	8.1847-04	6.7566-04	6.3021-04	6.1959-04
	IP	1.4568-03	1.4424-03	1.1266-03	9.1091-04	8.1619-04
35	IM	1.2572-03	7.7397-04	6.5016-04	6.1174-04	5.9263-04
	IP	1.4178-03	1.4384-03	1.1360-03	9.2259-04	8.2603-04
36	IM	1.1936-03	7.2787-04	6.2453-04	5.9338-04	8.8285-04
	IP	1.3456-03	1.4329-03	1.1442-03	9.3350-04	8.1925-04
37	IM	1.1099-03	6.8019-04	5.9899-04	5.7517-04	5.6721-04
	IP	1.3711-02	1.4259-03	1.1513-03	9.4360-04	8.4582-04
38	IM	9.9963-04	6.3100-04	5.7347-03	5.5715-04	5.5176-04
	IP	1.3495-03	1.4172-03	1.1571-03	9.5286-04	8.5970-04
39	IM	8.4017-04	5.8044-04	5.4812-04	5.3933-04	5.3655-04
	IP	1.2767-03	1.4028-03	1.1649-03	9.7997-04	8.7980-04
	IM	5.2024-04	5.2020-04	5.2028-04	5.2028-04	5.2028-04

180

I	Q	OLCP	PCT CHG	BETASC	OLCSC	PCT CHG	BETABS	OLCABS	PCT CHG	ETAU(CONT)
1	0.0000	8.5534-02	-100.00	1.8522-04	0.0000	.00	0.0000	7.1834-09	-100.00	1.4315-02
2	0.0000	6.4361-02	-100.00	2.1632-03	0.0000	.00	0.0000	8.1514-08	-100.00	1.3393-02
3	0.0000	5.7267-02	-100.00	4.2409-03	0.0000	.00	0.0000	1.5957-07	-100.00	1.3463-02
4	0.0000	5.2792-02	-100.00	6.3757-03	0.0000	.00	0.0000	2.3978-07	-100.00	1.3463-02
5	0.0000	4.9506-02	-100.00	8.5532-03	0.0000	.00	0.0000	3.2153-07	-100.00	1.7361-02
6	0.0000	4.6914-02	-100.00	1.0766-02	0.0000	.00	0.0000	4.0471-07	-100.00	1.7357-02
7	0.0000	4.4775-02	-100.00	1.3008-02	0.0000	.00	0.0000	5.0853-07	-100.00	1.7355-02
8	0.0000	4.2957-02	-100.00	1.5276-02	0.0000	.00	0.0000	1.0996-06	-100.00	1.7354-02
9	0.0000	4.1376-02	-100.00	1.7567-02	0.0000	.00	0.0000	2.1485-06	-100.00	2.2952-02
10	0.0000	3.9980-02	-100.00	1.9880-02	0.0000	.00	0.0000	3.8842-06	-100.00	2.2952-02
11	0.0000	3.8468-02	-100.00	2.2758-02	0.0000	.00	0.0000	6.7657-06	-100.00	2.2961-02
12	0.0000	4.0938-02	-100.00	2.5313-02	0.0000	.00	0.0000	1.3357-05	-100.00	2.1843-02
13	0.0000	4.7303-02	-100.00	2.7789-02	0.0000	.00	0.0000	2.4241-05	-100.00	2.1593-02
14	0.0000	5.2607-02	-100.00	3.0197-02	0.0000	.00	0.0000	4.1216-05	-100.00	2.1556-02
15	0.0000	5.9772-02	-100.00	3.2547-02	0.0000	.00	0.0000	6.6519-05	-100.00	2.1556-02
16	0.0000	6.5824-02	-100.00	3.4845-02	0.0000	.00	0.0000	1.5364-04	-100.00	2.1554-02
17	0.0000	7.1748-02	-100.00	3.7099-02	0.0000	.00	0.0000	2.2279-04	-100.00	2.1553-02
18	0.0000	7.7552-02	-100.00	3.9311-02	0.0000	.00	0.0000	3.1472-04	-100.00	2.1553-02
19	0.0000	8.3246-02	-100.00	4.1486-02	0.0000	.00	0.0000	4.3519-04	-100.00	2.1560-02
20	0.0000	8.8821-02	-100.00	4.3628-02	0.0000	.00	0.0000	5.9046-04	-100.00	2.1560-02
21	0.0000	9.4284-02	-100.00	4.5740-02	0.0000	.00	0.0000	7.8795-04	-100.00	2.1561-02
22	0.0000	9.9533-02	-100.00	4.7823-02	0.0000	.00	0.0000	1.0362-03	-100.00	2.1561-02
23	0.0000	1.0432-01	-100.00	4.9879-02	0.0000	.00	0.0000	1.2617-03	-100.00	1.6171-02
24	0.0000	1.0875-01	-100.00	5.1406-02	0.0000	.00	0.0000	1.5260-03	-100.00	1.6172-02
25	0.0000	1.1257-01	-100.00	5.2920-02	0.0000	.00	0.0000	1.8343-03	-100.00	1.6172-02
26	0.0000	1.1632-01	-100.00	5.4421-02	0.0000	.00	0.0000	2.1625-03	-100.00	1.6172-02
27	0.0000	1.2003-01	-100.00	5.5910-02	0.0000	.00	0.0000	2.6071-03	-100.00	1.6172-02
28	0.0000	1.2369-01	-100.00	5.7388-02	0.0000	.00	0.0000	3.0350-03	-100.00	1.6172-02
29	0.0000	1.2729-01	-100.00	5.8856-02	0.0000	.00	0.0000	3.6342-03	-100.00	1.6172-02
30	0.0000	1.3084-01	-100.00	6.0313-02	0.0000	.00	0.0000	4.2634-03	-100.00	1.6172-02
31	0.0000	1.3435-01	-100.00	6.1761-02	0.0000	.00	0.0000	4.9746-03	-100.00	1.6172-02
32	0.0000	1.3856-01	-100.00	6.3103-02	0.0000	.00	0.0000	5.7035-03	-100.00	1.6172-02
33	0.0000	1.4274-01	-100.00	6.4434-02	0.0000	.00	0.0000	6.7017-03	-100.00	1.6172-02
34	0.0000	1.4689-01	-100.00	6.5754-02	0.0000	.00	0.0000	7.7412-03	-100.00	1.6172-02
35	0.0000	1.5102-01	-100.00	6.7063-02	0.0000	.00	0.0000	8.9155-03	-100.00	1.6172-02
36	0.0000	1.5512-01	-100.00	6.8362-02	0.0000	.00	0.0000	1.0249-02	-100.00	1.6172-02
37	0.0000	1.5919-01	-100.00	6.9652-02	0.0000	.00	0.0000	1.1730-02	-100.00	1.6172-02
38	0.0000	1.6323-01	-100.00	7.0931-02	0.0000	.00	0.0000	1.3173-02	-100.00	1.6173-02
39	0.0000	1.6725-01	-100.00	1.4502-01	7.8646-04	8339.80	4.3213-08	2.7347-02	-100.00	3.411-02

SOLFLX = 1.27C3-02   OLCSOL = 0.0000   PCT CHG = 0.00

ANGLE		EPS	W	W1	RG			
1	57.311	8.000-01	0.000	6.845-04	2.223-03	2.209-02	5.689-02	7.364-02	4.516-02
2	76.658	8.000-01	0.000	6.845-04	2.223-03	2.209-02	5.689-02	7.364-02	4.516-02
3	50.000	8.000-01	0.000	6.845-04	2.223-03	2.209-02	5.689-02	7.364-02	4.516-02
4	79.715	8.000-01	0.000	6.845-04	2.223-03	2.209-02	5.689-02	7.364-02	4.516-02
5	17.619	8.000-01	0.000	6.845-04	2.223-03	2.209-02	5.689-02	7.364-02	4.516-02

FREG GOURP 29000 CM**-1 TO 29800 CM**-1

INTENSITIES

I	HRATE	FLUX	87.21	76.66	60.00	39.71	17.62
1	8.0275-04	5.4105+00	0.0000	0.0000	0.0000	0.0000	0.0000
2	8.3330-04	5.3652+00	1.1297+00	1.2219+00	1.0724+00	9.6534-01	9.1972-01
3	4.8769-04	5.3177+00	3.8417-01	7.9091-02	3.8278-02	2.6885-02	2.3197-02
4	2.3779-04	5.2900+00	1.1600+00	1.2352-01	1.0711-01	9.6001-01	9.1307-01
5	1.8144-04	5.2737+00	6.2493-01	1.5094-01	7.4391-02	5.2403-02	4.5202-02
6	1.2169-04	5.2635+00	1.2447+00	1.2477+00	1.0693+00	9.5457-01	9.0650-01
7	8.5832-05	5.2565+00	8.0305-01	2.1984-01	1.1003-01	7.7758-02	6.7066-02
8	6.3042-05	5.2517+00	1.2045+00	1.2528+00	1.0643+00	9.4725-01	8.9851-01
9	4.7838-05	5.2481+00	9.3696-01	2.8584-01	1.4526-01	1.0290-01	8.8752-02
10	3.6931-05	5.2454+00	1.3084+00	1.2534+00	1.0573+00	9.3874-01	8.8965-01
11	2.8122-05	5.2433+00	1.2243+00	3.4835-01	1.7983-01	1.2775-01	1.1021-01
12	2.1468-05	5.2409+00	1.1219+00	1.2543+00	1.0450+00	9.2950-01	8.8026-01
13	1.6762-05	5.2390+00	1.3141+00	4.0873-01	2.1369-01	1.5226-01	1.3140-01
14	1.3332-05	5.2375+00	1.1610+00	1.2470+00	1.0397+00	9.1975-01	8.7050-01
15	1.0772-05	5.2364+00	1.3407+00	4.6556-01	2.4680-01	1.7639-01	1.5229-01
16	8.8152-06	5.2354+00	1.1951-01	1.2414+00	1.0299+00	9.0962-01	8.6049-01
17	7.2990-06	5.2346+00	1.3413+00	5.1951-01	2.7911-01	2.0012-01	1.7287-01
18	6.1014-06	5.2340+00	1.2513+00	1.2347+00	1.0194+00	8.9918-01	8.5027-01
19	5.1456-06	5.2335+00	1.3453+00	5.7039-01	3.1061-01	2.2343-01	1.9313-01
20	4.3722-06	5.2330+00	1.2470+00	1.2271+00	1.0085+00	8.8850-01	8.3988-01
21	3.7404-06	5.2326+00	1.3455+00	6.1842-01	3.4128-01	2.4631-01	2.1305-01
22	3.2189-06	5.2323+00	1.3141+00	1.2186+00	9.9714-01	8.7758-01	8.2935-01
23	2.8204-06	5.2320+00	1.3452+00	6.8777-01	3.8709-01	2.8078-01	2.4313-01
24	2.5353-06	5.2318+00	1.3299+00	1.2043+00	9.7898-01	8.6043-01	8.1292-01
25	2.2857-06	5.2317+00	1.3407+00	7.5071-01	4.3087-01	3.1416-01	2.7237-01

Additional intensity rows (87.21, 76.66, 60.00, 39.71, 17.62):

87.21	76.66	60.00	39.71	17.62
1.3332+00	1.1884+00	9.6002-01	8.4287-01	7.9625-01
1.3387+00	8.0762-01	4.7263-01	3.4644-01	3.0076-01
1.3418+00	1.1708-01	9.4031-01	8.2496-01	7.7937-01
1.3322+00	8.5390-01	5.1236-01	3.7759-01	3.2828-01
1.3413+00	1.1518+00	9.1992-01	8.0675-01	7.6233-01
1.3246+00	9.0491-01	5.5009-01	4.0763-01	3.5492-01
1.3194+00	1.1313+00	8.9890-01	7.8825-01	7.4514-01
1.3105+00	9.4600-01	5.8586-01	4.3653-01	3.8068-01
1.3089+00	1.0675+00	8.7727-01	7.6951-01	7.2783-01
1.2681+00	9.8251-01	6.1968-01	4.6431-01	4.0557-01
1.2535+00	1.0860+00	8.5507-01	7.5055-01	7.1341-01
1.2861+00	1.0147+00	6.5160-01	4.9096-01	4.2957-01
1.2377+00	1.0611+00	8.3234-01	7.3139-01	6.9292-01
1.2777+00	1.0430+00	6.8164-01	5.1650-01	4.5269-01
1.2250+00	1.0347+00	8.0909-01	7.1206-01	6.7537-01
1.2114+00	1.0675+00	7.0909-01	5.4092-01	4.7493-01
	1.0067+00	7.8536-01	6.9258-01	6.5777-01
	1.0885+00	7.3626-01	5.6423-01	4.9629-01
	9.7723-01	7.6116-01	6.7297-01	6.4015-01
	1.1064+00	7.6090-01	5.8645-01	5.1678-01
	9.4608-01	7.3653-01	6.5325-01	6.2252-01
	1.1178+00	7.8324-01	6.0239-01	5.3158-01
	9.2172-01	7.1780-01	6.3840-01	6.0929-01
	1.1276+00	7.9462-01	6.1772-01	5.4589-01
	8.9639-01	6.9885-01	6.2352-01	5.9608-01

					ALBEDO.EARTH.BTMDE = .3710+00
26	2.0660-06	5.2315+00	1.2582+00	1.1355+00	6.3244-01	5.5571-01
27	1.8681-06	5.2314+00	1.1971+00	8.7006-01	6.0860-01	5.8208-01
28	1.6957-06	5.2313+00	1.2471+00	1.1427+00	8.2459-01	5.7305-01
29	1.5432-06	5.2312+00	1.1817+00	8.4270-01	5.9166-01	5.5571-01
30	1.4025-06	5.2311+00	1.2354+00	1.1481+00	6.6003-01	5.8591-01
31	1.2799-06	5.2310+00	1.1652+00	8.1420-01	5.7871-01	5.5557-01
32	1.1683-06	5.2309+00	1.2910+00	8.1427-01	6.7201-01	5.9829-01
33	1.0711-06	5.2308+00	1.1471+00	1.1522+00	6.2101-01	5.4347-01
34	9.7855-07	5.2307+00	1.2100+00	7.8473-01	6.8574-01	6.1019-01
35	8.9504-07	5.2307+00	1.1549+00	1.1549+00	6.8534-01	5.2043-01
36	8.2151-07	5.2306+00	1.1270+00	7.5405-01	5.4102-01	5.2160-01
37	7.4889-07	5.2305+00	1.1963+00	1.1565+00	6.9704-01	6.3254-01
38	7.7976-07	5.2305+00	1.1041+00	7.2219-01	5.3389-01	5.0451-01
39	0.0000	5.2305+00	1.1820+00	1.1568+00	7.0023-01	6.4299-01

SOLAR FLUX = 1.0162+01   VERT. COMP. OF SOLAR FLUX = 8.6014+00

-183-

FREQUENCY-INTEGRATED QUANTITIES   700 CM**-1 TO   29800 CM**-1

I	HRATE	FLUX
1	-4.8248-03	1.3000+00
2	-5.5030-03	1.5738+00
3	-5.5575-03	1.8867+00
4	-4.1129-03	2.1737+00
5	-3.0628-03	2.4076+00
6	-2.0365-03	2.5817+00
7	-1.2822-03	2.7020+00
8	-6.4450-04	2.7725+00
9	-1.7043-04	2.8091+00
10	1.8675-03	2.8187+00
11	2.5001-03	2.7140+00
12	9.0074-04	2.4951+00
13	3.5853-04	2.4093+00
14	8.4598-05	2.3744+00
15	-1.2667-04	2.3670+00
16	-2.8134-04	2.3781+00
17	-3.9504-04	2.4027+00
18	-4.7905-04	2.4374+00
19	-5.3622-04	2.4794+00
20	-5.7095-04	2.5263+00
21	-5.8574-04	2.5762+00
22	-5.7456-04	2.6271+00
23	-5.6143-04	2.6776+00
24	-5.7083-04	2.7149+00
25	-4.8642-04	2.7463+00
26	-4.2546-04	2.7717+00
27	-3.4690-04	2.8077+00
28	-2.4058-04	2.8320+00
29	-9.1201-05	2.8478+00
30	1.8721-04	2.8573+00
31	3.3215-04	2.8616+00
32	3.6409-04	2.8200+00
33	5.7282-04	2.7860+00
34	9.3958-04	2.7584+00
35	1.5558+03	2.6967+00
36	2.0059-03	2.5946+00
37	5.2526-03	2.4186+00
38	2.5705-02	2.0674+00
39	0.0000	3.1390-01

FLUX SPECTRUM

WAVENUMBER INTERVAL	FLUX, UPPER BCY	FLUX,GRC	FL.11	FL.23
700 TO 720	-4.110539+00	-4.916562+00	-2.529305+00	-2.554430+00
	5.410620+00	5.230458+00	5.243338+00	5.232031+00
29000 TO 298CC				

185

APPENDIX C

A DETAILED RADIATION MODEL FOR CLIMATE STUDIES;
COMPARISONS WITH A GENERAL CIRCULATION MODEL RADIATION SUBROUTINE

W. J. Wiscombe and B. E. Freeman

Systems, Science and Software
La Jolla, California 92037

1. INTRODUCTION

An atmospheric radiative transfer computer code has been developed, tested and applied to the calibration of the radiative transfer subroutine of one of the climate dynamics computer codes. The code to be described below has the objective of calculating radiative fluxes of short and long wave radiation in order to determine highly accurate atmospheric heating rates. Through this formulation, which takes account of frequency and angular dependence, scattering from molecules and aerosols, and general surface boundary conditions, we hope to make available a radiative transfer benchmark code serving as a standard for comparison with calculations containing less comprehensive treatments.

In several intensively investigated problems of atmospheric motion the role of radiative transfer is an important one. One of these is the global circulation of the atmosphere in which short and long wave radiation form a major subsystem of the strongly interactive radiative-fluid dynamic atmospheric system. In investigations of climate the geographical and seasonal dependence of the heating of the atmosphere interacting with surface albedo and cloud cover provides the source of energy for the atmospheric circulation. Another actively investigated field of fluid dynamics in which radiation plays a role is the planetary boundary layer. Diurnal changes within this layer give rise to winds and clouds having profound influence on Man. To mention a few of the phenomena induced by the heating of the atmosphere near the ground there are slope winds, land-sea breezes, heat island effects and radiation and advection fogs. Finally, on the micro-scale the environment of plants and animals is largely determined by the radiation properties of their immediate surroundings.

A number of the phenomena mentioned above have been the subject of detailed theoretical investigations within the last decade. If the results of these studies are to be of value in a predictive sense it is clear that the treatment of radiative transfer must be sufficiently quantitative to determine the time and space dependence of the atmospheric heating rate.

We shall return to the question of how accurate, in principle, a theoretical description of atmospheric radiative transfer can be made. Even within the framework of commonly made approximations, however, the radiative transfer calculation is a very large one. In fact the radiative transfer calculation is more time consuming than the fluid dynamic calculation by a substantial factor. This is principally due to the larger number of independent variables required to describe the radiation field as compared with the fluid field. In addition to spatial coordinates there are angular and frequency variables as well. Consequently, all calculations of the time-dependent behavior of an atmospheric fluid dynamic system have employed additional simplifying approximations in order to reduce the amount of calculation to solve the radiative transfer equations. In our presentation we plan to report the tests of one approximation scheme by comparing the results of our benchmark radiative transfer calculation with that of the Mintz-Arakawa global circulation model as used at the RAND Corporation for climate dynamics calculations.

In the perspective of the above discussion the objectives of our investigation are as follows:

(1) Formulate a theoretical treatment of atmospheric radiative transfer oriented to the determination of heating rates in the atmosphere. The treatment must be applicable to arbitrary conditions of insolation, surface boundary condition, and atmospheric distribution of gaseous and particulate absorbers and scatterers;

(2) Within basic well-justified approximations, develop a computer code which incorporates the best available techniques and data. The resulting computer code should qualify as a standard for comparison with radiation routines contained in fluid dynamics codes. Economy of calculation is considered to be of secondary importance compared to the above objective;

(3) Apply the computer code to the calibration of a radiation routine of a climate dynamics general circulation model (GCM).

As suggested above, there are several different classes of radiation treatments. The radiation subroutines of the fluid dynamic codes contain simplifying assumptions in order to achieve computational speed. These calculations must be performed repeatedly for many spatial positions and at many time steps during a typical fluid dynamic calculation. Examples of the treatment of radiation for GCM's are discussed by Manabe and Strickler (1964), Sasamori (1968) and Joseph (1966). Radiation in the planetary boundary layers is considered by Atwater (1971). At the other extreme, atmospheric spectroscopic investigations call for a very detailed treatment of narrow frequency intervals. In this case, interest in angular dependence and state of polarization, in addition to absorption line profile information, produces more information than is needed for atmospheric heating and greatly increases the computational expense. Examples of this approach are to be found in the extensive calculations of Dave (1968), Sekera (1963), and of Thompson and Wells (1971).

Only a few calculations have been reported which give a detailed treatment of the entire spectrum with the objective of evaluating the radiative heating of the atmosphere. Such a treatment is that of Rasool and Schneider (1971) who examine the effects on global climate of increases in aerosols and CO_2. They employ high resolution in the specification of the model atmosphere and in the frequency dependence in the IR. However, the angular distribution and interaction of scattering and absorption are treated very approximately. Another detailed radiation calculation of planetary atmospheres is that of Hunt and Grant (1969) who investigate the effect of high clouds on IR radiation emerging from the atmosphere. They calculate accurately the radiative transfer due to scattering and absorption but use an idealized phase function and low frequency resolution. As is discussed in greater detail below, our formulation attempts to remedy the weaknesses of both of these formulations.

2. FORMULATION OF THE RADIATIVE TRANSFER PROBLEM

The objectives of the radiation code discussed in the Introduction dictate that certain approximations which reduce its complexity can be made. We identify these approximations in this section and comment on each in a sentence. To reiterate the objectives of the study, we desire an accurate treatment of the radiative heating rate of the troposphere consistent with the level of atmospheric data obtainable from GCM calculations and global observations. These data are limited at present but we anticipate substantial improvement in them in the future and design our calculation accordingly.

Several approximations of physical processes have been made:

(1) The emissivity and absorption coefficient of the atmospheric constituents are assumed to be that appropriate to local thermodynamic equilibrium. This approximation, which requires molecular collisions to maintain thermodynamic equilibrium populations of those states participating in radiative transitions, is valid in the troposphere where the atmospheric pressure is high.

(2) The radiation field can be considered to be unpolarized. While molecular and Mie single scattering events result in partially polarized radiation, it has been shown (Howell, 1970) that the error resulting from a polarization-independent treatment is in many cases less than one percent.

(3) The air is assumed to be non-refractive. Refraction effects affect heating rates only for near-grazing angles of incidence of the solar beam and these angles occupy a very small fraction climatological events.

(4) Aerosols are assumed to be composed of uniform spherical particles with a homogeneous index of refraction. It is known that this assumption is not entirely valid for atmospheric aerosols; limited investigations indicate that scattering is not strongly dependent on shape and the theory of non-spherical particles is very much more difficult than for spheres.

Geometrical approximations which permit the radiation calculation to be treated as a stratified plane-parallel atmosphere are also implied:

(1) The atmosphere and boundary are taken to be plane-parallel. The atmosphere itself is well-approximated as plane when tropospheric radiation (where mean free paths are short) is being considered, when the clouds are stratified, and the sun angle is not near grazing incidence where curvature effects should be considered. The lower boundary must also be a horizontal plane.

(2) In order to carry out an average over the angle of azimuth, it is necessary that the quantity of interest be a scalar, such as the atmospheric heating rate.

A number of mathematical approximations have also been made. The discussion of these (discretization of angle, frequency, space) takes place in the next section along with the description of the computer code itself.

3.   DESCRIPTION OF THE CODE

The code has several unique features, among which are flexibility with respect to vertical zoning, ability to attain arbitrary accuracy by adjusting a few parameters, treatment of the combined line absorption-scattering problem and particularly of band overlap regions, and the generality of its surface boundary condition. These features, and others, are described in more detail below.

3.1   Transport Formulation

The central part of the code is that which solves the radiative transfer equation. The algorithm of Grant and Hunt (1969) has been chosen for this purpose. This algorithm is, in our estimation, the best currently available for the solution of the general monochromatic absorbing-scattering problem. It eliminates altogether the need for a cumbersome, and, in the presence of clouds, prohibitively expensive, scattering iteration procedure. It is computationally stable and economical, allows zones of arbitrary size, conserves flux provided only that the phase function is properly "normalized", and guarantees positive intensities regardless of the optical depth. It provides for error reduction by the adjustment of a few simple parameters, and furnishes error estimates for various quantities involved in the computation.

At present, the code assumes that zones are homogeneous with respect to the albedo for single scattering and the phase function; this permits the doubling method to be used for reflection and transmission matrices. However, since neither the Planck source term nor the solar source term (obtained after splitting the intensity into a solar and a diffuse part) are constant across zones, the normal doubling equations for source vectors cannot be used. We have derived doubling formulae for these inhomogeneous source vectors which permit them to be calculated with a minimum of computing time.

In the following discussion, space limitations force us to assume that the reader is familiar with the Grant and Hunt (1969) technique. Consider the zone of Figure 1, composed of 2^N primary layers of optical thickness $\Delta\tau$. Presume that the source in question varies across the zone according to $f(\tau)$, and that the source vectors for primary layer i are

$$\Sigma^{\pm}_{p,i} = \Sigma^{\pm}_{p} f(\xi_i) \qquad (1)$$

where the $\Sigma^{\pm}_{p}$ are independent of τ, and ξ_i is the mid-point of the primary layer,

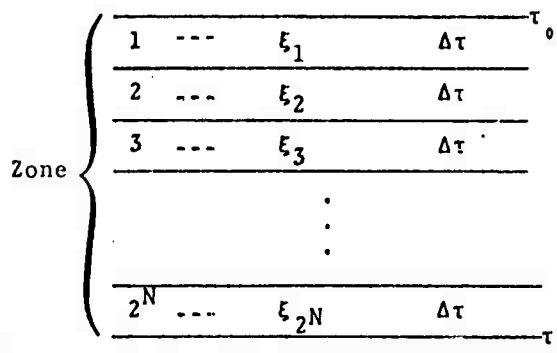$$\xi_i = \tau_0 + i\Delta\tau - \tfrac{1}{2}\Delta\tau \quad . \qquad (2)$$

Fig. 1. Zone, homogeneous with respect to single-scattering albedo and phase function, and composed of 2^N primary layers.

Because the layer superposition formulas for source vectors are linear in the source vectors, the superposition of any adjacent 2^n primary layers within the zone, beginning at the ith one, yields

$$\Sigma^{\pm}_{(i,n)} = \sum_{\ell=1}^{2^n} V^{\pm}_{n,\ell} \, f(\xi_{i+\ell-1}) \qquad (3)$$

(the expressions for the V's are not of interest here). The notation $\Sigma^{\pm}_{(i,n)}$ is a shorthand for

$$\Sigma^{\pm}_{i+(i+1) \, + \, \ldots \, + \, (i+2^n-1)} \quad .$$

For the solar source, we have

$$f(\tau) = e^{-\tau/\mu_0}$$

where μ is the cosine of the solar zenith angle. Assume that the first 2^n primary layers have been composed, so that $\Sigma^{\pm}_{(1,n)}$ are known. The next 2^n primary layers will then, by Eqs. (2) and (3), have source vectors

$$\Sigma^{\pm}_{(1+2^n,n)} = \sum_{\ell=1}^{2^n} V^{\pm}_{n,\ell} \, e^{-[\tau_0+(\ell+2^n)\Delta\tau-\frac{1}{2}\Delta\tau]/\mu_0}$$

$$= h_n \, \Sigma^{\pm}_{(1,n)} \qquad (4)$$

where

$$h_n = e^{-2^n\Delta\tau/\mu_0} \quad . \qquad (5)$$

Using Eq. (4), the source vectors for the combined layer of 2^{n+1} primary layers are given by the (source superposition) formulas

189

$$\Sigma^+_{(1,n+1)} = t_n \Gamma_n \left[r_n \Sigma^-_{(1+2^n,n)} + \Sigma^+_{(1,n)} \right]$$
$$+ \Sigma^+_{(1+2^n,n)}$$
$$= t_n \Gamma_n \left[h_n r_n \Sigma^-_{(1,n)} + \Sigma^+_{(1,n)} \right]$$
$$+ h_n \Sigma^+_{(1,n)} \tag{6}$$

$$\Sigma^-_{(1,n+1)} = t_n \Gamma_n \left[r_n \Sigma^+_{(1,n)} + \Sigma^-_{(1+2^n,n)} \right]$$
$$+ \Sigma^-_{(1,n)}$$
$$= t_n \Gamma_n \left[r_n \Sigma^+_{(1,n)} + h_n \Sigma^-_{(1,n)} \right]$$
$$+ \Sigma^-_{(1,n)} \tag{7}$$

where r_n and t_n are the reflection and transmission matrices for any layer of thickness $2^n \Delta\tau$ within the zone, and

$$\Gamma_n = (I - r_n r_n)^{-1} .$$

From the definition (5) of h_n,

$$h_{n+1} = h_n^2 . \tag{8}$$

Together, Eqs. (6-8) form a doubling scheme for the solar (or any exponential-in-τ) source. The scheme is initialized by

$$\Sigma^\pm_{(1,0)} = \frac{S_\nu \omega}{4\pi} e^{-(\tau_0 + \frac{1}{2}\Delta\tau)/\mu_0} \Delta\tau \begin{bmatrix} \frac{1}{\mu_1} \overline{P}_\nu(\pm\mu_1, \mu_0) \\ . \\ . \\ . \\ \frac{1}{\mu_m} \overline{P}_\nu(\pm\mu_m, \mu_0) \end{bmatrix}$$

$$h_0 = e^{-\Delta\tau/\mu_0}$$

and iterated from $n=0$ to $n=N-1$. (S_ν is the solar flux at frequency ν, ω is the albedo for single scattering, $\overline{P}_\nu$ is the azimuthally-averaged phase function, and $\mu_1, ..., \mu_m$ are the angular quadrature points.)

For the Planck source,

$$f(\tau) = B_\nu[T(\tau)]$$

where B_ν is the Planck function and T is the temperature. In order to derive doubling formulas for this source, a more tractable function than $B_\nu[T(\tau)]$ is needed. For zones across which the temperature change ΔT is not large ($\Delta T < 10°K$) it can be shown by expanding the Planck function that

$$f(\tau) = B_0 + B'(\tau - \tau_0)$$

reasonably approximates the variation of B_ν across the zone of Figure 1, where

$$B_0 = B_\nu[T(\tau_0)] , \quad \text{and}$$

$$B' = \frac{B_\nu[T(\tau_1)] - B_\nu[T(\tau_0)]}{\tau_1 - \tau_0} .$$

Consider a sublayer of thickness $2^n \Delta\tau$ ($0 < n < N$) beginning at $\tau = \tau_0$. Across this sublayer, write $f(\tau)$ as a linear combination of a constant part and an anti-symmetric part:

$$f(\tau) = \alpha_n f_c^n + B' f_L^n , \quad \tau_0 \leq \tau \leq \tau_0 + 2^n \Delta\tau ,$$

where $f_c^n = 1$, $\quad \alpha_n = B_0 + 2^{n-1} \Delta\tau B'$,

and $f_L^n = \tau - 2^{n-1} \Delta\tau - \tau_0$. $\tag{9}$

We now derive the doubling formulae for the source vectors $Y_n^\pm$ and $Z_n^\pm$ corresponding to f_c^n and f_L^n. The major advantage of working with Y and Z is that they are symmetric and anti-symmetric, respectively:

$$Y_n^+ = Y_n^- \equiv Y_n \qquad Z_n^+ = -Z_n^- \equiv Z_n$$

(these relations may be proved inductively). The doubling formula for Y_n is straightforward, since the corresponding source f_c^n is homogeneous across the zone:

$$Y_{n+1} = [t_n \Gamma_n (r_n + I) + I] Y_n . \tag{10}$$

Consider the source vector Z_{n+1} corresponding to the source function

$$f_L^{n+1} = \tau - 2^n \Delta\tau - \tau_0 , \quad \tau_0 \leq \tau \leq \tau_0 + 2^{n+1} \Delta\tau .$$

We treat this source function separately in the two halves of the interval:

$$f_L^{n+1} = f_L^n - 2^{n-1} \Delta\tau , \quad \tau_0 \leq \tau \leq \tau_0 + 2^n \Delta\tau ,$$

$$f_L^{n+1} = \tau - 2^n \Delta\tau - \tau_0 , \quad \tau_0 + 2^n \Delta\tau \leq \tau \leq \tau_0 + 2^{n+1} \Delta\tau ,$$

$$= \tau' - \tau_0 = f_L^n + 2^{n-1} \Delta\tau ,$$

$$\tau_0 \leq \tau' \leq \tau_0 + 2^n \Delta\tau .$$

The corresponding source vectors are

$$\Sigma^{\pm}_{(1,n)} = Z^{\pm}_n - 2^{n-1} \Delta\tau \ Y_n \quad ,$$

$$\Sigma^{\pm}_{(1+2^n,n)} = Z^{\pm}_n + 2^{n-1} \Delta\tau \ Y_n \quad .$$

Employing the source vector superposition formulae,

$$Z_{n+1} = t_n \Gamma_n [r_n \Sigma^{-}_{(1+2^n,n)} + \Sigma^{+}_{(1,n)}]$$

$$+ \Sigma^{+}_{(1+2^n,n)}$$

$$= [I + t_n \Gamma_n (I - r_n)] Z_n$$

$$+ g_n [I - t_n \Gamma_n (I - r_n)] Y_n \qquad (11)$$

where

$$g_n = 2^{n-1} \Delta\tau \quad .$$

Clearly,

$$g_{n+1} = 2 g_n \quad . \qquad (12)$$

Together, Eqs. (10-12) provide a doubling scheme for the Planck (or any linear-in-τ) source. The scheme is initialized by

$$Y_0 = (1-\omega)\Delta\tau \begin{bmatrix} 1/\mu_1 \\ \cdot \\ \cdot \\ \cdot \\ 1/\mu_m \end{bmatrix}$$

$$Z_0 = 0$$

$$g_0 = \frac{1}{2}\Delta\tau$$

and iterated from $n=0$ to $n=N-1$. The final values, Y_N, Z_N, and g_N, are combined just as the source functions in Eq. (9) are combined:

$$\Sigma^{+}_{(1,N)} = \alpha_N Y^{+}_N + B' Z^{+}_N$$

$$= (B_0 + g_N B') Y_N + B' Z_N \quad ,$$

$$\Sigma^{-}_{(1,N)} = \alpha_N Y^{-}_N + B' Z^{-}_N$$

$$= (B_0 + g_N B') Y_N - B' Z_N \quad .$$

More accurate piecewise-polynomial-in-τ approximations to $B_\nu[T(\tau)]$ are possible, at the expense of more com-

plicated source doubling formulas. In particular, we have derived economical quadratic and cubic schemes for future inclusion in the code (if the increased accuracy so obtained warrants their use).

The solar and Planck source vectors are simply added to give the total source vector.

3.2 Material Properties

The properties of the various gaseous, liquid, and solid constituents of the atmosphere enter the calculation of the absorption and scattering coefficients and phase function.

3.2.1 Scattering Treatments — Rayleigh scattering, with the non-negligible depolarization correction, is included following Penndorf (1957). A full Mie scattering calculation (for homogeneous spheres), with integration over a user-specified aerosol size distribution, is also included. Any of the commonly-used analytic aerosol size distributions (modified gamma, Gaussian, log-normal) are available as options, or the user may supply these data in card form. The complex index of refraction of water is tabulated over the entire frequency range of interest in the atmosphere, so that the accuracy with which the most important aerosols, clouds, are treated depends entirely on the accuracy with which the size distribution is known. The indices of refraction of other aerosol substances are tabulated as completely as available data permit.

Since the Mie scattering calculation can be costly, especially when clouds are present and the phase function must be calculated at many angles, an option is provided to use the Henyey-Greenstein phase function instead. The Mie phase function is then calculated at a relatively small number of angles and the single parameter in the Henyey-Greenstein function chosen to give a best fit at those angles. Several-parameter analytic phase functions are being sought in order to give greater freedom in this fitting process.

The Mie scattering sections of the code were checked against the tables of Deirmendjian (1969). In the integration over particle size, Deirmendjian picked integration intervals and tabular angles "by eye." In order to perform this integration by computer program an alternative procedure was devised. It involves a crude preliminary size integration, which is used to limit the size of the total interval of integration, to pick the integration mesh, and to establish the angular mesh on which the phase function is to be calculated. A Romberg integration is then done to obtain the final results.

If the phase function has too large a forward peak, it is truncated

191

after the fashion of Potter (1970) who finds that the resulting intensity errors are generally less than one percent. Flux errors are even smaller. By thus ensuring that the phase function does not have a strong angular dependence, accuracy can be obtained in fluxes using a relatively coarse angular specification of the intensity (3-7 Gaussian angles are currently being used).

3.2.2 Absorption Treatment

In addition to the continuum absorption due to Mie scattering, two other absorption continua are included in the code: the H_2O continuum in the 8-13μ window region; and the N_2 continuum around 4μ. Data for both of these continua are taken from McClatchey, et.al. (1970). McClatchey's group has also furnished what we find to be the best currently available transmission functions for molecular bands (barring a prohibitively expensive line-by-line calculation). These transmission functions are tabular fits to actual line-by-line calculations, with averaging intervals of 20 cm^{-1}. (Below 350 cm^{-1} we use the Goody random band model for the H_2O rotation band.) Transmissions are calculated separately for H_2O, for O_3, and for the uniformly mixed absorbers (CO_2, N_2O, CO, CH_4, and O_2). The scaling approximation is used with parameters chosen to give the best agreement with line-by-line calculations. The results are claimed to be accurate to better than 10 percent, and in most cases to better than 1-2 percent; the worst errors are in the wings of strong bands.

3.3 Splitting Into Monochromatic Problems

The Grant and Hunt algorithm is applicable to monochromatic problems. Unfortunately, in solving atmospheric radiative transfer problems, frequency groups may not be taken narrow enough that the absorption coefficient remains reasonably constant across them. Typically, a frequency group will be upwards of 20 cm^{-1} in width and will contain numerous absorption lines. Therefore, a further approximation is necessary.

The approximation we have chosen is suggested by some work of Grant and Hunt (1969) and of Yamamoto (1971). The idea expressed in Eq. (14) antedates their work, however, and may be traced to, for example, Cowling (1950).

Let the transmission function be

$$T_{\Delta\nu}(u) = \frac{1}{\Delta\nu} \int_{\Delta\nu} e^{-k_\nu u/\mu} \, d\nu \qquad (13)$$

where u is the scaled absorber amount. Fit $T_{\Delta\nu}$ with a sum of exponentials,

$$T_{\Delta\nu}(u) \cong \sum_{i=1}^{M} a_i \, e^{-k_i u/\mu} \qquad (14)$$

where M is small, $O(10)$ say (thus precluding the sum from being an ordinary quadrature for the integral, which would require hundreds or thousands of terms). If i_ν is the diffuse intensity, suppose that corresponding to Eq. (14) we have

$$i_{\Delta\nu} \equiv \frac{1}{\Delta\nu} \int_{\Delta\nu} i_\nu \, d\nu \cong \sum_{i=1}^{M} a_i i_i \quad . \qquad (15)$$

Each i_i is chosen to satisfy a monochromatic problem with absorption coefficient

$$k_i \frac{du}{dz}$$

(where z is vertical distance). Recombining the i_i according to Eq. (15), with the a_i determined by some fitting scheme leading to Eq. (14), produces the frequency-averaged intensity $i_{\Delta\nu}$.

Yamamoto (1971) explicitly assumes and Grant and Hunt (1969) tacitly assume that the above procedure is correct. However, they do not actually give a derivation beginning from the radiative transfer equation. The present authors find that a further assumption is needed, namely that

$$\frac{1}{\Delta\nu} \int_{\Delta\nu} i_\nu \, e^{-k_\nu u/\mu} \, d\nu \cong \sum_{i=1}^{M} a_i i_i \, e^{-k_i u/\mu} \, . \qquad (16)$$

Granting this, the splitting into monochromatic problems follows. We argue for the plausibility of Eq. (16) based on certain ideas about Lebesgue quadrature and about the behavior of i_ν. This point is considered more definitively by Freeman, Wiscombe, and England (1972).

It is difficult to obtain the fit in Eq. (14) in an automatic, stable, convergent fashion, since the problem of exponential-sum-approximation is notorious for its numerical ill-conditioning and general intractability (cf. Lanczos, 1956). Recently, however, Cantor and Evans (1970) devised a way of "factoring out" the ill-conditioned part of the problem, and their method has been incorporated into the code. It is accurate, computationally fast, has guaranteed convergence, and provides the unique best fit in the least-squares sense.

3.4 Boundary Conditions

The surface boundary condition is formulated in complete generality, allowing for the specification of the full bi-directional reflectivity. There are also provisions, in case less information is

available, to use the directional-hemispherical reflectivity or the hemispherical reflectivity (albedo). In the latter two cases, diffuse reflection is assumed. The emissivity is calculated from the reflectivity using Kirchoff's Law. In case only the directional or hemispherical emissivity is available, the directional-hemispherical reflectivity or albedo is calculated therefrom using Kirchoff's Law.

Theoretical derivations of rough-surface bidirectional reflectivities, with roughness specified by Cox and Munk's (1956) distributions for the sea surface and by McStravick's (1972) model for land surfaces, have been incorporated into the code. Various albedo data, such as that of Krinov (1947), have also been included.

4. TEST PROBLEMS

There are very few exact solutions in radiative transfer theory. Those that do exist, are for monochromatic problems only. We have tested the code against several such problems. For the case of no scattering, and using a realistic absorption coefficient (a Lorentz line) with pressure and temperature dependence, problems were run with various temperature profiles and surface boundary conditions and compared with the analytic solution. For a scattering test problem, comparisons were made with the Rayleigh scattering solutions tabulated by Sekera and Kahle (1966). Agreement in these cases was excellent.

Investigation is continuing into the accuracy of the approximation of Eq. (16). A detailed line-by-line transfer calculation is being designed, using a model line structure, to ascertain the limits of its validity.

5. COMPARISON WITH GCM CALCULATIONS

An application of our code is being made to the calibration of the radiation subroutine of the Mintz-Arakawa GCM as used in the climate dynamics research program at the Rand Corporation (Gates, 1971). Results of comparisons between the radiation treatment in that code and our code will be included in our presentation. These will consist of comparisons of radiative heating rates of the atmosphere for selected locations on the global surface. Atmospheric input data are taken from the GCM calculation.

6. REFERENCES

Atwater, M., 1971: The radiation budget for polluted layers of the urban environment. J. Appl. Meteor., 10, 205-214.

Cantor, D. and J. Evans, 1970: On approximation by positive sums of powers. SIAM J. Appl. Math., 18, 380.

Cowling, T.G., 1950: Atmospheric absorption of heat radiation by water vapor. Phil. Mag., 41, 109.

Cox, C. and W. Munk, 1956: Slopes of the sea surface deduced from photographs of sun glitter. Bull. Scripps Inst. Oceanog., 6, 401.

Dave, J.V., 1968: Transfer of solar ultraviolet radiation through the earth's molecular atmosphere. JQSRT, 8, 25-38.

Deirmendjian, D., 1969: _Electromagnetic scattering on spherical polydispersions_. Elsevier.

Freeman, B.E., W.J. Wiscombe, and W.G. England, 1972: The effects of meso-scale and small-scale interactions on global climate. Systems, Science and Software Report 3SR-1034, La Jolla, Calif.

Gates, W.L., E.S. Batten, A.B. Kahle, and A.B. Nelson, 1971: A documentation of the Mintz-Arakawa two-level atmospheric general circulation model. Advanced Research Projects Agency Report R-877.

Grant, I. and G. Hunt, 1969: Discrete space theory of radiative transfer I. Fundamentals. Proc. Roy. Soc. Lond. A, 313, 183.

Howell, H. and H. Jacobowitz, 1970: Matrix method applied to multiple scattering of polarized light. J. Atmos. Sci., 27, 1195-1206.

Hunt, G. and I. Grant, 1969: Discrete space theory of radiative transfer and its application to problems of planetary atmospheres. J. Atmos. Sci., 26, 963-972.

Joseph, J., 1966: Calculation of radiative heating in numerical general circulation models. Dept. of Meteorology Tech. Report No. 1, University of California, Los Angeles.

Krinov, E.L., 1947: Spectral reflectance properties of natural formations. Nat. Res. Council of Canada Tech. Trans. 439, Ottawa.

Lanczos, C., 1956: _Applied Analysis_. Prentice-Hall, p. 272.

Manabe, S. and R.F. Strickler, 1964: Thermal equilibrium of the atmosphere with a convective adjustment. J. Atmos. Sci., 21, 361-385.

194

McClatchey, R., et.al., 1970: Optical properties of the atmosphere. Air Force Cambridge Report AFCRL-70-0527, Cambridge, Mass.

McStravick, D.M., 1972: The effect of surface roughness on the reflected and emitted energy from a rough surface. Ph.D. Thesis, Rice Univ. Texas.

Penndorf, R., 1957: Tables of the refractive index for standard air and the Rayleigh scattering coefficient for the spectral region between 0.2 and 20μ. J. Opt. Soc. Amer., $\underline{47}$, 176.

Potter, J., 1970: The delta function approximation in radiative transfer theory. J. Atmos. Sci., $\underline{27}$, 943.

Rasool, S.I. and S.H. Schneider, 1971: Atmospheric carbon dioxide and aerosols: Effects of large increases on global climate. Science, $\underline{173}$, 138-141.

Sasamori, T., 1968: The radiative cooling calculation for application to general circulation experiments. J. Appl. Meteor., $\underline{7}$, 721-729.

Sekera, Z., 1963. Radiative transfer in a planetary atmosphere with imperfect scattering. The Rand Corp. Report R-1413-RR, Santa Monica, Calif.

Sekera, Z. and A. Kahle, 1966: Scattering functions for Rayleigh atmospheres of arbitrary thickness. The Rand Corp. Report R-452-PR, Santa Monica, Calif.

Thompson, B.C. and M.B. Wells, 1971: Scattered and reflected light intensities above the atmosphere. Appl. Optics, $\underline{10}$, 1539-1549.

Yamamoto, G., M. Tanaka, and S. Asano, 1971: Radiative heat transfer in water clouds by infrared radiation. JQSRT, $\underline{11}$, 697.